Lígia Regina Tomás Coelho

BSc. Biochemistry, FC-UL

Vascularization: plant decellularization and electrospinning techniques for the development of small and medium caliber blood vessels

Dissertation submitted in partial fulfillment
of the requirements for the degree of

Master of Science in
Biochemistry

Adviser: Jorge Carvalho Silva, Assistant Professor, NOVA University of Lisbon

Co-adviser: Carla Pinheiro, Assistant Professor, NOVA University of Lisbon

Examination Committee

Chairperson: Prof. Dr. José Ricardo Ramos Franco Tavares
Raporteur: Dr. Ana Margarida da Costa Macedo Fortes
Member: Prof. Dr. Jorge Alexandre Monteiro Carvalho Silva

FACULDADE DE CIÊNCIAS E TECNOLOGIA
UNIVERSIDADE NOVA DE LISBOA

October, 2018

Vascularization: plant decellularization and electrospinning techniques for the development of small and medium caliber blood vessels

This document was created using the (pdf)LaTeX processor, based in the "novathesis" template[1], developed at the Dep. Informática of FCT-NOVA [2].
[1] https://github.com/joaomlourenco/novathesis [2] http://www.di.fct.unl.pt

To the ones who helped this dream become a reality.

Acknowledgements

This thesis could never have come to fruition without the help of some amazing people who I was lucky enough to come in contact with along this entire year. This work is dedicated to them.

To the ladies at the Molecular Ecophysiology Lab at ITQB, Dr. Ana Fortunato and Dr. Olfa Zarrouk, for all the support and valuable suggestions given to me throughout the time I was there. A special thanks to Dr Ana for taking the time out of her busy schedule to guide me through the booking protocols of equipment, teach me about how everything works and especially, watering my plants on the days I couldn't go to the institute, so I could finish an experiment at the faculty.

To professor Pinto Ricardo at the Plant Biochemistry Lab at ITQB, for his help choosing and identifying plant varieties and always being interested on the project.

To Dr Susete Fernandes from the Polymeric and Mesomorph Materials Group at FCT-UNL, for helping me with the contact angle measurements and teaching me about the process.

To all the lab technicians and researchers who have aided me along the way, be it by their work or simple advice, with a special thanks to Hugo Matias for all his greenhouse help during the plant growth step.

To my lab colleagues Diana Querido, Bruno Guerreiro, Daniela Fernandes and Jeniffer Farias for making the hard days when nothing seemed to work much more bearable.

To my partner, David Moreira, for saving me multiple times from some serious informatics mishaps, for all the support and times he's helped me transport my work from the institute to the university.

Lastly, but surely not the least, to my wonderful supervisors professor Jorge Silva and professor Carla Pinheiro for giving me all the resources I needed to complete my work the best way I could. Thank you for always having the time to listen to me and give me precious advice even when your schedule seemed to have no wiggle room. Thank you for always being one email, text or knock on the door away and ultimately, thank you for always believing in me even before this project was even accepted and it was only a simple draft.

"Non quia difficilia sunt non audemus, sed quia non audemus, difficilia sunt."
It is not because things are difficult that we don't dare, it is because we don't dare that things are difficult.
- Seneca, Epistuale Morales 104.26

Abstract

Vascularization in complex human tissues remains a challenge in the field of tissue engineering. A functional vascular network, capable of providing oxygen and nutrients and the removal of metabolites, is mandatory for the regeneration of large organs. Recent research on whole organ decellularization has showcased advantages regarding biocompatibility and structural integrity on the resulting extracellular matrix. In this work, we explored the possibilities of two different scaffold building techniques, plant decellularization and fibre electrospinning, as natural and synthetic alternatives for the issue of vascularization. *Tetragonia tetragonioides* (Pallas) Kuntze, *Spinacia oleracea* L. and *Phaseolus vulgaris* L. leaves were successfully decellularized, with a nucleic acid reduction of 89 ± 11 %, 99.0 ± 1.0 % and 99.6 ± 0.4 % respectively. The structural integrity was highest for *T. tetragoniodes*. Re-seeding of the leaves with 3T3 fibroblasts and endothelial cells by conventional seeding and a perfusion re-cellularization for *S. oleracea* with 3T3 cells were also achieved. In parallel, we were able to produce polycaprolactone scaffolds interleaved with open channels and evaluate their cellular adhesion and proliferation. A three channel scaffold alongside thick polycaprolactone layers provided the best results. The scaffolds studied in this work may provide effective re-vascularization strategies upon incorporation in large-scale scaffolds for organ regeneration.

Keywords: Tissue engineering, ECM, 3T3, endothelial cells, PCL, PEO, *Phaseolus vulgaris* L., *Tetragonia tetragonioides* (Pallas) Kuntze, *Spinacea oleracea* L., SDS, Triton X-100.

Resumo

A vascularização em tecidos humanos complexos permanece um desafio no ramo de engenharia de tecidos. A existência de uma rede vascular que providencie oxigénio e nutrientes, bem como a remoção de metabolitos é essencial à regeneração de órgãos. Desenvolvimentos recentes acerca da descelularização de órgãos têm demonstrado vantagens relativamente à biocompatibilidade e integridade estrutural da matriz extracelular resultante. Neste trabalho, explorámos as possiblidades de duas técnicas de fabricação de *scaffolds*, a descelularização vegetal e a electrofiação de fibras, como sendo alternativas naturais e sintéticas ao problema da vascularização. Folhas de *Tetragonia tetragonioides* (Pallas) Kuntze, *Spinacia oleracea* L. e *Phaseolus vulgaris* L. foram descelularizadas com sucesso, com uma redução de conteúdo de ácidos nucleicos de 89 ± 11 %, 99.0 ± 1.0 % e 99.6 ± 0.4 % respectivamente. A integridade estrutural foi superior para *T. tetragonioides*. Foi possível efetuar o *seeding* de folhas com fibroblastos 3T3 e células endoteliais por seeding convencional bem como por perfusão de folhas de*S. oleracea* com células 3T3. Em paralelo, foram produzidos *scaffolds* de policaprolactona intercalados com canais abertos e avaliada a sua adesão e proliferação celular. Os melhores resultados foram obtidos para um *scaffold* de três canais juntamente com camadas espessas de policaprolactona. Os *scaffolds* utilizados neste trabalho poderão ser uma estratégia eficaz de re-vascularização quando incorporandas em *scaffolds* de larga escala para a regeneração de órgãos.

Palavras-chave: Engenharia de tecidos, 3T3, células endoteliais, ECM, PCL, PEO, *Phaseolus vulgaris* L., *Tetragonia tetragonioides* (Pallas) Kuntze, *Spinacea oleracea* L., SDS, Triton X-100.

Contents

List of Figures

List of Tables

Glossary

Anastomosis	A connection made surgically between adjacent blood vessels or other channels of the body.
Angiogenisis	Process through which new blood vessels form from pre-existing ones, often associated to a particular organ or tissue.
Angiosperm	A plant of a large group that comprises those that have flowers and produce seeds enclosed within a carpel, including herbaceous plants, shrubs and grasses.
Atheroma	An abnormal accumulation of material, mostly macrophages and debris, in the inner layer of the arterial wall.
Cotyledonary	Respective to the cotyledon, meaning an embryonic leaf in seed-bearing plants, one or more of which are the first leaves to appear from a germinating seed.
Dicot	Abbreviation of dicotyledon, meaning a flowering plant with an embryo that bears two cotyledons. Typically, they have broad stalked leaves with net-like veins.
Hypanthium	An enlarged cup or rim of tissue in flowers.
Hyperplasia	Increase in the amount of organic tissue, resulting from cell proliferation.
Hypoxia	Process where there is an inadequate oxygenation of the blood.
Parenchyma	A type of tissue in plants, typically soft and succulent, characterized by cells with thin walls and found mainly in the softer parts of leaves etc.
Patency	The condition of being open or unobstructed.
Proatherogenic	That promotes the formation of atheromatous deposits.
Protoxylem	The part of the primary xylem that develops first in a plant organ, consisting of narrow, thin-walled cells.

Saphenous vein	Large superficial vein of the leg.
Scaffold	Cell growth support structures composed of biocompatible materials, especially designed for cell attachment.
Seeding	To disperse or transfer cells onto a designed scaffold.
Senescence	Also known as biological aging, it refers to the condition or process of deterioration with age.
Thrombus	A stationary blood clot along the wall of a blood vessel, frequently causing vascular obstruction.
Xenotransplantation	Also known as heterologous transplant, it consists on the transplantation of living cells, tissues or organs from one species to another.

Acronyms

AEC	Adapted Euro-Collins solution.
bFGF	Basic Fibroblast Growth Factor.
Car	Carotenoid.
CB	Common Bean (*Phaseolus vulgaris* L.).
CHAPS	3-[(3-CholAmidopropyl)dimethylammonio]-1-PropaneSulfonate.
Chl	Chlorophyll.
CST	Common Sowthistle (*Sonchus oleraceus* L.).
DAPI	4,6-DiAmidino-2-PhenylIndole.
DMEM	Dulbeccos Modified Eagles Medium.
EC	Endothelial Cell.
ECH	EpiChloroHydrin.
ECM	Extracellular Matrix.
EDTA	Ethylene Diamine TetraAcetic acid.
EGTA	Ethylene Glycol TetraAcetic acid.
EtOH	Ethanol.
FBS	Fetal Bovine Serum.
GAG	Glycosaminoglycan.
NZ	New Zealand spinach (*Tetragonia tetragonoides* (Pallas) Kuntze).
PBS	Phosphate Buffer Solution.

PCC	Plant Cellular Culture.
PCL	PolyCaproLactone.
PD	Plant Decellularization.
PEG	PolyEthylene Glycol.
PEO	PolyEthylene Oxide.
PFA	ParaFormAldehyde.
PLA	Poly-Lactic Acid.
PLCL	Poly(l-Lactide-co-ϵ-CaproLactone.
PLGA	Poly(Lactic-co-Glycolic Acid).
PVP	Poly(Vinyl Pyrrolidone).
RC	*Rumex crispus* L.
SB	SulfoBetaine.
SCC	Scaffold Cellular Culture.
SDS	Sodium Dodecyl Sulfate.
SDS-PAGE	Sodium Dodecyl Sulfate PolyAcrylamide Gel Electrophoresis.
SEM	Scanning Electron Microscopy.
SMC	Smooth Muscle Cells.
U.T.S	Ultimate Tensile Strength.
VEGF	Vascular Endothelial Growth Factor.
VS	Viroflay Spinach (*Spinacea oleracea*).
WGS	Winter Giant Spinach (*Spinacea oleracea* L.).

Chapter 1

Introduction and Objectives

The interdisciplinary field of tissue engineering aims for the restoration, improvement or replacement of human tissues. As to achieve it, a scaffold must be biocompatible, in order to avoid unwanted host immune responses, allow for cellular attachment, migration, proliferation and differentiation and be controllably biodegradable in order to aid tissue construction. The material should also support the formation of the ECM (extracellular matrix) by promoting cellular mechanisms, provide biomolecular signals and have adequate mechanical properties in order to arrange a good cellular environment for the normal transit of cell factors and molecules [1]. It is then implanted onto the patient and degrades at an adequate rate as the cells proliferate in number, leaving, at last, a solely cellular tissue with no toxic degradation by-products. Although skin and cartilage tissues designed *in vitro* are already commercially used, whole-organ engineering is still far from safely transplantable in patients [2]. However, recent years have allowed for large scientific advances in biomaterials, stem cells, growth and differentiation factors and the creation of biomimetic environments, allowing for new scaffolds, new cellular techniques and an exponential growth in attempts at engineering living tissues. Nevertheless, major challenges still remain such as the need for more complex systems and the inability to produce functional and stable vascularized systems.

1.1 Vascularization

Blood vessels allow for the transportation of nutrients and oxygenated blood to cells as well as the removal of waste through a network that is subdivided into small capillaries. It plays a pivotal role on the cellular viability of the implanted tissue, especially in regards to parenchymal cells, co-determining their behaviour. This mechanism is limited by the fact that diffusion can only transport oxygen and nutrients at a distance of 100-200 μm from the nearest blood vessel. Although some neovascularization processes occur post implantation, as a reaction to hypoxia [3], this growth is limited to tens of micrometeres per day, a rate too low for an organ to be feasible unless previously vascularized [4].

In order to enhance vascularization several strategies have been investigated *in vitro* and *in vivo*, with methodologies such as pre-vascularization with or without the usage of angiogenic factors and scaffold design.

1.1.1 *In Vivo* Pre-vascularization

In vivo pre-vascularization is a technique based on a non-vascularized construct that follows a two-step programme. Firstly, a porous acellular scaffold is attached to the patient's artery, side to side, becoming vascularized post-implantation through cellular infiltration on the scaffold. After a time period of a few weeks, a microvascular network will be formed that can then be harvested an explanted to the host's target site.

This process allows for the scaffold to be immediately perfused after implantation. However, two separate surgeries are required and, since the vascular axis has to be removed from the first surgery's site, cells will have to reseed on the second surgery site, a process that can be tricky thanks to nutrient limitations that arise post implantation [5].

1.1.2 *In Vitro* Pre-Vascularization

In vitro pre-vascularization aids time management as vessels only need to grow into the outer regions of the vessel construct. However, as they cannot be surgically connected to the host's vasculature, perfusion occurs at a slower rate when compared to *in vivo* pre-vascularization [6]. Co-cultures using endothelial cells and, optionally, other cell lineages such as myoblasts and fibroblasts can be used as a way to initiate vascularization in a variety of tissues. In this technique, the cells are introduced into the desired tissue through either 3D multicellular spheroids or simple culture mixing, thus constructing a rudimentary vascular network that can be connected with the existing vasculature of the host's tissue, a process named anastomosis [7] [8]. The usage of a combined culture of both endothelial cells and

fibroblasts has been found to be particularly useful as fibroblasts have also been shown to modulate the formation of an endothelial cellular network [9].

1.1.2.1 Angiogenic Factors

Angiogenisis consists of the process where new blood vessels are formed, branching outwards from pre-existing ones in a deeply dynamic process comprised of several steps. Angiogenic factors arise from different sources, being produced by host cells due to an inflammatory response to tissue injury at the moment of or after implantation [10].

These factors can and have been successfully added to designed scaffolds in order to enhance vascularization. In fact, the formation of new vessels can be increased by factors such as VEGF (vascular endothelial growth factor) and bFGF (basic fibroblast growth factor) which stimulate the mobilization and recruitment of progenitor cells, thus accelerating the activation of the host's microvasculature at the implantation site [11]. In order to deliver them to the implantation site, growth factors are entrapped within a scaffold such as collagen, alginate and PLGA (poly(lactic-co-glycolic acid)). However, induced vessels have been found to be often disorganized, hemorrhagic and unstable [12], thus still requiring optimization.

Protein modification techniques have also been applied in scaffolds, by binding domains for angiogenic factors through fusion proteins. Although successful, issues were found regarding the delivery of pro-angiogenic factors towards a specific region. This issue has lead to the exploration of drug-delivery techniques such as loaded microspheres incorporated onto scaffolds. Still, as this process is highly dependant on cellular response, to date, it is seen as better suited as for conditions where these factors can be easier to control [13].

1.1.3 Scaffold Design

Scaffold design deeply affects the rate of vascularization post implantation as it influences its inherent characteristics. Druecke *et al.* has shown that vessel ingrowth rate into a poly(ether ester) block-copolymer scaffold is influenced by pore size, where the rate for small diameter pores is lower than the one for pores with a diameter between 200-300 μm [14]. The way pores interconnect with each other also plays a pivotal role as cell migration, and thus, vascularization, will only occur when pores are connected [15]. Although its shape and size can be varied through different fabrication techniques, their organization will remain random, leading to obstructed and partially connected pathways that could limit nutrient supply for the seeding cells as well as vessel ingrowth [16].

Currently, scaffold fabrication can be done through several methodologies such as phase separation, freeze-drying, self-assembly, gas foaming, rapid prototyping, electrospinning and tissue decellularization [17]. Organ decellularization has showcased advantages regarding

biocompatibility and structural preservation. The complexity of the microstructure of a decellularized ECM cannot be reproduced by any of the current scaffold fabrication methods, either alone or in combination thus making it an interesting approach to the issue of vascularization. Also, plant ECM holds several characteristics similar, to a certain extent, to animal ECM.

1.2 The Extracellular Matrix

The ECM is a fairly stable structural component whose main function is to provide physical scaffolding for cell growth and prolifertion. Nonetheless, it plays other important roles, by triggering key biochemical and biomechanical cues, required for tissue morphogenesis and differentiation profiles. It is a highly dynamic structure which is frequently remodelled via both enzymatic and non-enzymatic processes. Each tissue has an individual composition that differs between cellular lineages in a markedly heterogeneous fashion though their main composition remains the same throughout [18]. Cell adhesion and communication is also influenced by the ECM.

1.2.1 The Animal ECM

The Animal ECM is a complex network composed of three main types of molecules: proteoglycans , fibrous (substrate adhesive) proteins and structural components.

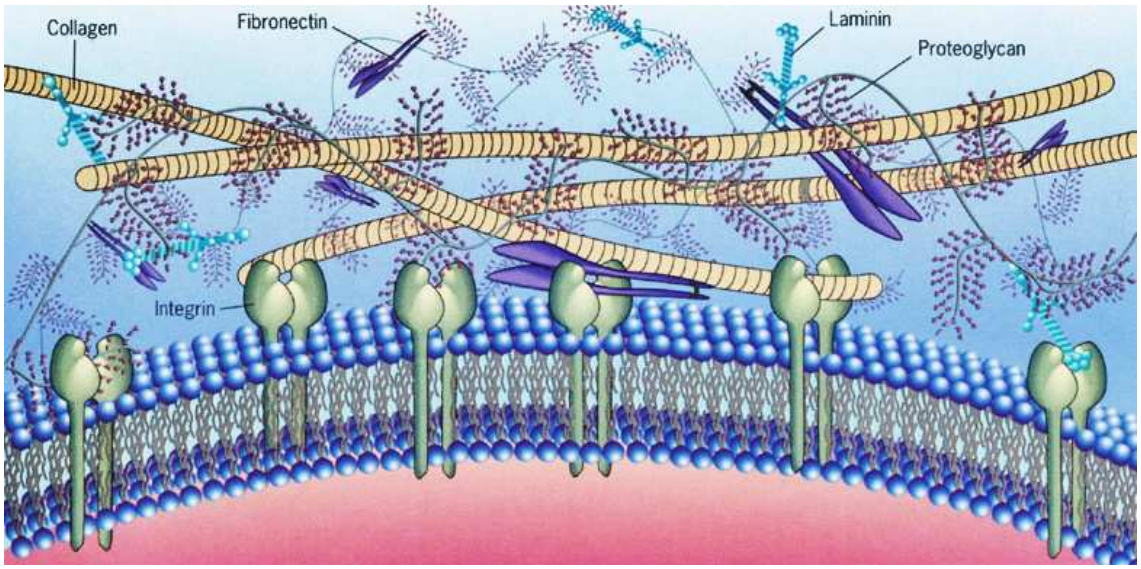

Figure 1.1: Pictorical representation of the ECM molecular organization. Fibrous proteins contain binding sites for each other as well receptors such as integrins which are located at the cell surface. The presence of proteoglycans is of great importance since they occupy the majority of the extracellular space. Adapted from Karp [19].

1.2.1.1 Proteoglycans and other glycoproteins

Proteoglycans are complex macromolecules, mainly comprised of GAG (glycosaminoglycans) chains covalently bound to a polypetide side chain. Their strong anionic charge allows them to attract counter-ions as well as water molecules in tissues, giving them their characteristic hydration properties and force-resilience [20] [18] [21].

Glycoproteins are comprised of olygosacharide chains covalently bound to a polypeptide side chains which, contrary to proteoglycans, are not negatively charged. Laminins are a group of heterotrimetric glycoproteins that play an important role both in cell adhesion and several other processes such as cellular differentiation and migration via their integrins. Integrins compile a family of cell surface receptors which mediate cell-matrix interactions by binding ECM fibrils and associating with actin filaments through cytoskeletal linker proteins. Each component of the linkage transmits forces that activate a plethera of signaling pathaways for cell survival [22]. Laminins also have the ability to bind to minor collagen species [23] [24] [25].

1.2.1.2 Fibrous proteins

I. **Collagen**

Collagen is the most common fibrous protein in humans, with an estimated 30% of all protein in the human body being Collagen Type I. It is arranged into fibrils in a triple-helical organizational fashion, which consists of three separate α chains, each of them twisted in the form of a left-handed helix. These chains wrap around each other in a highly ordained way, similar to a rope, producing the tight molecular structure which is then stabilized by inter-chain hydrogen bonds. Its structure gives collagen the ability to help maintain tissue integrity by giving the ECM the tensile strength required to endure mechanical stress as well its resistance to protease attacks. Collagen also plays a role in other mechanisms such as cellular adhesion and migration [24] [26] [21].

II. **Elastin**

Elastin's role relies on providing tissues its resilience and elasticity. Its structure comprises single tropoelastin subunits (precursors) that bind to each other, forming the fibre. Elastin fibres are covered by fibulin and fibrillin micro fibrils that play a role on its structural integrity [27] [24] [18].

III. **Fibronectin**

Fibronectin is a highly elastic glycoprotein located within the basement membrane of the ECM. It exists in two different forms depending on their solubility; soluble plasma and less-soluble cellular fibronectin. Its roles are diverse though it is intimately connected to ECM organization and the mediation of cell attachment and migration. It also has the ability to bind to other ECM components such as collagen, fibrin and heparan sulphate proteoglycans [28] [24] [18].

1.2.2 The Plant ECM

Over the last couple of decades, some biologists have adopted the term "extracellular matrix"as a way of assess the dynamic structure of the plant cell wall. The cell wall is mostly comprised of polysaccharides, such as cellulose, xyloglucans and pectins; glycans, lignin and proteins, all organized onto a paracrystalline lattice with ratios that vary between tissues, plant types, cellular differentiation state and environmental factors [29] [21] [30].

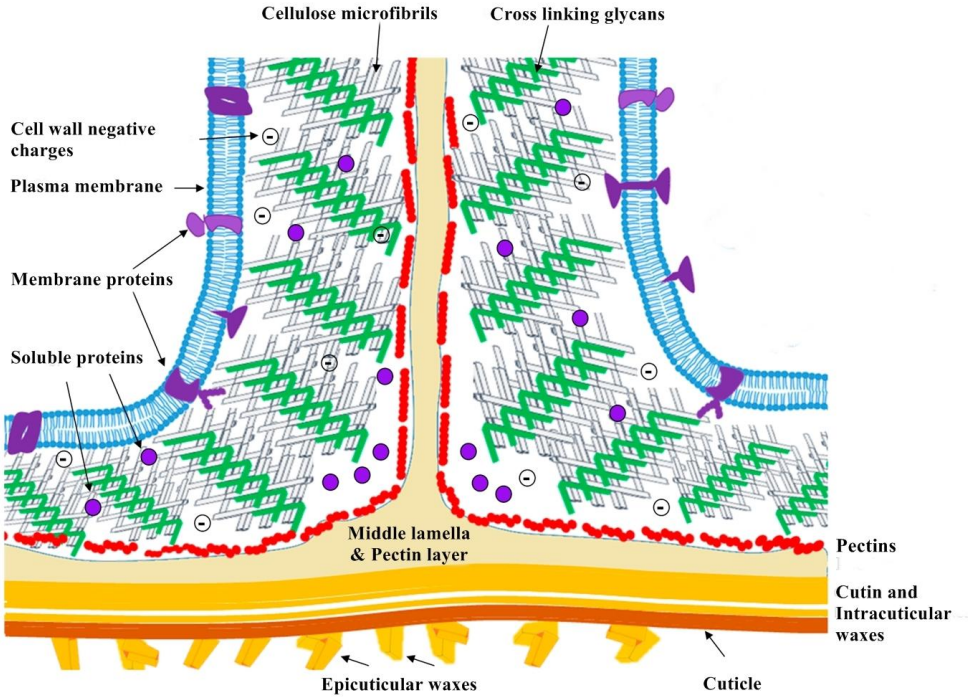

Figure 1.2: Schematical representation of the ECM of an angiosperm. Cellulose microfibrils (grey) intertwine with cross-linking glycans (green) forming an environment with a negative net charge that fronteirs the middle lamella through a pectin layer (red). Image adapted from Guimarães *et al.*[30]

1.2.2.1 Polysaccharides

I. **Cellulose**
Cellulose, $(C_6H_{10}O_5)_n$ is a fibrous water-insoluble polisaccharide that comprises the majority of the cell wall. Structurally, it is comprised of repeating glucose monomers attached end-to-end. It is bonded through its hydrogen, forming micro-fibrils which wind together, forming threads that coil around each other, creating a rope-like structure named macro-fibril. Micro-fibrils are then embedded onto a cross-linked matrix of hemicelluloses, pectins and glycoproteins [21] [31].

II. **Hemicellulose**
Hemicelluloses combine a diverse group of non-crystalline glycans which are bound to the cell wall, with xyloglucans accounting for the most predominant. Structurally, xyloglucans are similar to cellulose, only containing short side chains of xylose, galactose and sometimes a terminal fucose. They are tightly linked through hydrogen bonds with cellulose micro-fibrils, playing an imporant role in cell growth regulation [21] [31].

III. **Pectins**
Pectins are a family noncellulosic polysaccharides, containing galacturonic acid residues. They are highly hydrophilic, allowing to water to enter the cell wall, modulating its stretching ability. Nonetheless, they serve many purposes, playing an important role in ion transport and inducing the activation of defence responses and the accumulation of protease inhibitors [21].

1.2.2.2 Structural Proteins

Holding a predominant spot as the main proteic content, structural proteins hold key functions such as contributing for the control of cell wall assembly, hydration and permeability. Depending on their enrichment in certain amino acids and the presence of repeated sequence motifs, they can be classified into two groups; hydroxyproline-rich proteins and glycine-rich proteins that cross-link with the cell wall polissaccharides [30].

1.2.2.3 Lignin

Lignin is a hydrophobic polymer with differeing compositions depending on the plant source, particularly abundant in the cell wall of woody trees. It is rich in aromatic subunits which fills the spaces between cellulose, hemicellulose and pectin by being covalently bound to hemicellulose, cross-linking with the remaining polysaccharides. This fact turns lignin into a largely important in vascular and support tissues such as xylem tracheids and vessel elements, conferring the cell wall its strength [32].

1.3 Plant Leaf Anatomy

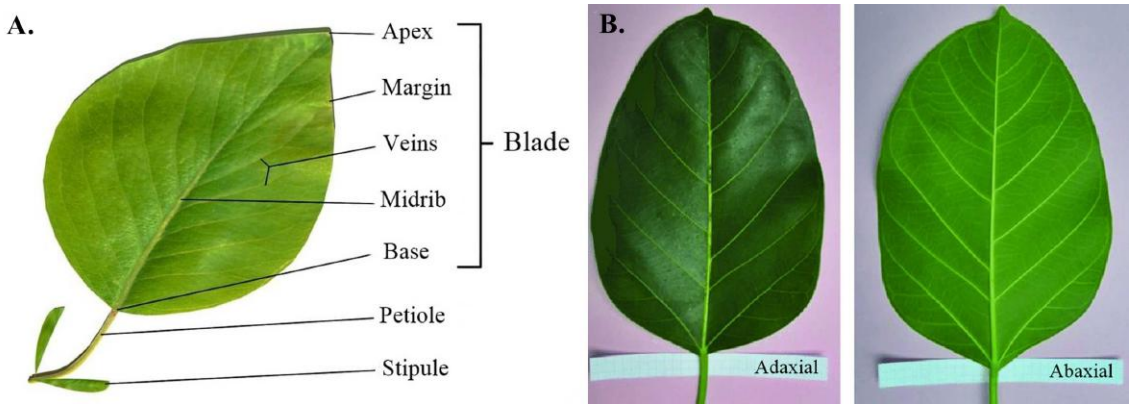

Figure 1.3: Plant leaf anatomy. A. The petiole attaches the leaf blade to the stem. Its dimensions vary between species. **B.** Adaxial vs Abaxial leaf surface. Image adapted from [33]

As to use the plant ECM for vascularization purposes, it is important to understand the anatomy of plant leaves. Although some differences can be found between plants, leaves possess basic features that are universal. Within the blade, commonly known as the leaf itself, nutrient transportation is delivered through the veins, comprised of vascular tissue. Secondary veins connect in a major vein named midrib, in a fashion that mimics the relationship between large animal vessels such as arteries and veins and their branching towards arterioles, venules and capilaries. Connecting the veins to the plant stem is the petiole, a thin stalk that can be absent in some plant species and allows for nutrients to be delivered from the plant stalk to the leaf.

1.3.1 Leaf Tissues

Leaves are highly organized structures, comprised of three different main tissues, the epidermis, the mesophyll and vascular tissue.

1.3.1.1 Epidermis

The epidermis consists of a single layer of tightly packed barrel-shaped cells which covers both surfaces of the leaf blade. It is involved by a continuous waxy layer of cutin named cuticle, which protects the leaf from dehydration due to transpiration. Special cells named guard-cells, regulate plant-environment gas-exchanges. In several species, trichomes can grow out of the epidermis, creating an irregular surface that, in some cases, helps protect the leaf from uninvited herbivores or insects through processes like stinging, or trapping [34].

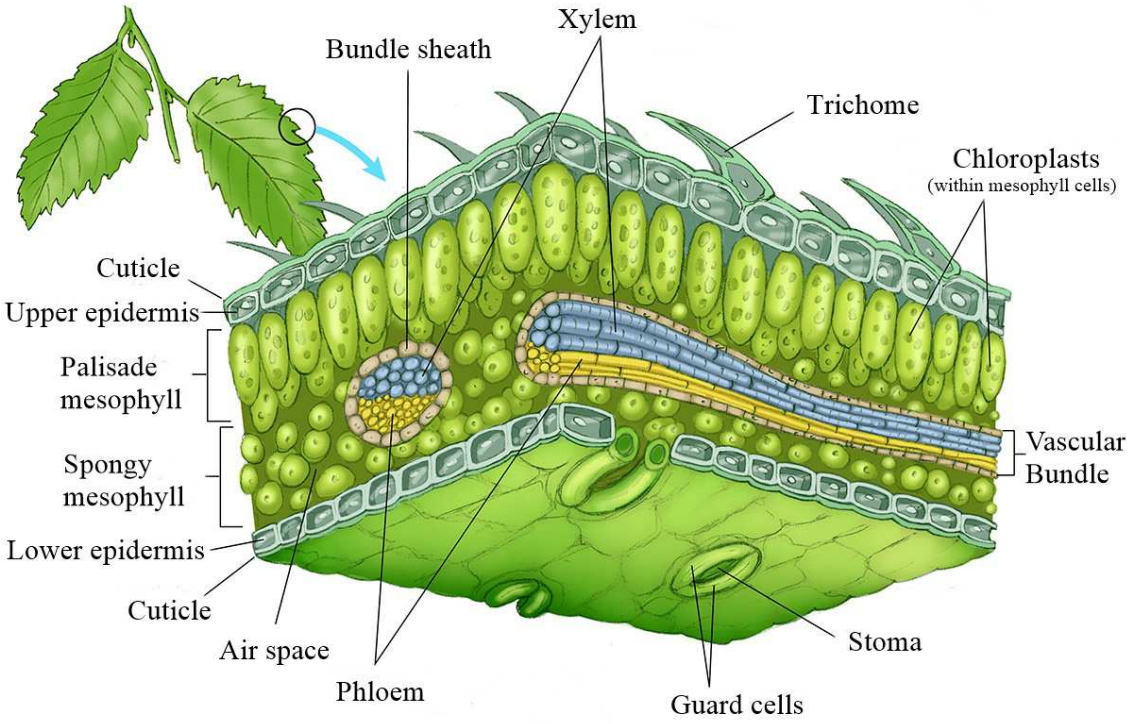

Figure 1.4: General representation of a dicot epidermis. The epidermal tissue includes several differentiated cell types such as epidermal cells (most numerous and least specialized, typically less elongated in dicots), guard cells, subsidiary cells, and epidermal hairs (trichomes). Adapted from Carlson [35].

I. **Cuticle**

The cuticle comprises two main lipidic components; insoluble cutin/cutan and soluble waxes.

Cutin is a polyester polymer of variable size, structurally comprised of C_{16} and C_{18} hydroxy and hydroxy-epoxy fatty acid monomers. **Cutan** is an alternative highly insoluble polymer with an unclear molecular structure. It differs from cutin with its ability to withstand alkaline hydrolysis. Together, they form the cuticle matrix. Depending on the plant species, the matrix can be formed by cutin, cutan or both at different weight percentages.

Cuticle waxes can be epicuticular or intracuticular, depending whether they are deposited on the surface or embedded onto the matrix. Together, they represent the plant's main barrier to water and solute transportation across the cuticle [36].

Currently, the cuticle is regarded as a lipidic layer that only interacts physically with the cell wall in short distances. The cutin matrix is embedded with intracuticular waxes and phenolic compounds throughout the cuticle, whereas polysaccharides populate only the cuticular region that interacts with the cell wall. Additionally, a layer of waxes on the cutin matrix creates the interface between the leaf and the involving atmosphere [37] [34].

II. **Trichomes**

Trichomes consist of a series of different outgrowths or appendages that come in a variety of shapes and sizes and can serve various functions. Mainly, trichomes have been found to have a protective role against insects, mostly due to its chemical secretions. As an example, bean leaves were used in the Balkan countries as a way to entrap bed bugs, being thrown on the floor and later burnt [34] [38].

1.3.1.2 Vascular Tissue

The plant vascular network allows for the transportation of nutrients and water throughout the plant, ending on the leaves. It comprises two main conductive tissues; the xylem, mainly involved in water and ions conduction from the soil, and the phloem which takes care of the transportation of water and organic molecules. This network will be taken advantage of in the present work.

I. **Xylem**

The xylem allows for the transportation of water and some ions under negative pressure. It can classified onto two types; the primary and the secondary xylem, depending on the stage and origin of growth. Additionally, it is comprised of tracheary elements, parenchyma cells and supporting cells, also named fibres. Regarding the tracheary elements, two types exist in the xylem; the tracheids and the vessel elements, comprised of the cell walls of dead cells arranged onto a "pipe-like"structure [39] [40] [34].

II. **Phloem**

Contrary to the xylem, the phloem is a living tissue which has the ability to transport, by an active mechanism, the organic compounds produced during the photosynthetic process. Living cells allow for the osmotic gradient to be maintained and protects the vascular system from leakage by the underlying pressure. It is comprised of sieve elements, parenchyma cells and supportive cells. Between the tube members there are sieve plates which are pores that regulate said transport [41].

1.4 Blood Vessel Anatomy

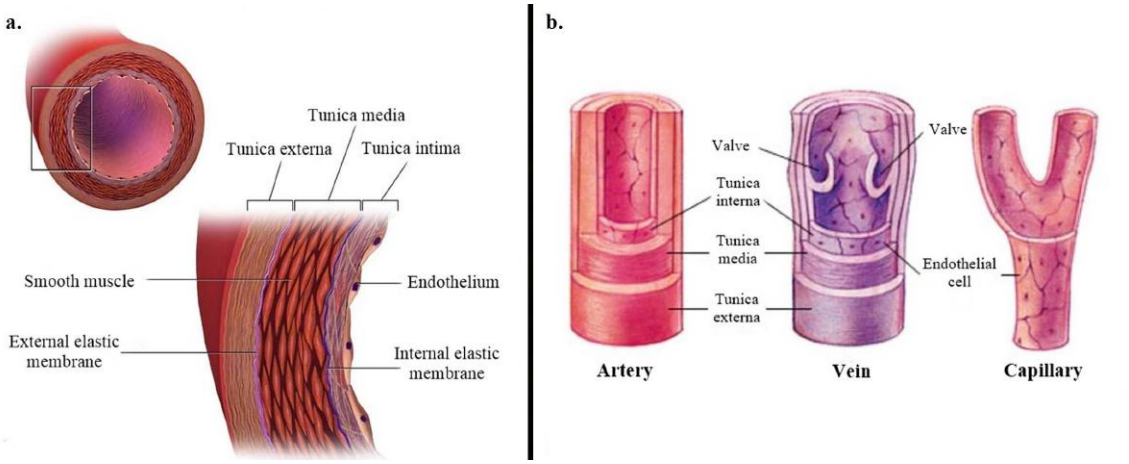

Figure 1.5: Anatomical structure of blood vessels. a. *Schematic representation of an artery wall.* Smooth muscle cells allow for it to withstand high physiological pressure. **b.** *Structural comparison between arteries, veins and capillaries.* In veins, valves help blood return to the heart from places where gravity has a bigger effect such as the saphenouos vein. Contrary to arteries, capillaries are less resistant to pressure since they are made of a single layer of endothelial cells. Adapted from Blausen and staff [42].

Blood vessels are key parts of the peripheral vascular system including all the vessels outside of the heart, which transport blood throughout the body. It is comprised of arteries and arterioles that transport oxygenated blood from the heart, veins and venules that transport low oxygenated blood to the heart, and capillaries which are branched out vessels. Structurally, they differ slightly, with arteries having thicker walls in order to withstand the high pressure pumped from the heart. However, both arteries and veins possess a wall composed of three tissue layers; the *tunica intima* (thinnest layer, comprised of a single layer of endothelium supported by a subendothelial one), the *tunica media* (thickest layer, contains smooth muscle cells, elastic fibers and connective tissue arranged in a circular fashion) and the *tunica adventia* (external layer made of connective tissue). In addition, all vessels possess a hollow space named lumen where the blood flows [43].

1.5 Tissue decellularization

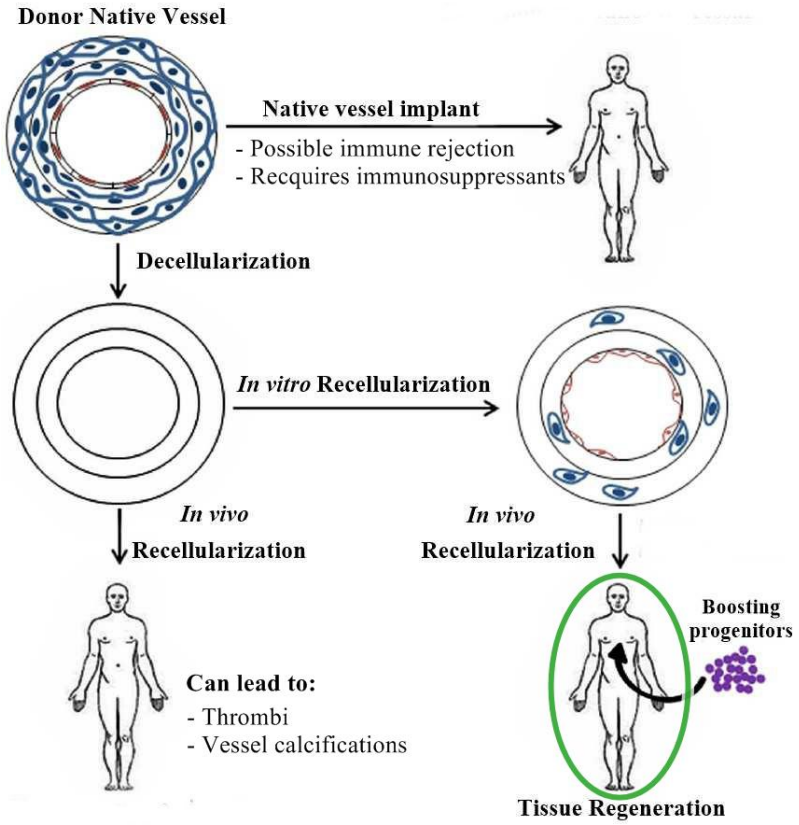

Figure 1.6: Advantages of *in vitro* recellularization when compared to other techniques. Decellularization helps reduce the risk of patient immune rejection since it can be seeded with autologous cells. The usage of an *in vitro* recellularization technique prior to implantation has also been known to reduce the risk of complications such as thrombus formation and calcifications with the added bonus of inducing the recruitment of progenitor cells *in vivo*. Image adapted from Moroni *et al.* [44]

Tissue decellularization aims for the isolation of the components of the ECM while keeping their structural integrity, through the removal of the tissue's inherent cells. The efficacy of the decellularization process can be assessed through different techniques such as histological staining with nuclei markers like DAPI, hematoxylin and eosin and the quantitative measurement of DNA [45]. These methods base themselves on the assumption that the removal of intracellular, membranous molecules and DNA are equally efficient. Also, since intracellular and membrane components possess surface antigens, the removal of these components allows for the reduction of a possible immune rejection due to xenotransplantation.

In order to decellularize an organ, in this case, plant leaf, several techniques can be used which fall onto the categories of physical, chemical, enzymatic and combined.

1.5.1 Chemical Decellularization Agents

1.5.1.1 Acids and Bases

Solutions with an extreme pH value can improve the efficacy of cellular removal through the catalysis of biomolecular hydrolytic degradation. **Acids** such as per-acetic have been used in order to remove residual nucleic acids where they have been found to solubilize cytoplasmatic components with no relevant structural disturbance on the ECM. This happens because even though collagen is partially removed, the sulfated GAGs are generally not affected [46]. However, since a balance between the removal of structural protein such as collagen and the removal of other components needs to occur, it is important to optimize both the concentration and exposure time to such agents.

Bases are commonly used for sample processing such as the removal of hair from skin samples [47]. Commonly used bases such as ammonium hydroxide, sodium sulfide and sodium hydroxide work by denaturing DNA. However, since they remove important growth factors and highly decrease the mechanical properties of the ECM through the disruption of collagen crosslinks, they are a more disruptive method than acids [48].

1.5.1.2 Detergents

Detergents are effective decellularization agents that work by solubilizing cell membranes and dissociating DNA from proteins. However, their common use in protein extraction procedures infers that they will also be disrupted from the ECM, thus having a negative effect on its structural integrity. This con can be managed by lowering both the concentration and exposure time as well as combining detergents with different agents.

I. **Ionic Detergents**

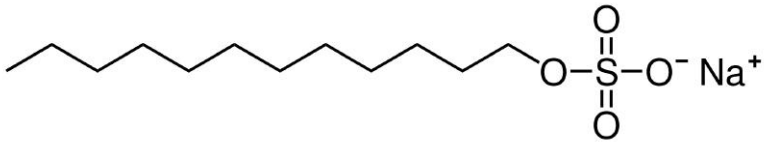

Figure 1.7: Chemical structure of SDS. The combination of its hydrocarbon tail with a terminal polar group gives this detergent its amphiphilic properties.

Ionic detergents such as SDS, Triton X-200 and sodium deoxycholate are highly efficient detergents that solubilize cytoplasmatic membranes, lipds and DNA [49]. The utilization of SDS comes from the fact that it is frequently used in order to aid the denaturation of proteins in SDS-PAGE electrophoresis, by interfering with both the hydrophobic interaction and the hydrogen bonds. In fact, SDS has been shown to

achieve an adequate cell removal in animal tissue while retaining proteins such as glycoproteins and collagens as well as retaining fiber orientation, making a huge difference regarding decellularization efficiency when compared with other agents. However, it is associated with a high GAG and growth factor removal and some structural disruption.

Triton X-200 has a greater structural disruption when compared to SDS, though it can only effectively work on thinner tissues, being more commonly used as a final agent [45].

II. **Non-Ionic Detergents**

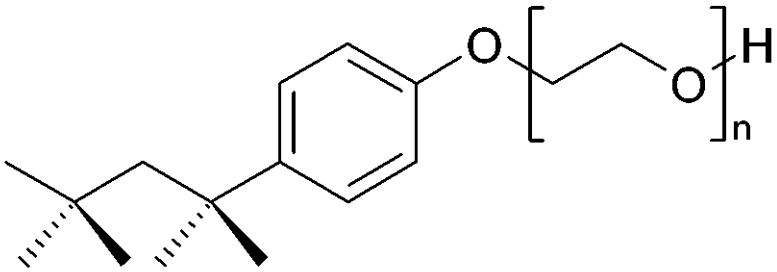

Figure 1.8: Chemical structure of Triton X-100. It is comprised of a hydrophilic polyethylene oxide chain and an aromatic hydrocarbon lipophilic group.

Non-ionic detergents are mainly used when it is pivotal to maintain as much of the structural protein integrity and enzyme activity as possible. They work by disrupting DNA-protein, lipid-lipid and lipid protein and, to a lesser extent, protein-protein interactions. Nonetheless, this lowers the efficiency of the process. Practical uses include tissue de-lipidation and the removal of cellular residues as a last step for tissues such as valve conduits [50].

In this category of detergents, Triton X-100 stands out in preference for decellularization procedures, due to its low structural disruption and high GAG removal [51].

III. **Zwitterionic Detergents**

Fairly less used, zwitterionic detergents own their name to the neutral charge in their hydrophilic groups, allowing them to protect the native state of proteins. Nonetheless, this characteristic does not come without cost, as their efficiency is much lower, thus only being used in thinner tissues such as the lung [52] or combined with ionic detergents [53]. Amongst this category lie detergents such as CHAPS, SB-10 and SB-16 [54], each with their own set of pros and cons. In fact, while SB-10 and SB-16 have been shown to better preserve the structure of ECM and remove cells when compared to ionic detergents [53], CHAPS improves collagen, GAGs and elastin retention [55] [56].

1.5.1.3 Alcohols

Alcohols are mainly used as dehydrating and lysing agents, since, when permeabilized, their hydroxyl groups can diffuse into the cell, replacing the intracellular water thus lysis the cell by a process of dehydration [57]. Oxidized phospholipids are proinflammatory and proatherogenic agents which can contribute to prosthesis calcification in valves and conduits [58]. Alcohols help fix this issues since they are known lipid dissolvers. However, alcohols such as ethanol and methanol can precipitate proteins and damage the ECM structure by altering the collagen structure through crosslinking [59].

1.5.1.4 Chelators

EDTA and EGTA bind divalent metal cations, mainly Ca^{2+} and Mg^{2+}, helping with the cellular dissociation from ECM proteins. As a result, they are particularly used in combination with trypsin and detergents in order to ensure a maximum cellular removal [48] [57] [60].

1.5.2 Enzymatic Methods

Enzymes are highly specific agents for the removal of cell residues and unwanted ECM components when accompanied by other methods. Nonetheless, special care must be held in order to remove enzyme residues which can hinder recellularization or induce an adverse immune response.

Examples used in decellularization protocols include endonucleases (eg. DNase, RNase), proteases (eg. trypsin, collagenase) and esterases (eg. phospholipase A2) which work in different ways. DNase and RNase catalyse the hydrolysis of the interior bonds of the nucleotide chains, while exonucleases catalyse the "exterior"terminal bonds, leading to the degradation of DNA or RNA. As such, they are mainly used as an additive to detergents in order to help remove residual DNA [61]. Since endonucleases cleave nucleotides mid-sequence, they are thought to be more effective than exonucleases at fragmenting DNA. Also, following this logic, non-site specific endonucleases would be more effective compared to site-specific ones [45].

Trypsin (EC 3.4.21.4) is perhaps, the most used enzyme in decellularization protocols. It is a serine protease which cleaves proteins on the carboxyl side of arginine or lysine unless the following residue is proline, detaching cell adherent proteins from the surface [62]. While trypsin has been shown to be effective as an adjuvant, long exposure times have been reported to damage the collagen matrix [47]. When compared to detergents, trypsin has a bigger impact on the structural integrity of elastin and collagen and a slower rate of cellular removal. However, it allows for a better preservation of GAGs [63] [64].

Other enzymes used include collagenase, dispase, thermolysin and lipase, which vary in structural disruption properties.

1.5.3 Physical Agents

1.5.3.1 Freeze–thaw cycles

Multiple freeze-thaw cycles have been shown to effectively lyse cells within tissues. However, its intracellular and membranous content are not eliminated unless they are processed afterwards [65] [66]. Freeze-thaw also produces minor disruptions on the ECM structure, with no significant alterations on its mechanical properties [67].

1.5.3.2 Agitation and Immersion

Perhaps the most commonly used techniques for tissue decellularization, protocols regarding the immersion of tissue in a solution with mechanical agitation have been published for different tissues such as the bladder [60], trachea [68], cartilage [69], dermis [48], and heart valves [70]. This technique allows for endless combinations of conditions which can be adapted to different tissues. For example, thin tissues such as the urinary bladder can be decellularized over a short period of time of a couple of hours of exposure to peracetic acid, when used a relatively aggressive agitation [71]. On the other hand, denser tissues such as the trachea or dermis require a longer exposure time and a combination of different solutions of alcohols, enzymes and/or detergents.

1.5.3.3 Perfusion

The process of perfusion decellularization consists on the usage of pressure gradients though the vascular system of the tissue or organ in order to improve the efficiency of the chemical decellularizing agents and facilitate the elimination of cellular debris, making it particularly useful for hollow tissues such as blood vessels.

Though used in tissues, the work of Wainwright *et al* has demonstrated the viability of perfusion based methods in the decellularization of porcine heart. For this, a retrograde coronary perfusion tactic was used, requiring the usage of trypsin and detergents, in cycles as well as a progressive increase in pressure [72].

In the work of Montoya *et al* [73], umbilical veins decellularized by luminal perfusion at a flow rate of 50 mL/min were compared to a simple rotary agitation of 100 rpm, showcasing a complete cellular removal and a diminuished cellular component retention with minimal damage to the ECM structure . Also, a combination of both perfusion and immersion can be

used in order to ensure a maximum removal of cellular content, as used by Wagner *et al* [74] in lungs.

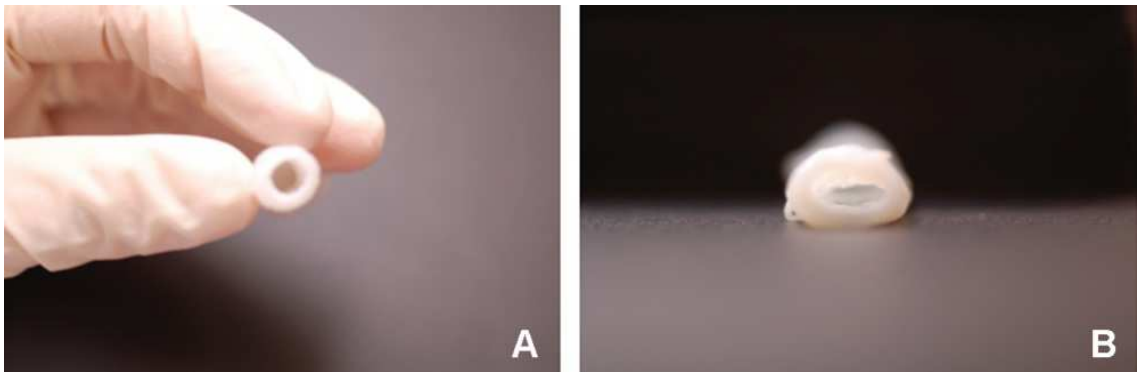

Figure 1.9: **Decellularized human umbilical vein. a.** Tissue decellularized through luminal perfusion. **b.** Tissue decellularized through agitation. Contrary to perfusion, some loss of rigidity is noticeable. Work and image published by Montoya *et al.* [73].

1.5.4 State of the art

1.5.4.1 Decellularization of cardiovascular components

Arteries have long been decellularized successfully. In 2003, Uchimura *et al.* have effectively decellularized porcine carotid artery and rat aorta using a 1g/mL PEG solution and DNase and re-seeded with rat vascular endothelial cells with a seemingly good conservation of mechanical properties [75].

Also in 2003, Dahl *et al.*'s work on porcine arteries has tested three decellularization methods. The one consisting of a two-step process presented the best results in terms of cellular content and structural properties, with a maximum stress pressure lowering from 6.6 ± 1.7 MPa for native arteries to 2.1 ± 0.7 MPa for the decellularized version. Step one consisted of a solution blend of 8mM CHAPS, 1M NaCl and 25 mM EDTA in constant agitation for a period of 11h. Step two swapped the zwitterionic detergent with an anionic one, SDS at a 1.8mM concentration for the same period of time. Both steps were performed in agitation in a 10% CO_2 environment at a temperature of 37°C. The scaffold was later rinsed with PBS and seeded with PKH-26-labeled porcine vascular SMCs, showcasing no obvious cytotoxicity [76]. The protocol has since been repeated by several groups such as Quint *et al.* [77] in 2011 who used a porcine carotid artery which was then implanted as an end-to-end graft and recellularized *in vivo*, showcasing good patency and collagen retention.

Porcine heart valves have also been successfully decellularized in 2008 by Liao *et al.* [78] by using 0.1% SDS followed by 0.5% Trypsin and 1% Triton X-100 and in 2012 by Dijkman *et al.* [79], using a solution blend of 0.25% sodium deoxycholate and 0.02% EDTA, both followed

by nuclease digestion. Both methods showcased little alteration on collagen content and mechanical properties with a preserved function.

Likewise, veins have suffered decellularization through several protocols, though not as popular as arteries. An example is a protocol used by Schaner *et al.* [80] in 2004 where human greater saphenous veins were decellularized through immersion with different SDS concentrations of 0.01, 0.025, 0.05 and 0.075% , the later having the best results. The resulting scaffolds possessed a 94% decellularization yield with similar *in vitro* burst strenght and collagen content to native veins, functioning properly with no dilation or rupture after 2 weeks of perfusion.

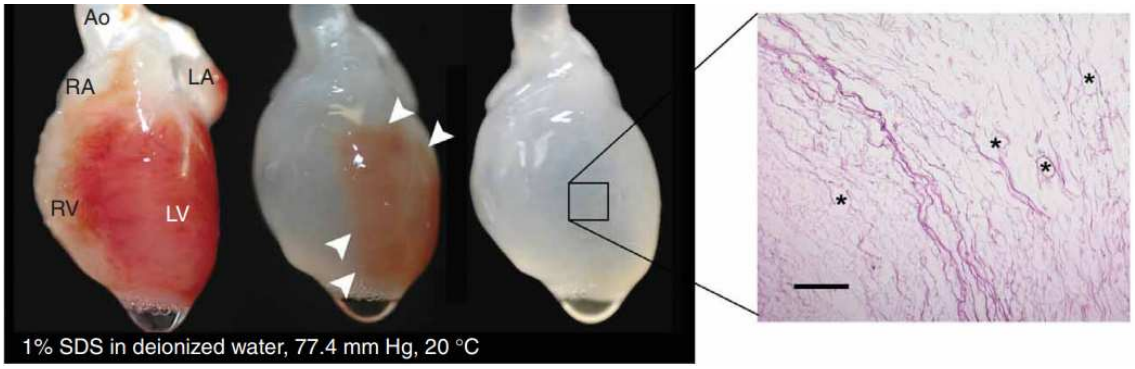

Figure 1.10: Decellularization process on rat heart. After 12h the heart becomes more translucent as the cellular material is removed through the right ventricle. HE staining showcases the conservation of large vasculature conduits (black asterisks). Ao, aorta; LA, left atrium; LV, left ventricle; RA, right atrium; RV, right ventricle. From Ott *et al.* [81]

Perfusion is a common technique especially in regard whole-organ decellularization. A great example was published in 2008 by Ott *et al.* [81] where rat hearts were decellularized by coronary perfusion of 1% SDS for 12h followed 1% Triton-X-100 for 30 minutes and an antibiotic solution for 124h. The scaffold was later reseeded with rat aortic endothelial cells with either intramural injection or perfusion into the vascular conduits, resulting in a biocompatible matrix with a perfusable vascular tree capable of being implanted.

1.5.4.2 Plant decellularization and blood vessels

Being an easily available and highly vascularized system, with a functional architecture similar to animal tissues, plant leaves are a promising ethically sustainable and environmentally friendly material regarding their possible use as a pre-vascularized scaffold for tissue engineering applications. Moreover, their high hidrophilicity allow for cellular expansion through long periods of time in a way that conforms to the microstructure of the plant's framework.

The idea of plant derived decellularized scaffolds is not new, starting to take a stand in the 2010's. The works of Modulevsky *et al.* have been especially featured, with the analysis of

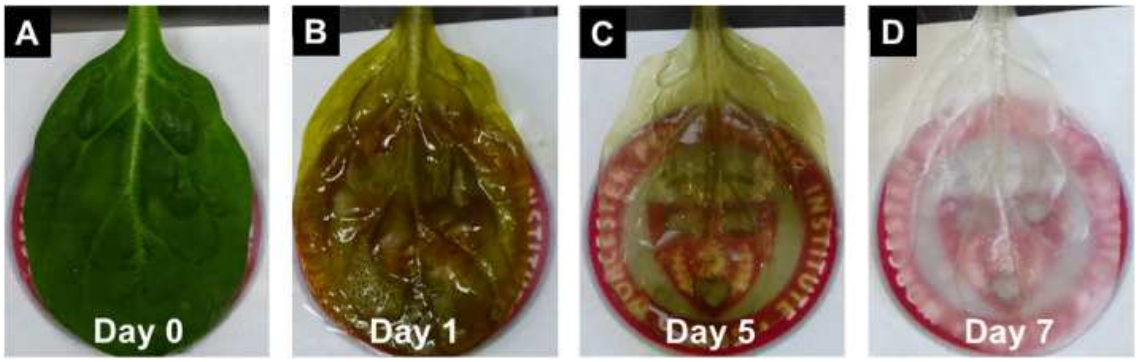

Figure 1.11: Decellularization timelapse in spinach leaf. After 5 days the leaf reaches a translucent green hue which is removed when a 10% sodium chlorite solution is added (image **d.**). Work and image published by Gershlaka *et al.* [82].

the properties of native hypanthium (floral tissue) of apples. Firsty, in 2014, the scaffold was successfully seeded with NIH3T3 fibroblasts, mouse C2C12 muscle myoblasts and human HeLa epithelial cells, remaining viable for up to 12 weeks [83]. Its ability to work as an implantable cellulose scaffold was later confirmed in 2018. The developed scaffold showcased an immune response that gradually disappeared as of the 8th week post implantation, with an active migration of fibroblasts and blood vessel formation [84].

However, the usage of plant decellularization techniques as a way to build vascularization was first shown by Gershlaka *et al.* In their article published in 2017, spinach leaves were treated with hexanes and later decellularized using a 10% SDS solution perfused through cannulas for 5 days after which a solution mix of 0.1% Triton-X-100 and 10% sodium chlorite bleach was perfused for an aditional 48h, both at a constant pressure of 152 mmHg. Post decellularization, the scaffolds retained patency and were capable of transporting microparticles. Later, they were reseeded with human mesenchymal stem cells and human pluripotent stem cell derived cardiomyocytes which adhered to the outer surfaces of the plant leaf. Particularly cardiomyocytes showcased their contractile and calcium handling properties over the course of 21 days [82].

Though not currently optimal, this brand new approach to the problem of vascularization has thus shown an immense array of possibilities for its usage since plant material is easy to get in a high quantity and its decellularization process is relatively cheap. Decellularized leaves can also be further enriched for optimal mechanical properties and enhanced animal cell adhesion.

1.6 Electrospinning

Electrospinning is a common technique where a highly viscous synthetic or natural polymeric solution is made into solid fibres, having a diameter between a few micrometers and a few nanometers, with the help of an electric field. The solution emerges at the end of a blunt needle or capillary tube to which a high voltage (usually between 10 and 30 kV) is applied. The interplay between surface tension and coulombic repulsion between like charges leads to the formation of a conical shape commonly named Taylor cone from which a solution jet emerges. The solution whips and elongates as it travels towards the collector due to the electrostatic repulsions between the surface charges, the Couloumbic force exerted by the external electrical field and solvent evaporation. [85] [86].

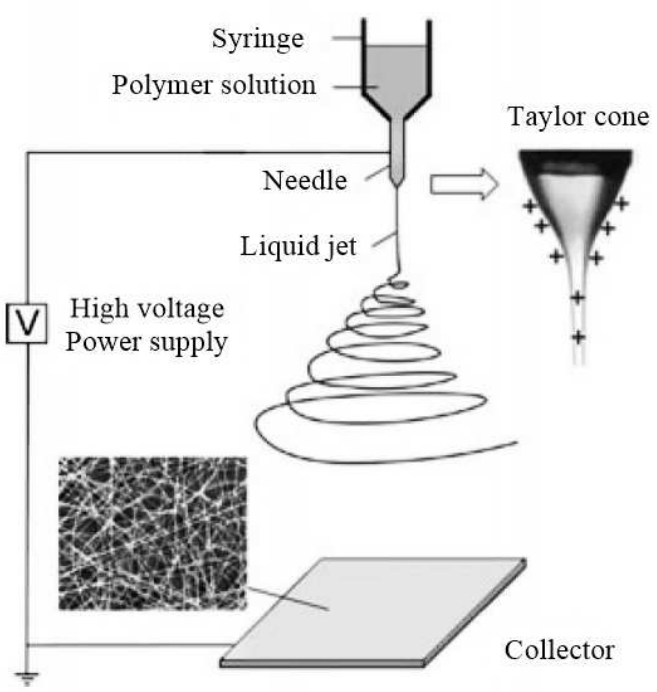

Figure 1.12: Basic electrospinning aparatus. The electrospinning technique allows for the production of non-woven nanofibers using an electric force to draw charged polymeric threads towards a moving or static collector. SEM image represents non-oriented fibres of PVP. Adapted from Li *et al.* [86].

These fibres can be aligned with the rotation of a cylindrical collector at a high speed since when the linear speed of the rotating cylinder matches that of the evaporated depositions, the fibres align in a circumferential manner. Thus, higher speeds will result at a tighter alignment whereas lower speeds will decrease the alignment.

In order to achieve this, a setup is placed consisting of a high voltage power supply, a syringe pump, a syringe, a spinneret (blunt tip metallic needle on which the voltage is applied)

and a grounded metallic collector. Also, optimization can be achieved through the manipulation of several different parameters. These include solution properties such as conductivity, viscosity and surface tension; environmental parameters such as air humidity, velocity and the temperature of the solution and process parameters such as the electric potential, flow rate, needle-collector distance, collector composition and its geometry [87].

The flexibility of the electrospinining technique allows it to be used with several different polymers, as long as they can be charged and have the necessary viscosity to be elongated towards the collector. In the present work two polymers will be used, PCL and PEO.

1.6.1 Polycaprolactone

PCL is a hydrophobic, semi-crystalline polymer, belonging to the poly(α-hydroxy) ester family that can be prepared through two different paths; the ring-opening polymerization of the cyclic monomer ϵ-caprolactone by a catalyst such as stannous octoate and the polycondensation of 6-hydroxyhexanoic acid [88]. Due to its biocompatibility and easy processing (low melting point and solubility in a wide range of organic solvents and miscibility with different polymers), PCL has turned into one of the most commonly used polymers for biomedical purposes [89]. In fact, PCL can be mixed with other polymers as a way to improve its characteristics, such as adhesion and stress crack resistance [90] and is known to be soluble in chloroform, carbon tetrachloride, benzene, toluene and dichloromethane at room temperature with a low solubility in acetone and acetonitrile and total insolubility in alcohol [91].

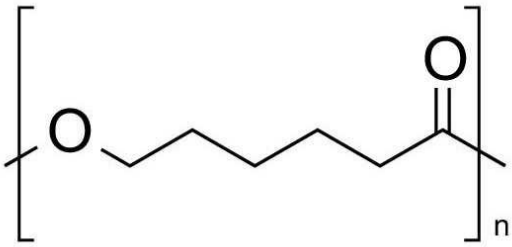

Figure 1.13: Chemical structure of PCL. Resulting from the ring opening polymerization of ϵ-caprolactone, PCL is a biodegradable polyether widely used in tissue engineering due to its mechanical properties.

Regarding its biodegradability, PCL can be degraded by micro-organisms such as bacteria and fungi in a span of months to years depending on the conditions, its molecular weight and degree of crystallinity. However, though some hydrolysis can occur [92], the polymer's degradation rate when implanted is very low since there is a lack of suitable enzymes *in vivo*. The hydrolytic degradation of this type of polymers occurs in two main steps. Firstly, water diffuses into its amorphous regions resulting in the cleavage of ester bonds and mass

loss. Once most amorphous regions are degraded, the actual hydrolytic degradation of the crystalline begins [93].

1.6.1.1 State of the art: polycaprolactone in blood vessel engineering

Throughout the last 15 years, several articles have been published regarding the usage of PCL in blood vessel engineering.

In 2004, Jeong *et al.* [94] have fabricated tubular, elastic and biodegradable scaffolds from poly(l-lactide-co-ϵ-caprolactone)(PLCL) at a 50:50 ratio which were seeded with smooth muscle cells and implanted onto mice, displaying an "excellent tissue compatibility". The scaffolds have also displayed a high elasticity, being able to withstand an extension of up to 210% with a 97

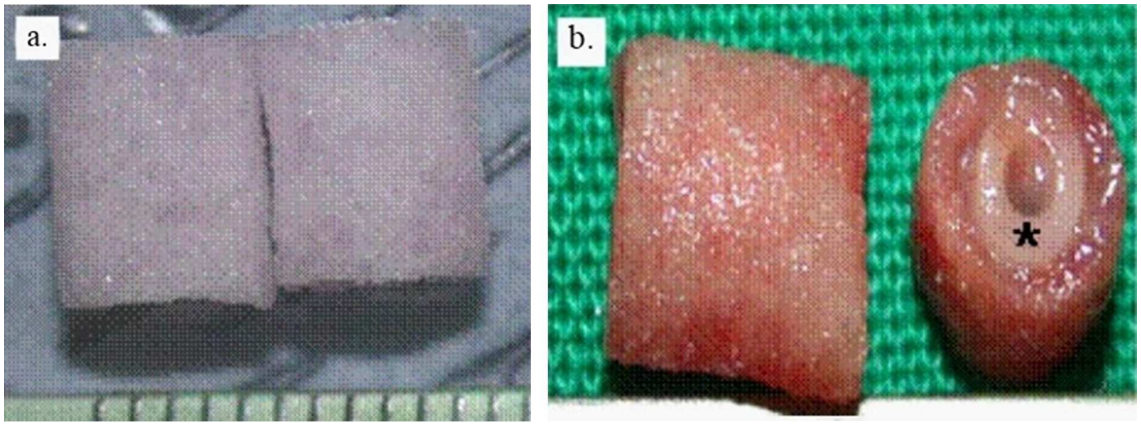

Figure 1.14: PLCL scaffold implanted into athymic mice. a. Scaffold before implantation. **b.** Explanted scaffold (black asterisk) after 8 weeks. Adapted from Jeong *et al.* [94]. Scale not provided.

Reaching 2005, multi-layered tubular scaffolds have been produced, such as the one made by Vaz *et al.* [95] containing an inner layer of PCL and an outer layer of a stiff polymer named poly-lactic acid (PLA), fabricated layer by layer through electrospinning. The resulting structure contained micro and nanofibers interconnected by pores of an average 10 μm, mimicking the natural anatomy of the blood vessel. Their mechanical properties were found to be acceptable, with a composite Young's modulus much higher than that of simple PCL.

In 2008, Nottelet *et al.* [96] produced electrospun PCL scaffolds averaging between 500-2500 nm diameter, creating 2 and 4 mm vessels. They showcased promising mechanical properties, with tensile stress values up to 7.4 MPa, much higher than the ones for native human blood vessels (1.4 MPa).

In 2009, Tillman *et al.* [97] analysed the stability of electrospun PCL/collagen scaffolds in a rabbit aortoiliac bypass model. After implantation *in vivo*, their results indicate an ability to support the adherence and growth of vascular cells and retain a high degree of structural

integrity and patency when exposed to physiological conditions. Also, the matrices were found to resist the adherence of platelets when exposed to blood.

However, in 2012, Valence *et al.*'s long-term *in vivo* study using electrospun PCL tubes in rat aorta for a period 18 months, has raised questions regarding the viability of PCL as an implantable scaffold. Though results seemed promising by the 6 month mark, with a rapid colonization of fibroblasts and macrophages and wide neovascularization, after 6 months, tissue regeneration began to regress with an increase of calcification, a reduced vascularization and both macrophage and fibroblast count and a cell regression in the hyperplasia of the *tunica intima* [98], a result that contradicts the previously published by Pektok *et al.* in 2008 [99].

Since then, PCL has been mainly used in conjunction with other materials such as collagen [100], gelatin [101] and alginate [102] [103].

1.6.2 Polyethylene Oxide

PEO $(CH_2CH_2O)_n$ is a polyether compound best known for its hydrophilic properties to which terminal hydroxyl groups contribute. However, its ether oxygens along the backbone must be considered in order to understand polymer/water interactions [104]. It can also be named PEG, which is applied to a lower molar mass, suggesting a glycolic chemical nature due to the significant contributions from the terminal hydroxyl groups [105].

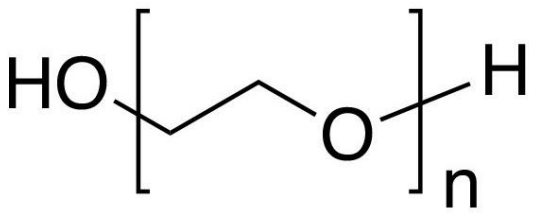

Figure 1.15: Chemical structure of PEO. Also known as PEG depending on its molecular weight, PEO is a hydrophilic polyether polymer with a high solubility in water which is largely used for various industries and applicabilities.

This polymer is soluble in both water and nonpolar solvents, being used in several different applications such as industrial, ion conduction in electrolyte batteries and biological, aiding the crystallization of macromolecules and coating metal surfaces in biomedical devices [104], since it has the ability to alter the interactions of cells and proteins with water and each other [106]. It can also be used as a surfactant since they are more biodegradable than the alkylphenol-based counterparts [104]. Its degradation in aqueous and organic solutions is accelerated by UV light, certain oxidizing agents, heavy metal ions and strong acids and occurs primarily through a process of autoxidation since hydroperoxides lead to chain cleavage [107].

1.7 Work plan and Objectives

The work presented concerns the development of a vascular network by taking advantage of the already existing transport complex characteristic of plant leaves. In order to achieve it, a decellularization technique will be used, a process that will be optimized throughout the presented work. Plant decellularization is a cheap and practical way of using the leaf's vasculature system without an immune response since the nuclear content is removed and both materials and reagents are easily available in large quantities.

Several approaches have been used in the past for the resolving of the problem of tissue vascularization. Thus, we have found important to compare this bio-approach to already known materials. Because of its well-known and proved behaviour, we have decided to test PCL as the main synthetic polymer. Its performance will be upgraded with the conjunction with PEO, due to its easiness to dissolve in water and low cytotoxicity, as to produce pores that can serve as aids for cellular migration.

The work at hand will aim to reach several objectives. Firstly, "Papo de Rola"common bean *Phaseolus Vulgaris* L. (CB), New Zealand spinach *Tetragonia tetragonioides* (Pallas) Kuntze (NZ), Winter Giant (WGS) and Viroflay (VS) spinach *Spinacea oleracea* L., *Rumex crispus* (RC) and common sowthistle (CST)*Sonchus oleraceus* L. will be grown in different conditions and selected considering their growth characteristics and decellularization behaviour. The decellularization process will then be optimized for the different leaf types available and its success assessed in terms of DNA quantification, mechanical properties and structural integrity. The fabrication of synthetic PCL/PEO scaffolds will also be optimized. All scaffolds will be seeded with mammalian cells, specifically 3T3 fibroblasts, Vero and endothelial cells (EC). Lastly, the adhesion, proliferation and spatial distribution will be analysed for the different scaffolds as to pinpoint the best option.

CHAPTER 2

MATERIALS AND METHODS

2.1 Plant Leaf Decellularization

2.1.1 Plant germination and growth

2.1.1.1 Plant germination

New Zealand spinach (*Tetragonia tetragonioides* (Pallas) Kuntze), Winter giant (*Spinacia oleracea* L.) and common "papo de rola"bean (*Phaseolus vulgaris* L.) seeds were both incubated and not incubated at 4°C for 7 days pior to germination in order to optimize a decrease in latency periods. Afterwards, the seeds were placed onto a Petri dish coated with humid paper along with the ones of common sowhistle (*Sonchus oleraceus* L.), and curly dock *Rumex crispus* L. and left to germinate.

2.1.1.2 Plant growth

After germination the above mentioned plants were transferred onto vases with a potsize 14 x 14.6 cm with a mixture of 1:1:1 soil, peat and sand and divided into 3 growth conditions; Plant Chambers, Lumigrow and Temperature-controlled conditions.

Plant Chambers: A FitoClima (AraLab Fitoclima 700 EDTU) plant chamber was set with a 12h/12h photoperiod (night/day) and a temperature amplitude of 17-22°C at 55-60% relative humidity.

Lumigrow: A room was illuminated with a Lumigrow Pro 325 ™ light set with a spectral output of 20% blue light (400-500nm), 5% green light (501-600nm) and 75% red light (601-700

nm) and set with a 12h/12h photoperiod (night/day) and a temperature amplitude of 17-22°C. The relative humidity was controlled at an amplitude of 50-60%.

Temperature-controlled conditions: Some of the remaining seedlings were placed onto a temperature controlled room set between 24-28°C.

All plants were watered with 50 mL of nutritive solution twice a month and regular water twice a week. Their growth was monitored in terms of leaf number and height and leaf dimensions measured 3 times a week.

2.1.1.3 Nutritive solutions

All solutions are adaptations from the ones published by D.I Arnon and D.R Hoagland [108] [109].

1M Macro Solution: 500 mL of solution were prepared with 100 mM KNO_3 (Merk), 30 mM $Ca(NO_3)_2.4H_2O$ (Sigma-Aldrich), 20 mM anhydrous $MgSO_4$ (Fluka) and 20 mM NaH_2PO_4 (Fluka).

A4 100x Solution: 25 mL were prepared with 9 mM H_3BO_3 (Merk), 2 mM $MnCl_2.4H_2O$ (Riedel de Haën), 0.4 mM $ZnSO_4.7H_2O$ (Merk) and 10 mM Fe(III)-EDTA (Sigma-Aldrich).

B6 10 000x Solution: 10 mL were prepared with 3 mM of $CoSO_4.7H_2O$ (Merk), 0.7 mM $(NH_4)6Mo_7O_{24}.4H_2O$ (Riedel de Haën), 0.5 mM $K_2Cr_2O_7$ (Merk), 2 mM NH_4VO_3 (Merk), 5 mM $CuSO_4.5H_2O$ (Merk) and 2 mM $NiSO_4.7H_2O$ (Fluka).

The final nutritive solution was prepared with a ratio of 100 mL Macro + 1 mL A4 + 100 μL B6.

2.1.2 Plant leaf conservation and transportation

2.1.2.1 Conservation assays

Five solutions were tested in terms of conservation potential for native leaves incubated at 4°C.

Adapted Euro-Collins: The prepared solution was adapted from the protocol published by Yamazaki *et al.* [110]. A 4x stock solution was prepared with 960 mM of D-glucose (Ducheta), 3 mM $Mg.SO_4.6H_2O$ (Fluka), 40 mM $KHCO_3$ (Merk), 116 mM K_2HPO_4 (Merk), 117 mM KH_2PO_4 (Merk), 168 mM $C_2H_3KO_2$ (Merk), 40 mM NaCl (Panreac) and 20 mM KCl (Sigma-Aldrich). The pH was set to 7.4 by using HCl 1M and the solution sterilized .

PEG 10% + Glucose: A 250 mL solution was prepared by using 2.5g of PEG 4000 (Fluka) and 10.8g D-Glucose (Ducheta) for a final glucose concentration of 240 mM and later sterilized by autoclave.

PEG 15% + Glucose, **PEG 20% + Glucose** and **PEG 15%** were prepared in a similar fashion.

Bean leaves were divided in sets of 4 (2 fully developed and 2 smaller, younger leaves) and placed in bags, each with 50 mL of the prepared solutions and left in the dark at 4°C. The conservation state of the leaves was visually monitored for 11 days.

2.1.2.2 Pigment Quantification

Sample weigh-in: The previously tested leaves, along with regular ones were cut into sections (while avoiding nerves), excess water removed with a paper towel and weighed.

Determination of water content: The weighed samples were divided onto two groups, one of which was incubated at 60°C. After 2 weeks, the samples were weighed again.

Pigment quantification protocol: Each sample was macerated on an iced mortar and placed onto an eppendorf tube where they were once more macerated with cold 90% acetone (Sigma-Aldrich) at a ratio of 4.5 mL per gram of fresh material. 1 mL of the supernatant was transferred onto another tube and centrifuged (Eppendorf Centrifuge 5415 R) for 10 min at 12 000 × *g* and 4°C. Once again, the supernatant was removed and placed onto another tube of which the absorvance was measured at 663, 645 and 470 nm in a Shimadzu UV-1603 UV-Vis spectrometer.

The formulas used were adapted Ramalho *et al.* [111] and Lichtenthaler [112] and corrected to μg.mg^{-1}.cm^{-2}.

$$Chla = 12.25Abs_{663} - 2.79Abs_{645} \tag{2.1}$$

$$Chlb = 21.50Abs_{645} - 5.10Abs_{663} \tag{2.2}$$

$$Chl(a+b) = 7.15Abs_{663} + 18.71Abs_{645} \tag{2.3}$$

$$Car(x+c) = \frac{1000Abs_{470} - 1.82Chla - 85.02Chlb}{99} \tag{2.4}$$

2.1.2.3 Plant transportation

After being grown, the plants were harvested for their leaves which were transported in bags containing a 15% PEG 4000 solution at a constant temperature of 4°C.

2.1.3 Plant leaf decellularization

All plant leaves tested were treated before the decellularization process as to remove cuticular waxes. In order to achieve it, a p.a solution of chloroform or acetone was used in repetition cycles of 10 or 15s and its effects on the leave's structural integrity assessed.

In all decellularization protocols, the samples were immersed in destilled water for a period of 7-15 days and the water was changed every other day.

2.1.3.1 Immersion protocols

Leaves were placed onto a glass crystalizer with 100 mL of decellularization solution and agitated at a rate of 100 rpm until transparency.

Conditions tested:

Table 2.1: **Immersion decellularization conditions for SDS and Triton X-100.** All samples were immersed in a SDS + Triton X-100 solution with varying concentrations. Total time displays the amount of days passed until the end of the assay, let it be for reaching full transparency or problems such as microbial contamination.

Plant	SDS (%)	Triton X-100 (%)	Total time (days)	Condition
VS & CB	1	5	34	**PD1**
	5	1	72	**PD2**
	1	10	72	**PD3**
VS	3	3	70-71	**PD4**
	5	3	75	**PD5**
CB	5	3	68-73	**PD6**
NZ	5	5	63-76	**PD7**
	5	1	76	**PD8**
	5	3	50	**PD9**
WGS	1	5	62	**PD10**
	5	3	62	**PD11**
	10	-	62	**PD12**
RC	5	1	42	**PD13**
	1	5	45	**PD14**

Table 2.2: Mixed immersion decellularization conditions. Under parenthesis is represented the amount of days passed with that particular concentration. Concentrations with the same days displayed represent a mixed solution of those compounds.

Plant	SDS (%)	Triton X-100 (%)	NaCl (M)	Bleach (%)	Step	Time (days)	Condition
VS	5	0.5	-	-	1	18	**PD15**
	-	-	-	0.5	2	6	
	5	-	-	-	1	16	**PD16**
	-	3	-	0.5	2	6	
CB	-	3	0.2	-	-	19	**PD17**
	1	3	0.2	-	-	64	**PD18**
RC	-	5	0.2	-	-	19	**PD19**
	-	1	0.2	-	-	45	**PD20**
	5	-	0.2	-	-	19	**PD21**
	1	5	0.2	-	-	19	**PD22**
	2	3	0.2	-	-	45	**PD23**

Table 2.3: Detergent-free decellularization conditions. Condition 24 is seeded onto an acetate buffer made with 100 mM $C_2H_3NaO_2$ (Sigma-Aldrich) and 100 mM CH_3COOH (Sigma-Aldrich) per 100 mL of solution. Condition 25 is seeded onto a potassium bicarbonate buffer built with 84 mM $KHCO_3$ (Sigma-Aldrich) per 100 mL of solution.

Plant	Ethanol (%)	pH	Bleach (%)	Total Time (days)	Condition
VS	4	4	-	7	**PD24**
	4	8.5	-	7	**PD25**
	-	-	0.5	7	**PD26**

2.1.3.2 Perfusion protocols

Two perfusion methods were tested where pressure came from either gravity or a pump.

Gravity-based perfusion: Leaves were perfused through a blunt needle along the petiole with a decellularization solution placed at a 1.5 m height difference. The samples were placed onto two sets of four which lead through plastic tubes, to two different flasks containing 1L of different decellularization solutions. The leaves are immersed onto a glass tin containing 1L of the respective solution. In order to improve the usability of the solution, two tubes were placed at the specific tin height where the solution reaches a 1L volume and connected to two peristaltic pumps which revert the excess solution to the flasks above.

Figure 2.1: Gravity-based decellularization setup. The chosen decellularization solution is perfused through plastic tubes onto blunt needle tips towards the leaves, which are also immersed onto the same decellularization solution inside glass tins. Setup built at FCT-UNL.

Pump-based perfusion: Likewise, the leaves were immersed and set onto the support in a similar fashion. A peristaltic pump circulates the decellularization solution from the tin to the leaves. A sensor was placed underneath the pump pressure converted to a voltage value, read by a multimeter. The sensor setup used was built by Ana Pádua [113] and allowed for the calculation of the pressure exerted onto the leaves by a simple calibration curve between pressure and voltage. The pressure was found to oscillate slightly along the process between 81 and 100 mmHg.

2.1.4 Plant histology

Decellularized and native leaves were stained using an adapted version of the protocol proposed by Tolivia [114]. The safranin solution was made using a ratio of 75 mL ethanol p.a (Panreac), 25 mL H_2O, 1 g Safranin O (Sigma-Aldrich), 1 g sodium acetate (VWR chemicals) and 2 mL formaldehyde.

2.1.5 Optimization of the decellularized material

2.1.5.1 Gelatin coatings

Epichlorohydrin (ECH) treatment: Decellularized leaves were cut onto circular sections, 10 mm in diameter. The samples were immersed in 10mM ECH (Sigma-Aldrich) solution containing 67mM NaOH and incubated for 2h at 50°C. They were then removed from the solution and rinsed with distilled water until neutral. The used protocol was retrieved from Zeng *et al.* [115].

Gelatin solutions: Bovine skin type B (Sigma-Aldrich) and porcine skin (Sigma-Aldrich) gelatin solutions were produced at a concentration of 0.5, 2, 4 and 5% in water and sterilized by autoclave at 120°C. 500 μL of the 0.5, 2 and 5% solutions were added to the scaffolds placed on 24-well microplaques and left overnight. The solutions were later removed and washed with PBS and seeded according to the protocol shown in section 2.3.1.

2.1.6 Mechanical Tests

Plant scaffolds were cut into sections and their dimensions measured. The samples were then mounted in a tensile testing machine from Rheometric Scientific using a load cell of 20 N. Load was applied at a rate of 1 mm/min with a clamps separation of 2 mm.

2.1.7 Scaffold DNA assessment

2.1.7.1 DNA extraction and quantification

Samples of regular and decellularized CB, VS and NZ were cut onto approximately 0.3g aliquots while avoiding the petiole and vein area, frozen with liquid nitrogen, throughly macerated and placed onto 2 mL microcentrifuge tubes. The following protocol was adapted from Keb-Llanes **et al.** [116].

Extraction Buffer A (EBA): 50 mL were prepared with the following concentrations: 100 mM Tris-HCl buffer (pH 8.0), 20 mM EDTA (Sigma-Aldrich), 1.4 M NaCl (Panreac), 4% (w/v) polyvinylpyrrolidone (PVP) (Merk) and 0.1 % (w/v) ascorbic acid and autoclaved. 2% (w/v) hexadecyltrimethylammonium bromide (CTAB) (Sigma-Aldrich) and 30 μL of β-mercaptoethanol (Sigma-Aldrich) were added the day of the experiment.

Extraction Buffer B (EBB): 50 mL were prepared with the following concentrations: 100 mM Tris-HCl buffer (pH 8.0), 50 mM EDTA (Sigma-Aldrich) and 100 mM NaCl (Panreac) and autoclaved. 30 μL of β-mercaptoethanol were added the day of the experiment.

TE Buffer: 100 mL were prepared using 10 mM of Tris-HCl (pH 8.0) buffer and 1 mM EDTA (Sigma-Aldrich).

Firstly, 300 μL of EBA, 900 μL of EBB and 100 μL of SDS 20% (Sigma-Aldrich) were added to the tubes containing the samples and further ground with a tube pestle. The tubes were spun on vortex for 2 min and incubated at 65°C for 15 min. Afterwards, they were placed on ice and 410 μL of cold 5 M potassium acetate solution (Merk) were added. The tubes were mixed by inversion and placed on ice for 5 min, after which they were centrifuged at 16 000 × *g* for 15 min in a refrigerated (4°C) Eppendorf 5415R centrifuge. 1 mL of the supernatant were then transferred to a new microcentrifuge tube, added 540 μL of ice cold isopropanol (Riedel del Haën) and incubated in ice for 40 min. The tubes were again centrifuged at 16 000 × *g* for 15 min and the pellet washed with 500 μL of 70% ethanol (Scharliau). The dry pellet was again ressuspended using 600 μL of TE and 500 μ of ice cold isopropanol and again centrifuged, discarded the supernatant washed with ethanol and left to dry. Once dried, the pellets of regular CB and VS were resuspended with 50 μL TE and the remaining ones with 30 μL.

DNA quantification was performed using a NanoDrop ND-2000C spectrofotometer.

2.1.7.2 Agarose Gel

The extracted samples were loaded onto a 1 % (w/v) agarose (Seakem) gel in 1x TAE (Tris-Acetate-EDTA buffer) added with Gel Red Nucleic Gel Stain 10 000 ×, using 5 μL of sample diluted onto 5 μL of loading solution (Sigma-Aldrich). A Gene Ruler^{TM} DNA Ladder Mix ready to use marker was used.

The gel was run for 30 min at 100 V and observed with a BioRad GelDoc^{TM} XR^{+} Imaging System.

2.2 Electrospinning

2.2.1 Condition screening

2.2.1.1 PCL

A 10% (w/w) PCL (Sigma-Aldrich)in chloroform solution was electrospun using different combinations of flow, needle to collector distance, tension and rotation velocity.
Conditions tested: Flow: 0.5, 0.7 and 1 mL/h
Distance: 15 and 20 cm
Tension: 12 kV
Velocity: 200, 400, 600, 800, 1000, 1200 and 1400 rpm

2.2.1.2 PEO

A 20% (w/w) PEO 100 kDa (Sigma-Aldrich)in chloroform solution was electrospun using different combinations of flow, needle to collector distance, tension and rotation velocity.
Conditions tested:
Flow: 5, 7 and 9 mL/h
Distance: 7 cm
Tension: 6, 7 and 8.5 kV
Velocity: 200, 400 and 600 rpm

2.2.2 Construction of the layered scaffolds

Scaffolds were built using PCL and PEO in a layered fashion. PCL was electrospun horizontally to the collector while PEO was electrospun vertically because of the solution's high viscosity.

2.2.2.1 PCL hydrophilicity optimization

Production of non-aligned PCL fibres: A 10% PCL solution was electrospun for 5h with a 0.7 mL/h flow, a distance of 20 cm and tension of 12 kV at a velocity of 150 rpm. The electrospun fibers were cut onto circular sections, 10 mm in diameter.

Hydrophilicity tests: In order to turn the PCL fibres hydrophilic, three approaches were tested.

The first approach consisted on putting the fibers in contact with a 67 mM, 100 mM, 250 mM, 500 mM and 1M NaOH solution and placed on a desiccator for 0, 10, 20, 30, 45, 60, 90, 120 and 180 min.

Table 2.4: Layered scaffolds produced. The layers were produced based on the same electrospinning conditions for each solution regarding rotation velocity, flow, tension and distance to the collector and are presented in their real deposition order from left to right. **PCL electrospinning conditions:** PCL 10%, 600 rpm, 0.7 mL/h, 12 kV, 20 cm. **PEO electrospinning conditions:** PEO 20%, 400 rpm, 9 mL/h, 7 cm, 8.5 kV.

Deposition times for the scaffolds produced

Scaffold	PCL	PEO	PCL	PEO	PCL	PEO	PCL
S1 & S2	15 min	10 min	30 min	-	-	-	-
S3, S4 & S5	2h	15 min	30 min	-	-	-	-
S6	1h30	15 min	30 min	-	-	-	-
S7 & S8	2h30	15 min	30 min	15 min	45 min	-	-
S9 & S10	2h30	15 min	30 min	15 min	30 min	15 min	45 min
S11	3h30	15 min	45 min	15 min	45 min	15 min	1h
S12 & S16	3h30	15 min	1h	15 min	1h30	-	-
S13 & S15	3h30	15 min	2h	-	-	-	-
S14 & S17	3h30	15 min	1h	15 min	1h	15 min	1h30
S19	6h	15 min	2h	-	-	-	-
S20	6h	15 min	1h30	15 min	2h	-	-
S21	6h	15 min	1h30	15 min	1h30	15 min	2h
S22	5h	15 min	2h	15 min	2h	15 min	3h
S23	5h	20 min	2h	20 min	2h	20 min	4h
S24	6h	15 min	5h	-	-	-	-

In the second approach, the fibres were exposed to a p.a solution of ethanol for a period of 15 or 30 min, washed with water, and placed onto a 0.5M NaOH solution. The samples were then divided onto two groups, in one of which they were placed onto a desiccator. Both groups were exposed to the NaOH solution for a period of 30, 60 or 90 min.

In the third approach, the sample were exposed to a p.a ethanol solution for a period of 15 or 30 min and left in contact with a 0.5M NaOH solution for 30, 60 or 90 min outside of the desiccator before being washed with water.

All samples were incubated at 37°C for 1 week after the test in order to dry completely and later, their contact angle was measured.

Contact angle measurements: Treated and untreated circular PCL samples with a diameter of 10 mm were cut in half and taped down to the equipment's collector. Their static contact angles were measured at room temperature through the hanging frop method using an OCA20 contact angle measuring instrument (DataPhysics Instruments GmbH, Filderstadt, Germany). Water microdrops (volume 5 μL, Ultrapure type II water) were generated with an electronic micrometric syringe and deposited on the substrate surface according to the so-called pick-up procedure. The contact angle was determined after 5 s of the moment of the drop deposition and settle. Image acquisition, analysis and contact angle determination was performed using the SCA20 v.4.3.12 software (Dataphysics Instruments GmbH, Filderstadt,

Germany). The angles were calculated using the Young-Laplace model. Each sample had a total of two drops dispensed in different regions and each condition was measured a total of six times. The results correspond to the average and are presented with the respective standard deviations.

2.3 Cellular Assays

2.3.1 Scaffold seeding

Each decellularized leaf and electrospun scaffold was cut circular sections, 10 mm in diameter and seeded with either Vero (monkey kidney epithelial cells), 3T3 (mouse fibroblasts) or ECs (rat aorta endothelial cells) at a cell density of 40kc/cm^2. Plant scaffolds were placed directly onto 24 well microplaques while the electrospun ones were placed onto hollow Teflon cylinders in order to diminish the number cells fallen to the bottom of the well.

All cells were cultivated in DMEM (Dulbeccos Modified Eagles Medium, Sigma-Aldrich D5030) supplemented with 1.0 g/L D-glucose (Gibco, 15023-021), 3.7 g/L sodium bicarbonate (Sigma-Aldrich, S5761), 1% GlutaMAX™ (L-alanyl-L-glutamine dipeptide, Life Technologies, 35050-038), 1% sodium pyruvate (Gibco, 11360039), penicillin (100U/ml) and streptomycin (100 g/mL) (Invitrogen, 15140122), 10% FBS (Fetal Bovine Serum, Invitrogen, 10270106).

Plant scaffolds were sterilized by being immersed in 70% ethanol solution for 3 days and then irradiated with ultraviolet radiation for 20 min. Electrospun scaffolds were simply immersed in 70% Ethanol.

2.3.2 Perfusion re-cellularization

Gelatin test: Initially and due to material availability, whole decellularized leaves of New Zealand spinach were divided onto three groups. The first group, comprising leaves that were treated with ECH, perfused with a solution of 4% bovine skin gelatin or 4% porcine skin gelatin through the petiole. The second group was comprised of leaves that were not treated with ECH but were still perfused with a 4% bovine gelatin solution. The third group was comprised of a single leaf immersed in a 70% ethanol solution which was treated as a control sample. The following steps are shared by the test mentioned bellow.

Untreated leaves test: As to improve on the previous test's results, whole decellularized leaves of Viroflay spinach were immersed in a 70% ethanol solution overnight and sterilized by UV irradiation for 20 min the following day. Phenol-red dye was added to a DMEM/3T3 blend at a ratio of 1:5 v/v and perfused through the petiole of the leaf until the veins were well-coated with the red liquid. The culture was then left incubating for 4 days in a 60 mm petri dish.

2.3.3 Resazurin tests

Resazurin is a non-fluorescent blue dye which can be used as a redox marker for cellular viability. Its low cytotoxicity allows for the following of a cellular culture over time. This method is based on the fact that resazurin is reduced to resorufin, a pink fluorescent dye by metabolically active cells. This reaction can be followed by UV-Vis spectroscopy since resazurin possesses an absorbance peak at 601 nm while resorufin has it at 571 nm.

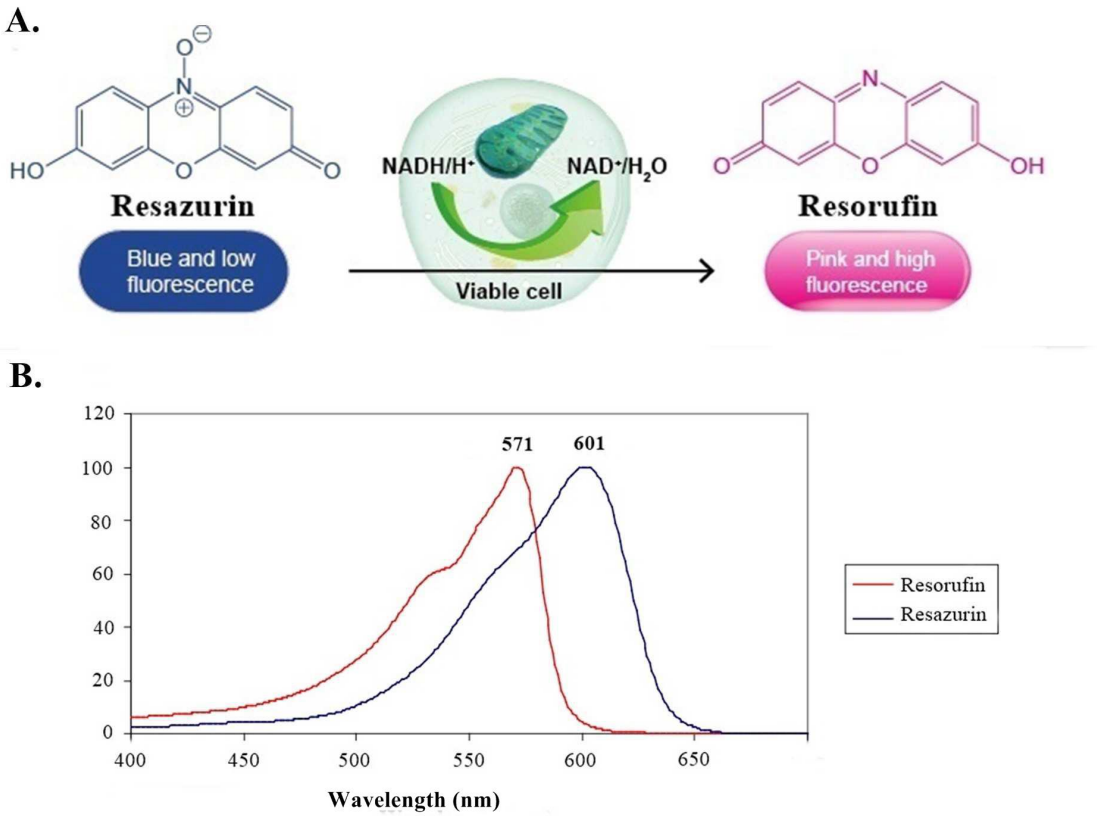

Figure 2.2: Resazurin and Resorufin. a. Resazurin is reduced to resofurin by the NAD coenzyme on metabolically active cells. Image adapted from [117]. **b.** Resazurin and resorufin UV-Vis absorbance spectra. Image adapted from [118].

2.3.3.1 Optimal resazurin for EC and 3T3 cell lines

EC and 3T3 cells were seeded on two 96-well microplaques and left to adhere for a day. Four resazurin (Alpha Aesar) solutions in PBS^- buffer were made with a concentation of 0.4 mg/mL, 0.2 mg/mL, 0.1 mg/mL and 0.05 mg/mL.

Conditions tested: With a ratio of 90% DMEM/ 10 % Resazurin: Resazurin 0.4 mg/mL, 0.2 mg/mL, 0.1 mg/mL and 0.05 mg/mL with respective controls.

With different ratios DMEM/PBS^-: 10% Resazurin 0.2 mg/mL with a 90/0, 80/10, 70/20, 60/30, 50/40, 40/50, 30/60, 20/70, 80/10 and 0/90 DMEM/PBS ratio.

2.3.3.2 Plant leaf scaffold seeding and resazurin tests

Different scaffolds coming from different plant species were seeded and cell proliferation monitored. The cultures performed are presented bellow.

Table 2.5: Cell cultures performed using decellularized plant scaffolds. All cultures were performed using DMEM medium supplemented with FBS and, aside from culture PCC5, the cells were seeded with the leaf's abaxial surface facing upwards. Cell adhesion was calculated on the day after cell seeding.

Culture	Cell Lineages	Plant	Total Days	Observations
PCC1	3T3, EC and Vero	VS	12	Regular adhesion and proliferation test.
PCC2	3T3, EC, Vero	CB	14	Added bovine gelatin test.
PCC3	3T3, EC	VS	4	Porcine and bovine gelatin and ECH test.
PCC4	3T3, EC	NZ	4	2% porcine and bovine gelatin test.
PCC5	3T3	VS	4	Single reading, perfusion culture.

2.3.3.3 Electrospun fibres seeding and resazurin tests

Different layered conditions were seeded and its cellular proliferation monitored. The cultures performed are presented bellow.

Table 2.6: Cell cultures performed using layered electrospun scaffolds. All cultures were performed using DMEM medium supplemented with FBS. Cell adhesion was calculated on the day after cell seeding.

Culture	Cell Lineages	Total Days	Observations
SCC1	3T3, EC	3	Hydrophilic PCL, scaffolds S17, S20, S21, S23 and S24.
SCC2	3T3, EC	6	Scaffolds S11, S12, S14, S15, S16 and S17.
SCC3	3T3, EC	4	Hydrophilic PCL, scaffolds S11, S17, S21 and S23.

2.4 Imaging techniques

2.4.1 Nuclei staining imaging

Leaf and electrospun scaffolds were observed using DAPI, a nuclear fluorescent stain which is able to penetrate the cell membrane and bind strongly to adenine-thymine rich regions of DNA in both living (with a lower efficacy) and dead cells. Since its absorption peak when bound to double stranded DNA is 358 nm and its emission peak reads at 461 nm, it is excitable by UV light and detectable through a blue/cyan filter [119].

In order to be used, the samples were washed 2 times with a PBS and fixed with a 3.7% solution of para-formaldehyde for 20-30 minutes at room temperature. The samples were washed again twice with PBS^{-} and a 0.3 μM DAPI solution was added at room temperature and left for 30 min.

2.4.2 Scanning Electron Microscopy

The morphology of both plant and electrospun scaffolds with and without adhered EC and 3T3 cells was characterized by SEM. The samples with adhered cells were washed twice with PBS and fixed for 3 days using 3.7% PFA at 4°C. They were then rinsed 3 times with sterile water, cut into sections, mounted on an aluminium board using double-sided adhesive tape and left to dry at room temperature. The samples were then coated 15 nm with iridium using a Quorum sputter coater. The samples were then observed with a Zeiss Auriga Cross Beam SEM-FIB operated at an accelerating voltage of 2 kV in varying magnifications.

CHAPTER 3

RESULTS AND DISCUSSION

3.1 Plant leaf decellularization

3.1.1 Seed germination

The work at hand is based on the decellularization of five plant species: New Zealand spinach (NZ), Winter Giant spinach (WGS), Viroflay Spinach (VS), "Papo de Rola"Common Bean (CB), Sowthistle (CST) and *Rumex crispus* (RC).

NZ (*Tetragonia tetragonioides* (Pallas) Kuntze) is an edible leafy vegetable indigenous from eastern Asia, Australia and New Zealand. Its leaves have a triangular shape, measuring 3-15 cm in length and are thick, with big nerves that are not highly tapered and covered in papillae trichomes. Contrary to the name, NZ is not a spinach, since it belongs to the *Aizoaceae* family, commonly known as "ice plants"though this plant prospers best at a temperature of 15-23°C. In order to germinate, it is recommended for the seed to be immersed into warm water for a 3-12h before planted. However, we found the cooling at 4°C for a period of at least 3 days prior to germination to have a better effect. This plant was chosen for the robustness of its leaves as well as defined veins and high leaf production.

WGS (*Spinacia oleracea* L.)is a frost resistant spinach variety best suited for sunny environments of 7-15°C. Their leaves are larger than other varieties, triangular in shape and arrange themselves around the flowering stem, being larger at the bottom and smaller and more tender on top. This variety was chosen as a way to link the work with its literature background, the article published by Gershlak *et al.* [82], since it did not declare the variety used. However, we have found it to be hard to cultivate in the tested conditions, with the flowering stem appearing quite early in the development, leading to smaller leaves with smaller petioles. Also,

the leaves had a tendency to get rigid and curl around themselves early in the development, making it hard to work with (see fig 3.1).

VS follow the same pattern of growth of WGS. However, this variety possesses smaller triangular leaves with a larger petiole and is best suited for a temperature of 12-24°C, making the flowering stem appear much later in the development timeline, resulting in a larger sample size of pre-flowering leaves. This variety was used as an alternative to WGS, as its optimal temperature was much closer to the tested conditions.

Figure 3.1: Plants grown in Fitoclima. a. Common Bean **b.** *Rumex sp. c.* Viroflay spinach **d.** Winter giant spinach. WGS leaves, though bigger than VS leaves, have a tendency to curl around themselves, making them hard to work with.

CB (*Phaseolus vulgaris* L.) is an annual plant that belongs to the *Leguminosae* family, best suited for a temperature of 15-27°C . Its leaves come in two different forms, both with a thin and highly branched vascular network. Cotyledonary leaves are larger and heart shaped and come as a single pair while the remaining leaves are more elongated with a thinner outer point. This plant has the advantage of, like all legumes, germinating easily and growing fairly

quickly as well as having the ability of self-pollinating, making it easier to have seeds to use when repeating the experiment. We have chosen to use the "papo de rola"variety as means of connecting this work to the national germplasm as well as having already been used for several purposes at ITQB.

CST (*Sonchus oleraceus* L.) is a biennial herb characterized by its bright yellow flowers and elongated leaves with a saw teeth-like perimeter. Though it prefers warmer climates and plenty of sunshine, it can tolerate most soil types, being considered as an invasive species in most parts of the world. This plant was helpful as a means to compare the growth pattern of other plants, since it grows easily.

RC (*Rumex crispus* L.) is an invasive plant characterized by having clusters of small, usually brick-red flowers carried above its smooth reddish green leaves, with distinctive wavy or curled edges, defined veins and large petioles, which were thought to be very useful for perfusion decellularization.

3.1.2 Plant growth patterns

In order to know more about the behaviour of the plants used, they were germinated and grown under three different conditions: Fitoclima, Lumigrow and Non-Controlled conditions. However, due to lack of space, not all plants were grown into all three environments.

CB, WGS and RC were grown in both Fitoclima and Lumigrow. Due to its height, all Fitoclima grown CB were transferred to Lumigrow after 21 days.

CB plants were easy to both germinate and grow, with healthy looking leaves of average size, good vascularization and bright green color. CB's placed on Lumigrow grew a bit faster than the ones in Fitoclima. WGS were grown for a period of 43 days in both conditions but its growth was poor, with thick leaves of heterogeneous color which would curl around themselves, making them hard to use for the purpose at hand. We also found them hard to germinate, even after storing them at 4°C for a period of 15 days. Their growth was slow and interrupted by the appearance of a flowering stem fairly early in the development. These characteristics were present in both Fitoclima and Lumigrow grown WGS most likely due to the temperature being too high. Due to these reasons, we have ruled out WGS as a contender to decellularization.

RC plants were perhaps the most different between conditions. Though similar in terms of height and number of leaves, RC leaves grown on Lumigrow were significantly different in color, with a red-ish brown tint all throughout the plant. This color disappeared when transferred to Fitoclima. However, the number of leaves achieved in both conditions was much lower than expected. In the wild, RC can have between 30-50 leaves of varying sizes, while the maximum leaves gathered was only 6. In order to improve this issue, a better view on RC necessities such as soil type and ideal temperature should be investigated. However,

other circumstances occurred which deemed this plant as not ideal for the work at hand, which will be shown on section 3.1.4.3.

CST and VS were grown in all three conditions. Contrary to what was expected, CST had some difficulties developing in the Temperature-Controlled conditions, with thin round delicate leaves and stalk which had a tendency to bend. This problem was solved by increasing sunlight exposure. On the other hand, Lumigrow grown CST developed much faster with resistant stalk and leaves of a similar layout as the ones found in the wild. However, like RC, they showcased a red-ish brown tint, specially in the abaxial side, most likely due to the exposure to an incomplete light spectrum. Fitoclima grown plants found themselves in the middle of the scale, with medium robustness and green leaves of a regular design. VS was grown after it was noticed that WGS did not have a growth behaviour suited for the task at hand. Like CST, non controlled conditions led to a worse performance. However, the difference between Lumigrow and Fitoclima was more noticeable, with the plant growing in leaf number a little faster with bigger leaves to work with.

Lastly, NZ was the only plant tested in one condition, Lumigrow, due to the fact that it did not grow in any other. Also, the difficulties in germination and growth made it so that only one plant was able to be grown in this phase of the work. Nonetheless, the plant grew for a period of 53 days, after which it provided 83 leaves which were used for the decellularization process at hand. This problem was later overcome, with the seeds being stored at 4°C for a period of 4 months prior to the next germination, after which the plants grew normally with a high leaf yield.

The graphics regarding the number of leaves achieved during the testing period for the tested conditions can be seen in the following page. This data, along with visual observation, has allowed us to choose which plant varieties would follow the next step (VS, CB, RC and NZ) and how much time it would take to harvest them in the desired growth stage. In fact, it is possible to observe differences between the growth conditions, with Lumigrow having similar (RC, CB) or better (VS, WGS) results. Along with this, the dimension of the leaves was also monitored.

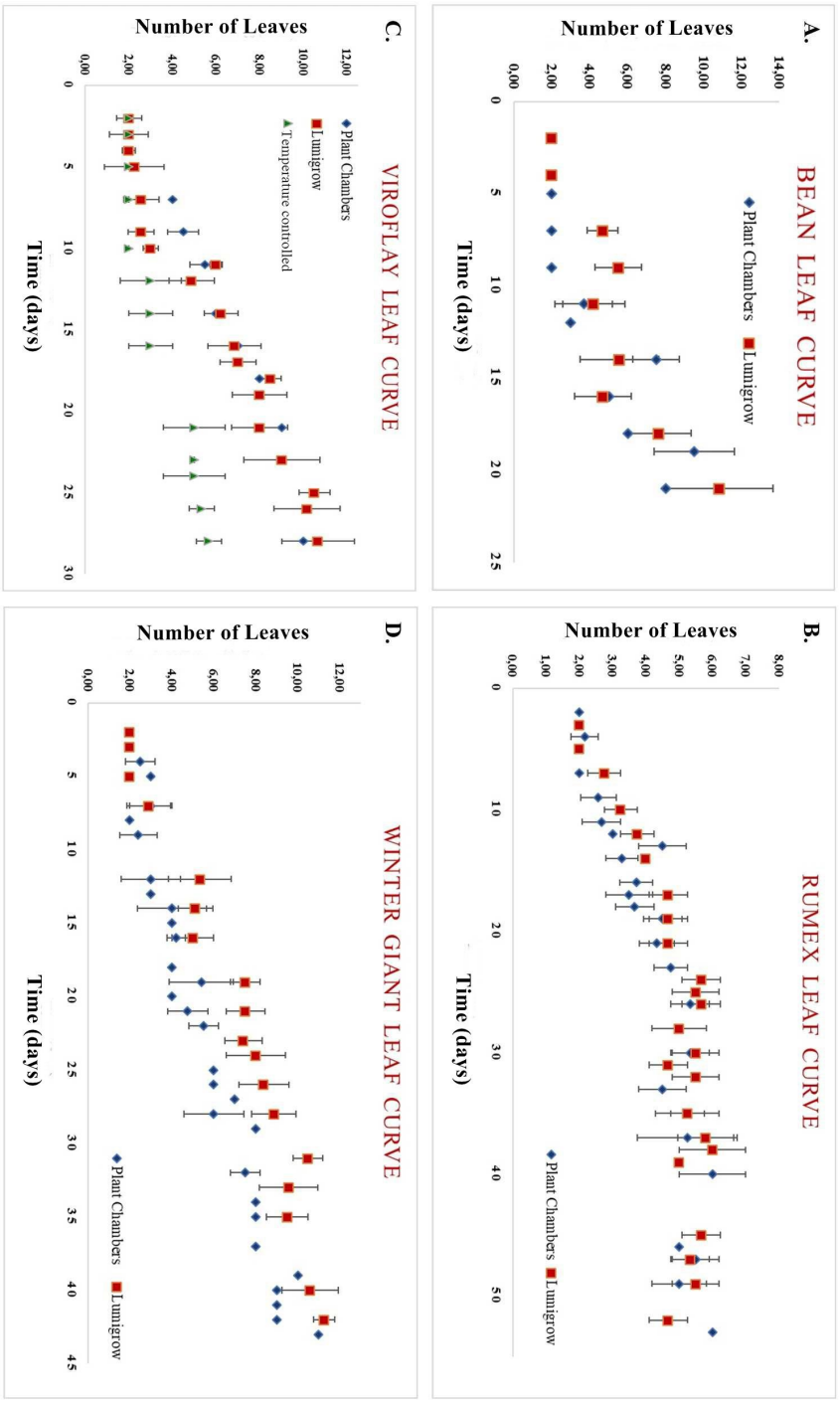

Figure 3.2: Leaf number assessment in different plant varieties. A. Common bean. **B.** *Rumex sp.* **C.** Viroflay spinach. **D.** Winter Giant spinach. While a slight difference between Lumigrow and Fitoclima grown plants can be observed in **a.** and **b.**, this difference increases in **c.** and **d.**. In **c.**, a significant decrease in leaf number in non-controlled conditions can be observed when compared to the latter. Values are an average of 20, 8, 28 and 8 replicas regarding CB, RC, VS and WGS respectively, for Plant Chambers and Lumigrow. Temperature controlled VS values are an average of 6 replicas.

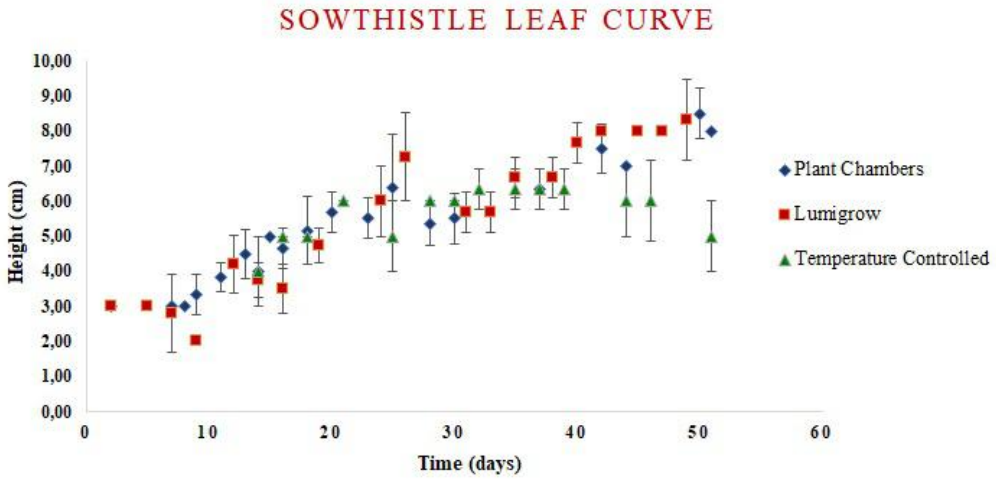

Figure 3.3: Leaf number assessment in common sowthistle Values are an average of 10, 10 and 4 replicas regarding Plant Chambers, Lumigrow and Temperature controlled respectively.

3.1.3 Plant leaf conservation and transportation

Due to the fact that the plants used were grown at ITQB while the decellularization equipment was situated at FCT-UNL, it was necessary to keep the leaves in optimal condition along the trip as well as store them for future use. For this purpose, five solutions were tested: Adapted Euro-Collins (AEC), PEG 10% + Glucose (P10G), PEG 15% + Glucose (P15G), PEG 20% + Glucose (P20G) and PEG 15% (P15). Since bean leaves were noticed previously as being the most susceptible to decomposition, they were the ones used for the test, both cotyledonary and regular.

After 11 days, the leaves were observed, reaching the following conditions. P15G and P20G supported a medium to good conservation of all tested leaves, with a slight mollification of the structure. P10G seemed worse, with 75% fairly conserved leaves and one which began to decompose. In P15, the best condition tested, all leaves maintained a similar structural integrity to native leaves. In AEC, the opposite occurred, with all leaves in a advanced stage of decomposition.

PEG has been used for several purposes, such as rat [120] and bovine blastocyst [121] vitrification and as a perfusion solution for the preservation of liver [122] and kidney [123] by preventing cell swelling. Though not as common nowadays, it was fairly used in combination with other compounds, from which one was usually a sugar. This lead us to use glucose, whose concentration was mimicked from the prepared AEC solution. Introduced by Collins in 1969, this solution was once very popular in organ preservation, particularly for liver and pancreas transplantation, before falling out of use in the late 1980's.

Since the leaves themselves were not sterilized, the glucose in P15G, P10G, P20G and AEC has seemingly fed micro-organisms that would later decompose the material. In the case

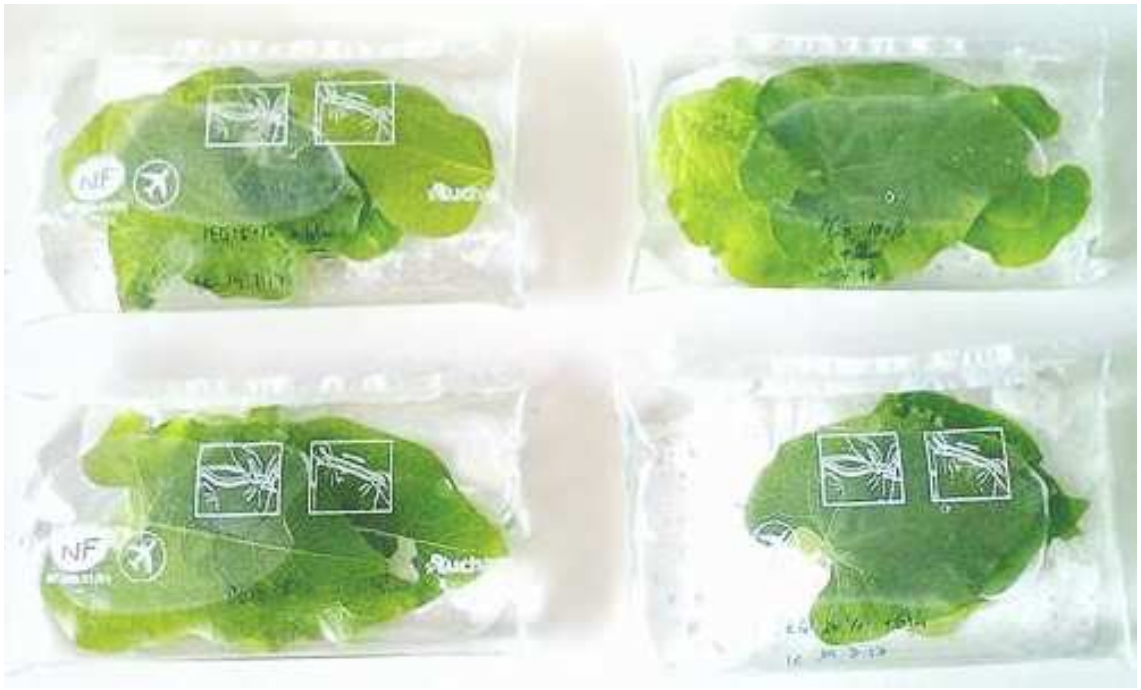

Figure 3.4: Leaves setup for conservation assays. Each bag contains 2 cotyledonary leaves and 2-3 regular ones immersed in 100 mL of conservation solution.

of P15G and P20G, that decomposition was in part hindered by PEG.

3.1.3.1 Pigment quantification

Photosynthetic pigments can be indicators of plant senescence. Carotenoids in particular are essential to the elimination of reactive oxygen species in damaged tissue as well as act as a cellular protector against photo-oxidative damage.

Contrary to what was expected, AEC which was visually seen as the worst performing solution actually had a bigger quantity of both Chlorophyll a (Chla) and Chlb. Since the pigments were extracted manually, it is possible that AEC leaves, which were much more fragile, made it so more pigment was able to be extracted rather than more pigment actually being in the leaves themselves.

P15 and P20G present a similar pigment mass when compared FCB (control, fresh CB). With this information, we can now distinguish between P15G and P20G, something that had not been possible by visual observation alone. P10G can also be excluded since pigment values are quite lower than the control F (fresh leaves) condition.

This analysis leaves us with two options to choose from, P15 and P20G. In order to distinguish them, ANOVA tests were performed. The values obtained are shown in table 3.1.

Table 3.1 showcases P15 and P20G as being the most similar to F. Though theoretically, P20G had achieved the best results, with 3/4 of parameters having a *p-value* higher than 0.05,

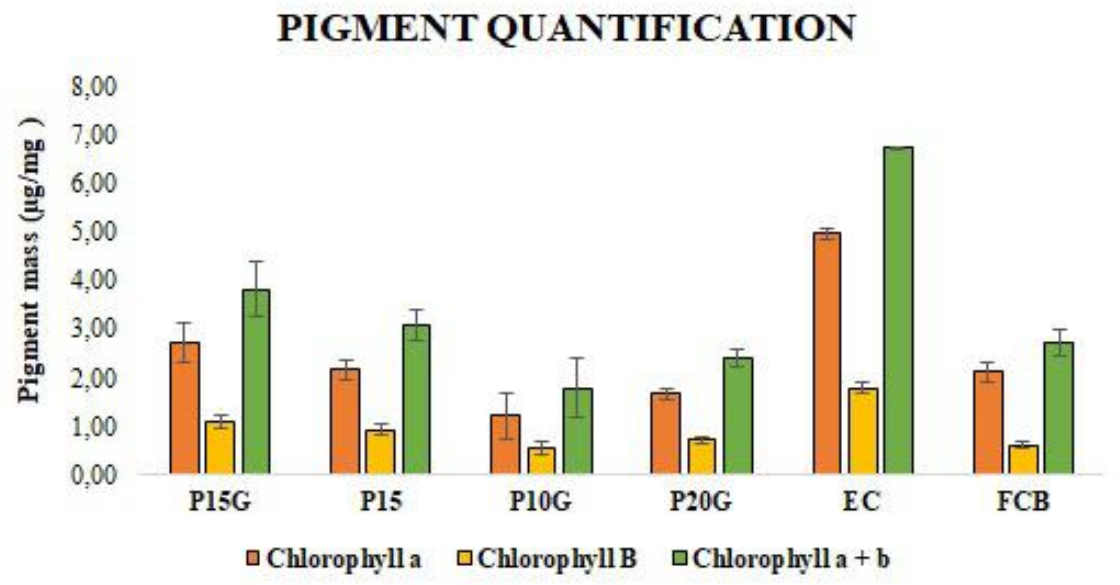

Figure 3.5: Pigment quantification in bean leaves after leaf conservation assays. Values presented per dry weight. Chlorophyl a, b and a+c in P15G, P15, P10G, P20G, AEC and F(fresh leaves, control condition). All conditions have a $\frac{Chla}{Chlb} > 1$ ratio. The values are an average of four replicates for each condition.

Table 3.1: A-NOVA *p-value* tests obtained between FCB and the remaining conditions. Chlorophyll a, b, a + b and carotenoids (xantophylls and carotenes) (x + c) *p-values* were analysed. *p-values* bellow 0.05 represent a statistically significant difference of values between the conditions.

ANOVA test *p-values*

Pigment	P15G	P15	P10G	P20G	AEC
Chl a	**0.110**	**0.842**	0.042	**0.106**	0.001
Chl b	0.007	0.027	**0.630**	**0.282**	0.002
Chl a + b	0.047	**0.298**	0.085	**0.298**	0.001
Car xantophyll + carotenoid	0.007	0.002	0.001	0.001	-

we have pondered whether the addition of glucose would improve the chances of microbial growth. For this, among all reasons mentioned above and being easier to produce, P15 was chosen as the preservation and transportation solution for all harvested leaves.

3.1.4 Decellularization procedures

3.1.4.1 Chloroform vs Acetone treatment

In order to increase the penetration of the decellularization solutions, cuticle waxes were solubilized with organic solvents, from which we have tested chloroform and acetone.

Firstly, VS and CB were treated 8 min with chloroform or acetone and then rinsed. This led to a large structural damage in chloroform treated leaves which did not happen in acetone. The amount tested was later decreased to three 30s cycles followed by a 60s one, which was also too damaging. The best chloroform cycle program was found to be three 15s cycles for VS, two 15s cycles for CB and three 60s cycles for NZ. The changes in programs are due to the leaves' rigidity. In the case of RC, three chloroform cycles of 5 min each were necessary. Acetone was found to be too mild for all leaves tested, though it helped in pigment removal.

3.1.4.2 Perfusion Decellularization

Our initial approach to decellularization was based on simple perfusion through the leave's petiole. This protocol was similar to section 2.1.3.2 except the decellularization solution was only perfused and the solution flasks were set at a height of 1.5m. Using equation 3.1 and knowing that 1×10^5 Pa = 760 mmHg, it is possible to calculate the pressure to which the leaves were subjected throughout the process.

$$P = \rho.g.h \tag{3.1}$$

Considering a fluid density similar to water, P = $997 \times 9.8 \times 1.5$ = 14.656 kPa, equivalent to a theoretical pressure of 112 mmHg. RC and VS leaves were mounted onto the perfusion equipment and left with a SDS 10% (left side) and Triton X-100 10% solution (right side). After a week, all leaves started to degrade, with the ones subject to SDS covered in a crystallized SDS build-up. Also, no decellularization was visible. The experiment was later repeated with a concentration of 5% for both detergents with similar results.

In order to fix this problem, the leaves were both perfused and immersed in the decellularization solution and the height was increased to 1.95 m, leading to a theoretical pressure of 140 mmHg. Nonetheless, though the build-up and degradation problem ended, the leaves continued to not decellularize properly. As an example, figure 2.1 showcases RC and VS leaves after 32 days of decellularization with the described method. This could be due to several factors such as the theoretical exerted pressure not being representative of reality, inadequate solution concentration and problems with embolism at the perfusion site (which we believe to be most probable). Since the decellularization process is rough on the structural integrity of the sample as it is, we have decided not to worsen it by increasing pressure. Thus, a pump

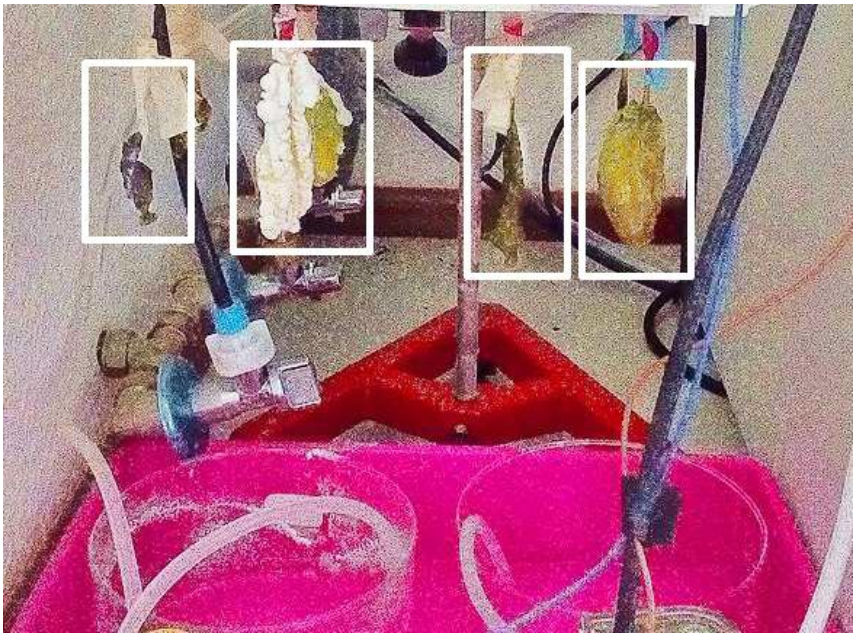

Figure 3.6: Immersion-free perfusion decellularization results. Both R and V leaves were subjected to a SDS 5% (left side) or a Triton X-100 5% solution. After a week, all leaves withered with crystallized SDS build-up being observable on the left set of leaves.

system imbued with a voltage sensor was used in order to monitor and control the pressure to which the leaves were subjected.

Equation 3.2 showcases the calibration curve obtained.

$$y = 43.83x - 0.87911 \tag{3.2}$$

The pressure is set in mbar which was converted to mmHg with the rate of 1 mbar = 0.75 mmHg. It is possible to conclude that this technique should be used as an additional step after a different method of decellularization rather than by itself, since it was unable to succeed on its own. For this reason, we have decided test different protocols of immersion decellularization, whose results and procedures are shown in the following section.

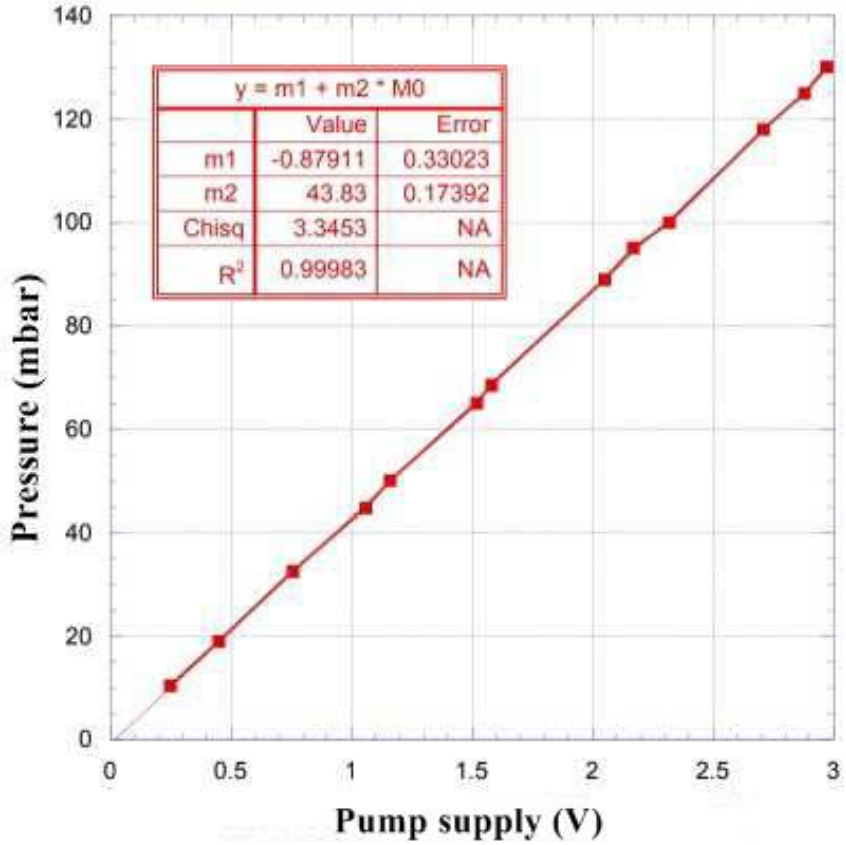

Figure 3.7: Calibration curve for the decellularization setup. Voltage monitoring allows for an easier reading of the pressure exerted by the inserting hydraulic pump onto the leaves, thus protecting them from damage.

3.1.4.3 Immersion decellularization

Several different conditions were tested either by immersion alone or mixed with perfusion.

PD24-26 (see table 2.3), aimed to observe the effect of pH in the process. In PD25, acetone removed pigment from the leaf at a faster rate than the other conditions. However, after 30 days, the leaves didn't show much difference compared to figure 3.8. Also, decellularization occurred simply around the veins rather than inside them. We have thus considered PD25 as a good first step prior to other decellularization procedures.

Section 3.1.4.2 demonstrated the difficulty in decellularizing RC. PD13-14 and PD19-23 (see table 2.1 and 2.2 respectively), aimed to find which condition would overcome this problem.

Unfortunately, no differences were observed between the conditions and the control even after 45 days, the exception being PD13, where some decellularization can be visible in the corners of the leaf. This was most likely due to the high concentration of SDS. Nonetheless, the difference was not enough to actually decellularize the leaves. Also, conditions PD19,

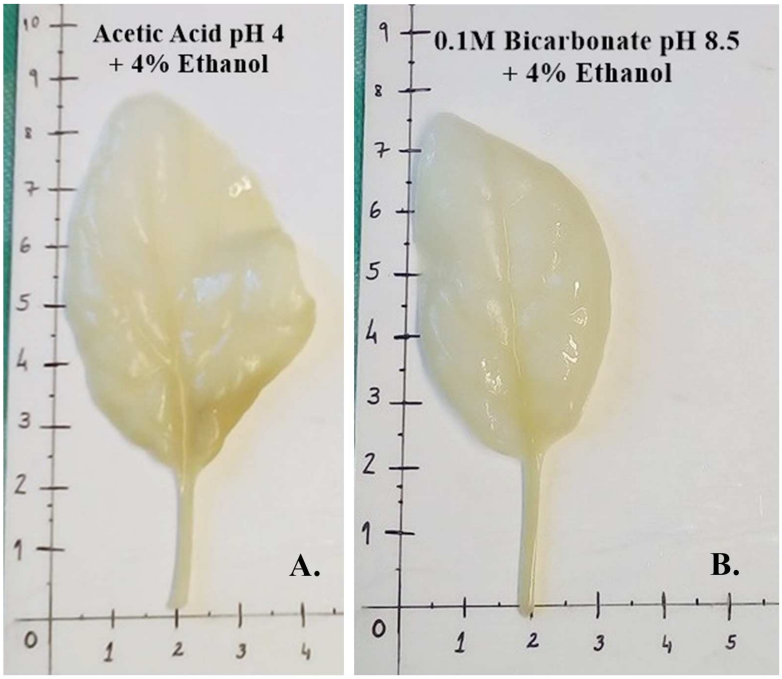

Figure 3.8: pH effect in VS leaves after 7 days of decellularization and an 8 min treatment with acetone. A. Condition PD24. **B.** Condition PD25.

Figure 3.9: RC leaves subjected to different decellularization solutions after 19 days. 13. 5% SDS + 1% Triton X-100. **14.** 1% SDS + 5% Triton X-100. **19.** 5% Triton X-100 + 0.2M NaCl. **20.** 1% Triton X-100 + 0.2M NaCl. **21.** 5% SDS + 0.2M NaCl. **22.** 1% SDS + 5% Triton X-100 + 0.2M NaCl. **23.** 2% SDS + 3% Triton X-100 + 0.2M NaCl. **C.** H_2O (Control).

21 and 22 were severely damaged, due to a large fungus outgrowth. This was largely due to the severe reaction between SDS and NaCl which prevented the detergent from reaching the leaves and properly decellularizing them, allowing them to degrade, providing a good medium for fungi to grow . This reaction was expected since SDS has a net negative charge which is largely attracted by the sodium cations present in NaCl. Since Triton X-100 is a non ionic detergent, this reaction did not occur. The experiment was later repeated with a simple 5% SDS solution with no improvement in results. For all reasons said above, RC was excluded as a feasible option.

PD15-16 (see table 2.2) allowed to understand the hypochlorite bleach effect. Though

large visual differences were noted, as seen in figure 3.10, they also resulted in a large structural damage with the leaves acquiring a gelatinous texture.

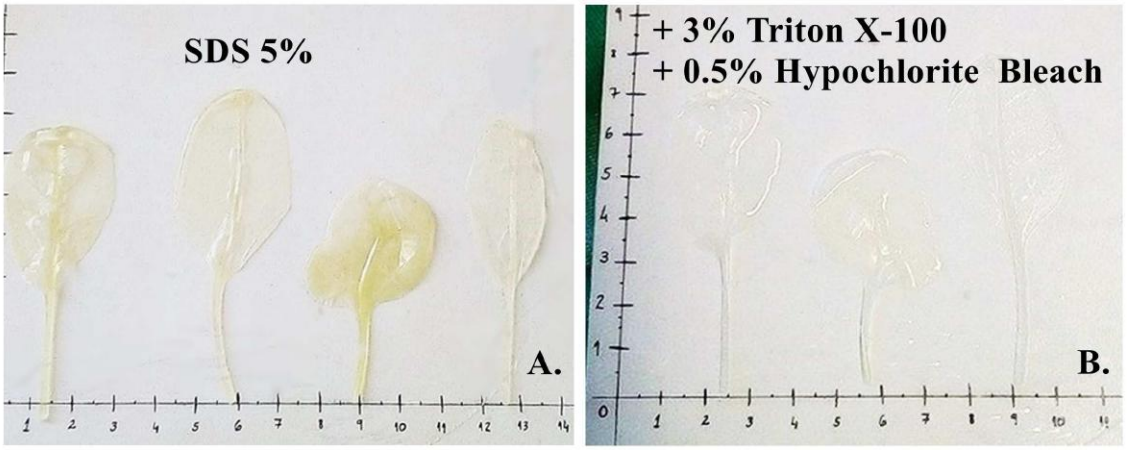

Figure 3.10: PD16 condition before and after the addition of hypoclorite bleach and Triton-X 100. A. VS leaves were immersed acetone for 8 min pior to exposure to a 5% SDS solution for 16 days. **B.** Exposure to 3% Triton X-100 + 0.5% Hypochlorite Bleach for 6 days has led to total transparency of the leaves.

In order to better analyse the effects of the process on VS leaves, they were stained with safranin O, a pigment that allows for the observation of cell nuclei and cellulose. Though a high decellularization is visible, trichomes appear to remain though they might have collapsed due to the burst of its comprising cells. Due to the leave's observable structural status, it is likely that most of the discolouration is due to the chemical disruption of cellulose links rather than actual nuclei removal.

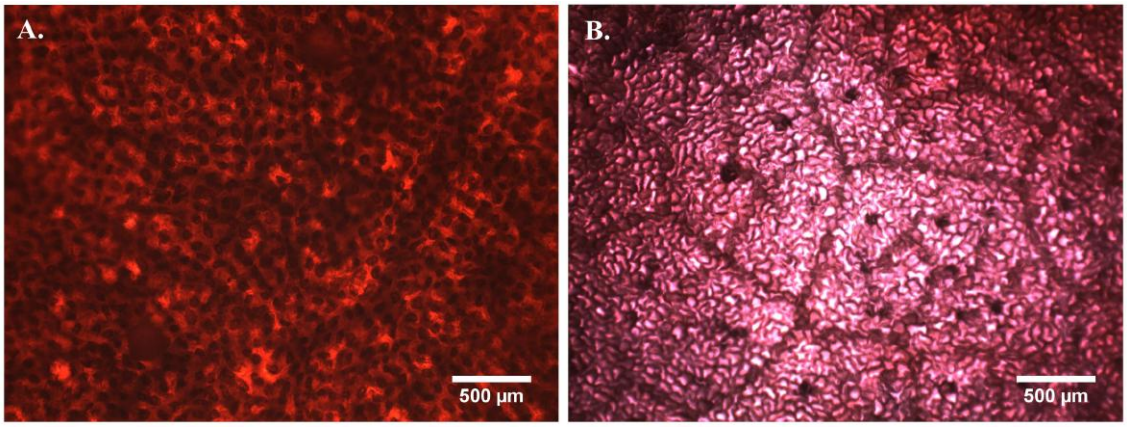

Figure 3.11: Safranin O staining of PD16 pre and post-decellularization A. Native V leaves. **B.** PD16 leaves. A large loss of nuclei is noticeable which appears to be lower in vascular tissue. Trichomes (large dark dots) are mainly undamaged.

The following conditions had their waxes solubilized by chloroform rather than acetone. The effect of NaCl was also tested in CB in PD17-18, (see table 2.2). Though PD17 led to the

same SDS/NaCl "salting out"reaction, as expected from an ionic detergent, PD18's behaviour was quite more interesting. In fact, CB leaves did not show much decellularization at all during the first 30 days. Afterwards, a large abrasion occurred with little discolouration of the tissue, which ended as a milky white colour after being immersed in bleach for 5 days. The anatomy of CB leaves was pinpointed as a disadvantage, since its fine point tends to break while being shaken, particularly in non cotyledonary leaves.

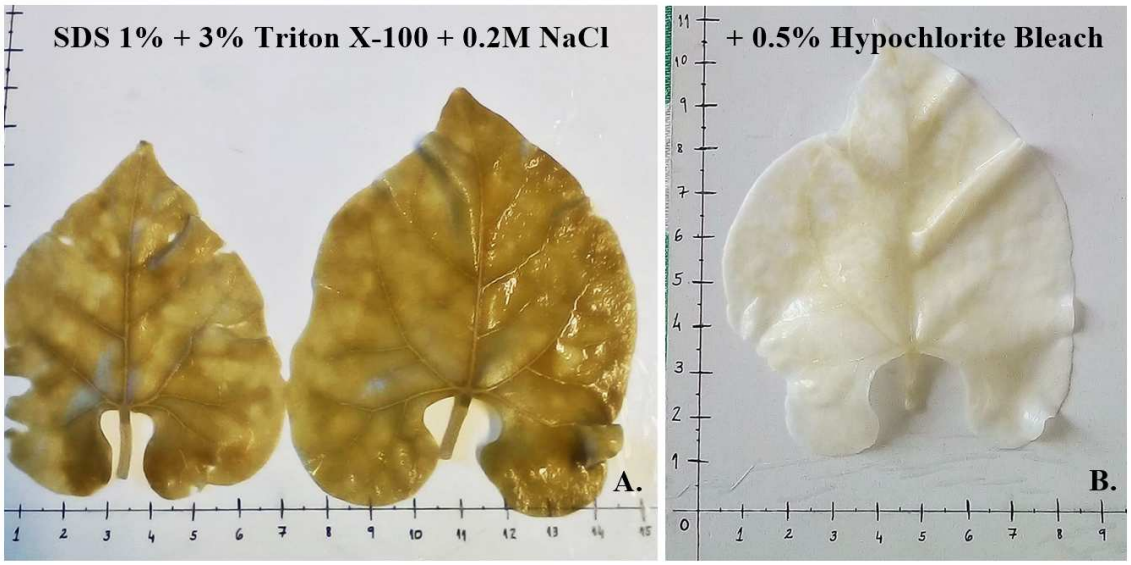

Figure 3.12: PD18 condition before and after added hypochlorite bleach. A. B leaves prior to adding 0.5% hypochloride bleach **B.** B leaves after 3 days of added bleach. Though the color largely improved, no additional decellularization is apparent.

PD1-PD12, (see table 2.1), were based on different concentrations of SDS and Triton X-100. Triton based conditions had a lower rate of decellularization while SDS based had a higher one. However, being SDS a relatively harsh detergent, a compromise between the rate of the process and structure retention needed to be evaluated. A concentration of 10% (PD12) was seen as too damaging with the leaves breaking off in chunks. On the other hand, PD3 (Triton 10% + SDS 1%) was not able to completely decellularize VS or CB even after 72 days.

It is important to note that the total time presented is not an optimal one since this work was also a timeline experiment. This was done as a way to understand exactly when and how much it was possible to decellularize the leaves, a value that was noted as being between 30-50 days for 5% SDS + 1% Triton X-100 and SDS 3% + 3% Triton X-100 solutions, depending on their toughness, variety and stage of development.

It was possible to understand the optimal conditions for the decellularization of different plants. Young or post-flowering leaves of VS and WGS were found to be best suited for a solution of 3% SDS + 3% Triton X-100. On the other hand, tougher leaves such as adult VS and WGS and all NZ types found the best results with 5% SDS + 1% Triton X-100. CB leaves

had the best results with a solution of 5% SDS + 3% Triton X-100. These conditions were used in further assays.

Figure 3.13: PD6 and PD2 conditions after full decellularization. A. Condition PD6. Though some damage occurred in the leave's tissue, its vascular network remained mostly intact. **B.** Condition PD2.

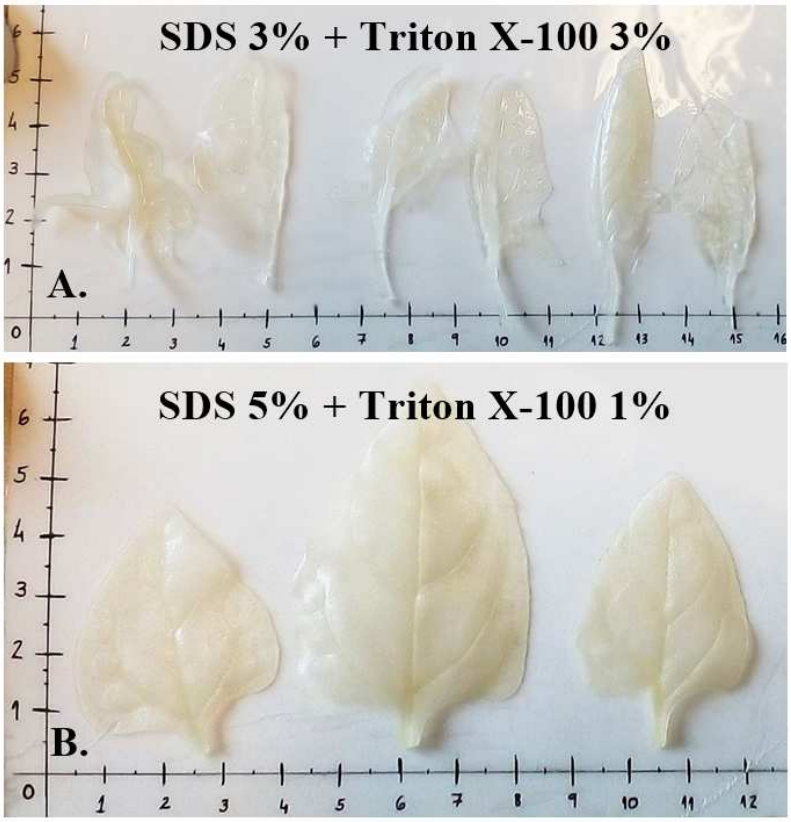

Figure 3.14: PD4 and PD8 conditions after full decellularization. A. Condition PD4. Post flowering VS leaves were used which decellularized relatively quickly with a great structural conservation. **B.** Condition PD8. NZ leaves do not get fully transparent due to their roughness.

3.1.4.4 Decellularization: conclusions

Table 3.2: **Main conclusions gathered from the decellularization process.** It was possible to achieve an observable decellularization through the usage of different SDS and Triton X-100 concentrations which were adapted to each leaf species and variety needs.

Experiment	Tested procedure	Observations
-	Chloroform and acetone assays for wax solubilization prior to decellularization	**VS and WGS:** three 15s chloroform cycles; **CB:** two 15s chloroform cycles; **NZ:** three 60s chloroform cycles.
PD24-26	pH 4.0 and 8.5 in VS	Partial decellularization only outside the leaf's veins.
PD13-14 & PD 19-23	SDS, Triton X-100 and NaCl in RC	No observable decellularization.
PD15-16	Hypochlorite bleach in VS	Large structural damage with no decellularization.
PD17-18	SDS, Triton X-100, NaCl and hypochlorite bleach	Large structural damage with no decellularization.
PD1-12	SDS and Triton X-100	**Optimal conditions:** **1. Young and post-flowering VS and WGS:** 3% SDS + 3% Triton X-100. **2. Mature VS and WGS, all NZ:** 5% SDS + 1% Triton X-100. **3. All CB:** 5% SDS + 3% Triton X-100.

3.1.5 DNA quantification and agarose gel

As to assess the effectiveness of decellularization, several techniques were used. DAPI staining results are shown in section 3.3.2 along with the resazurin tests. Both regular and decellularized leaves were subject to a DNA extraction and quantification protocol. The results were confirmed visually *via* agarose gel.

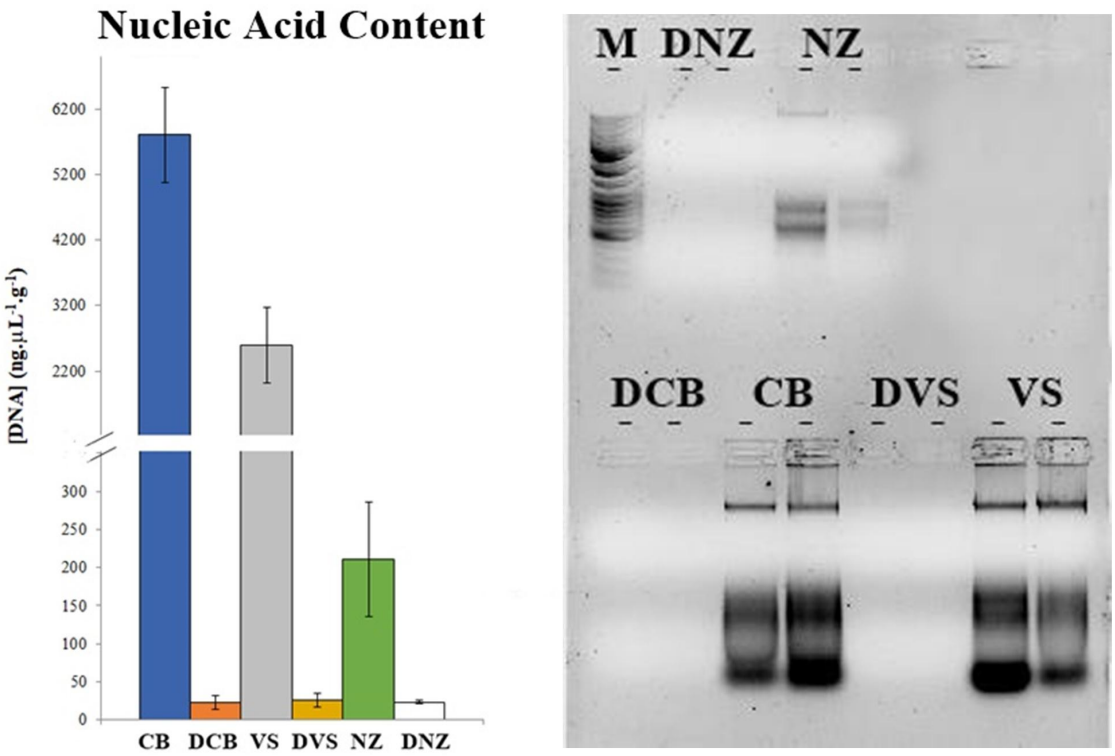

Figure 3.15: Leaf DNA quantification and obtained agarose gel. DCB: Decellularized common Bean **DVS**: Decellularized Viroflay **DNZ**: Decellularized NZ. Decellularized leaves obtained from each decellularization protocol were included in the essay. The black asterisks indicate the sample application site for the decellularized samples. Values are an average of triplicates.

Due to its density, a large difference can be seen regarding the actual concentration values of DNA in the different leaf types. Also, contrary to CB, both VS and NZ have "fleshier"leaves, due to its higher vacuole content, a reason that might also explain the discrepancy.

In order to analyse the obtained values, it is important to understand whether the extracted DNA has a high level of purity. For that, the Abs_{260}/Abs_{280} [124] ratio can be used. A value of 1.8 is typical of a relatively pure DNA. When lower, it can indicate a protein contamination and when higher, a RNA one. By observing the values shown in table 3.3, we can see a slight contamination of RNA in the regular leaves and protein in the decellularized ones. This, however, is expected, for two reasons. Firstly, since we were not able to use a commercial kit nor an RNase treatment, the extracted DNA is deemed to be "dirtier". Secondly,

when decellularized, the concentration of DNA becomes so low that an otherwise small protein contamination becomes more significant. Nonetheless, since the RNA concentration in the leaves is also affected by the decellularization process, it is important for the retrieved conclusions.

By analysing the results, we can conclude that the decellularization process appears to have been successful, with a DNA loss of 99.6 ± 0.4% for CB, 99.0 ± 1.0% for VS and 89 ± 11% in the case of NZ.

Table 3.3: Leaf nuclear content quantification. A large decellularization yield can be observed for all species, with CB having the best results. Values are an average of triplicates.

Leaf Type	Nucleic content concentration ($ng.g^{-1}$)	Abs_{260}/Abs_{280}
CB	5811 ± 726	2.12 ± 0.17
VS	2598 ± 579	2.12 ± 0.16
NZ	211 ± 75	2.14 ± 0.01
Decellularized CB	23 ± 9	1.64 ± 0.07
Decellularized VS	26 ± 9	1.77 ± 0.03
Decellularized NZ	23 ± 2	1.83 ± 0.08

3.1.6 Mechanical Tests

Human vessels have a non-linear stress-strain demeanour with two different regions of relatively linear behaviour; the lower modulus, which is said to be the mode of operation for vessels enduring physiological pressures and will be our comparison focus, and the upper modulus regions. For the lower region, the reported Young's Modulus vales are inserted onto a 0.2-0.6 MPa interval [125]. Likewise, our decellularized plant scaffolds also showcased two different modulus regions.

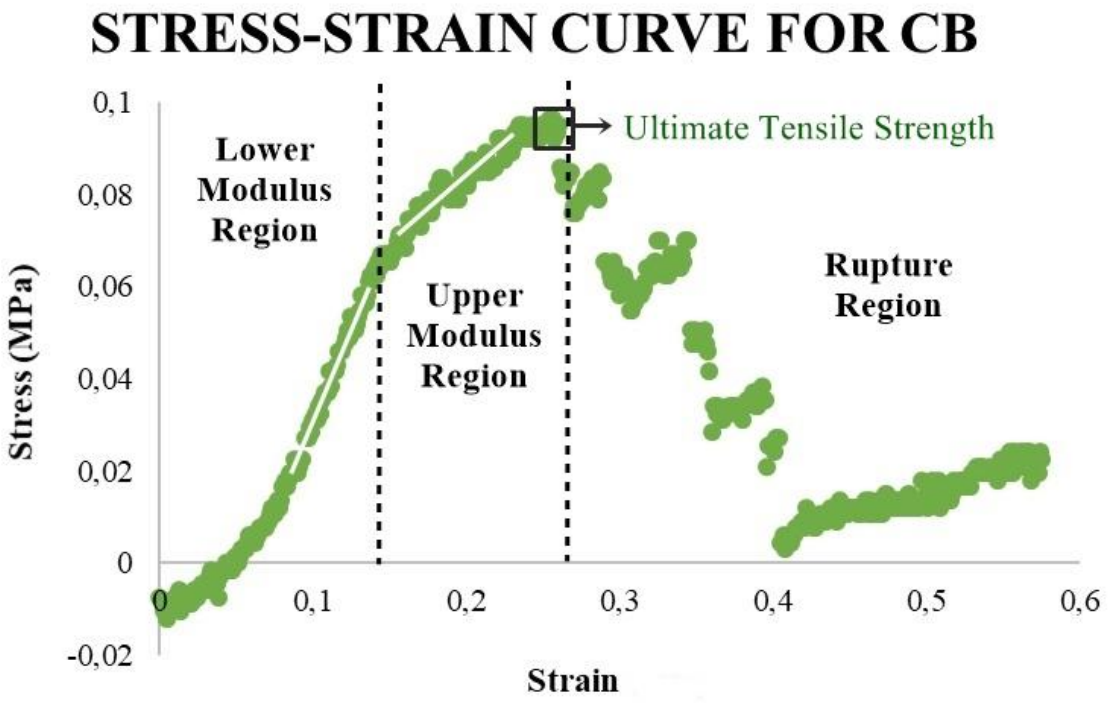

Figure 3.16: Stress-strain curve for decellularized CB. Two different modulus regions can be distinguished, similarly to human vessels, before their rupture.

The Young's Modulus values were determined for the decellularized vessels of CB, NZ and VS from which NZ had the most similar behaviour to human vessels, at 0.62 ± 0.07 MPa. Also, an ECH treatment is seen to weaken the structure, with the Ultimate Tensile Strength (U.T.S) decreasing by almost half. However, though stiffer, with a Young's Modulus of 0.81 ± 0.08, CB vessels are seen to be able to withstand higher pressures, with an U.T.S of 0.34 ± 0.01 MPa. As for VS vessels, a larger fragility is observed.

Table 3.4: Young's Modulus and Ultimate Tensile Strength values for decellularized scaffolds. For the scaffolds treated with ECH, only NZ were able to be tested since CB and VS were of such fragility that they could withstand the slighter tension without breaking. CB presented the highest U.T.S result, thus being able to withstand higher pressures. Values are an average of five replicas.

Young's Modulus (MPa)

CB Vessel	NZ Vessel	NZ ECH	VS Vessel
0.81 ± 0.08	0.62 ± 0.07	0.68 ± 0.08	0.13 ± 0.04

Ultimate Tensile Strenght (MPa)

CB Vessel	NZ Vessel	NZ ECH	VS Vessel
0.34 ± 0.01	0.19 ± 0.03	0.07 ± 0.02	0.09 ± 0.04

3.2 Electrospinning

3.2.1 Condition screening

Several fabrication conditions were tested, observed, and the diameter and angle of deviation from the average orientation was calculated. The range of testing was chosen based on the Final Activity Report for the Introduction to Scientific Investigation in Biomedical Engineering written by Diana Querido in 2016.

In order to build the desired matrices, each polymer layer should intertwine in a net-like fashion while keeping the structure's consistency. To ensure this, the fibres should keep a certain level of alignment while not being fully aligned, which was achieved at a rate of 600 rpm for PCL and 400 rpm for PEO. Low velocities led to thicker fibres with a high level of disorder while higher ones led to thin brittle fibres with an increased level of organization. The potential applied to PEO was chosen based on fibre uniformity, as lower voltages made it so the polymer was not stretched properly,resulting on fibres of irregular diameter.

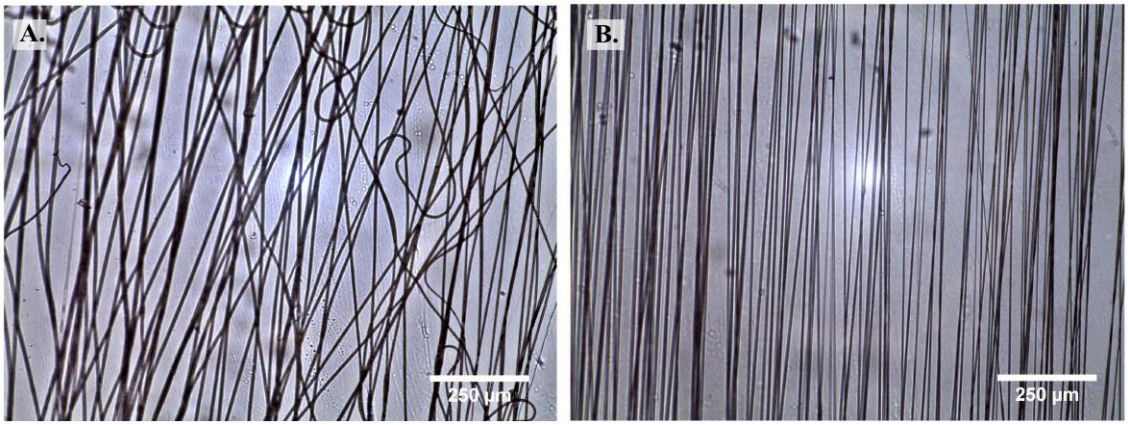

Figure 3.17: Effect of electrospinning velocity on PCL fibre morphology. All conditions had a flow of 0.7 mL/h and potential of 12 kV for a concentration of 10%. **A.** 200 rpm. The fibres are partly aligned along the circumferential direction of the collector. **B.** 1600 rpm. The fibres appear aligned with a lower diameter.

PCL fibres are seen to maintain their diameter uniformity even at extremely high velocities. As a way to quantify the degree of alignment, the angles for each fibre of each condition were measured and an average was calculated and the standard deviation determined. The value of standard deviation of the difference between the average fibre angles and each fibre angle was named **Alignment Number**. The more aligned the fibres, the lower the number. Its correlation to each condition is shown in figure 3.17.B.

PEO fibres share the tendencies regarding diameter and alignment. However, they tended to stick each other, uniting onto a single thicker fibre that was easily broken due to an incomplete evaporation by the time they reached the collector. Also, higher velocities led to the

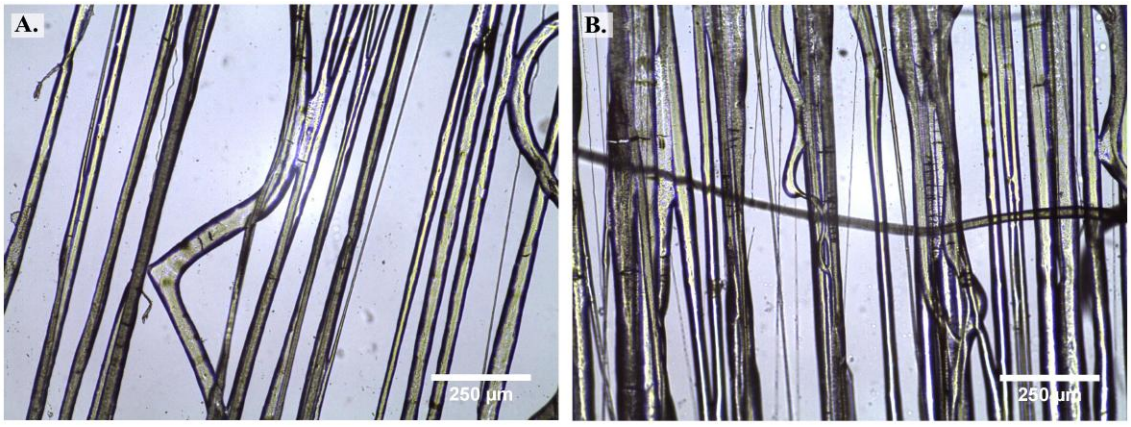

Figure 3.18: Effect of electrospinning velocity on PEO fibre morphology. All conditions had a flow of 5 mL/h and potential of 8 kV for a concentration of 20%. **A.** 200 rpm. **B.** 600 rpm. Values are an average of four replicates.

appearance of thin fibres at a greater number the higher the electric potential. We have found 8.5 kV to be a middle ground between the polymer stretch and the formation of several of the thin fibres.

Similarly to PCL, PEO fibres follow the tendency of a having a larger diameter when a larger flow is applied. However, due to the solution's high viscosity, they tend to align at lower collector velocities. 400 rpm was found to be the most consistent velocity in terms of diameter uniformity and alignment.

Having in mind the previous information, a PCL flow of 0.7 mL/h was chosen, which led to the production of fibres having a mean diameter of 5.4 ± 1.3 μm. For PEO, a higher flow was chosen in order to produce larger fibres of a measured diameter of 43 ± 6 μm and thus, larger cell migration pathways. Also, the solution of 20% PEO was electrospun vertically at a low distance of 7 cm in order to better control fibre positioning at the collector. In conclusion, the parameters chosen for PCL were of 10% concentration, 600 rpm velocity, 0.7 mL/h flow, 12 kV tension and 20 cm distance and for PEO, 20%, 400 rpm, 9 mL/h, 8.5 kV and 7 cm.

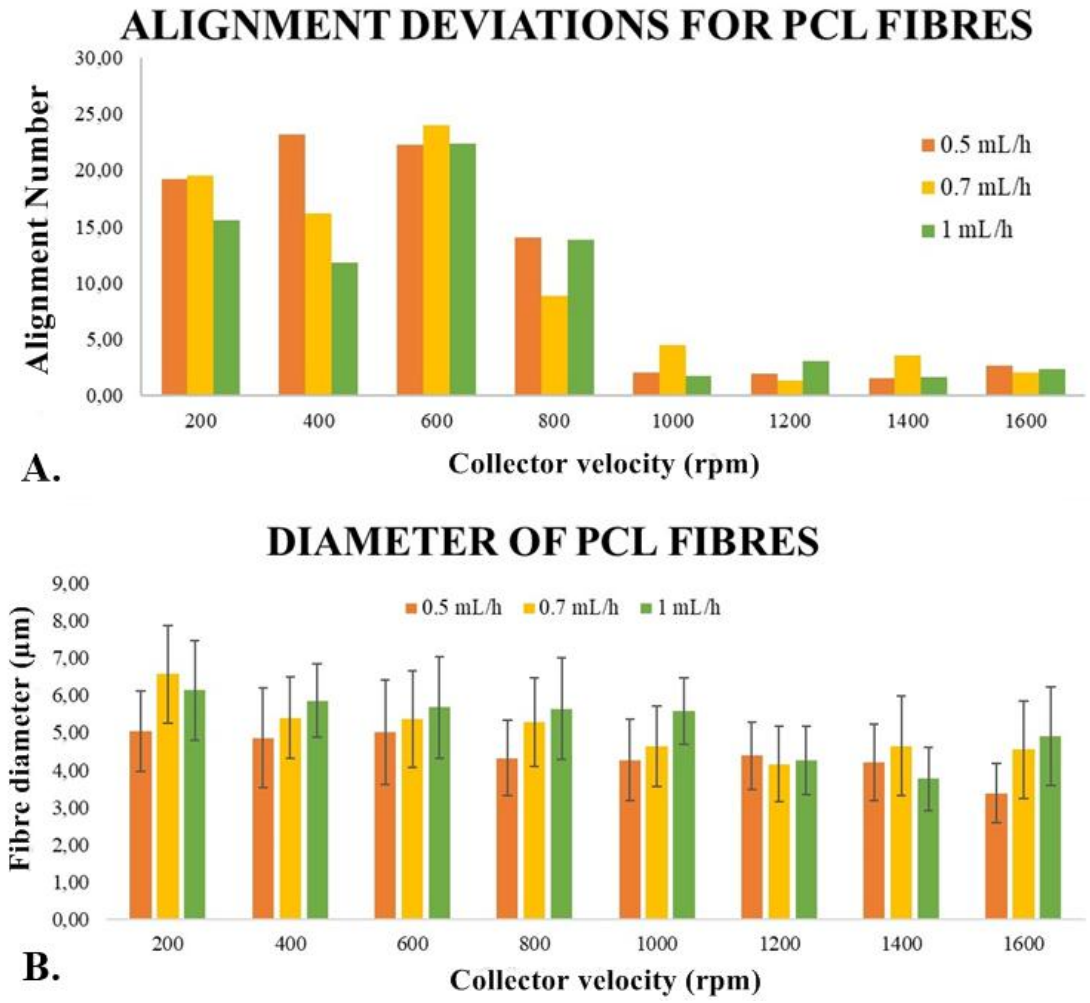

Figure 3.19: Characteristics of PCL electrospun fibres. A. Alignment assessment. Fibres tend to have a higher alignment at a higher velocity and flow. **B.** PCL fibre diameter. A slight tendency can be observed for fibres to be thinner at higher velocities and lower flows. Values are an average of four replicates.

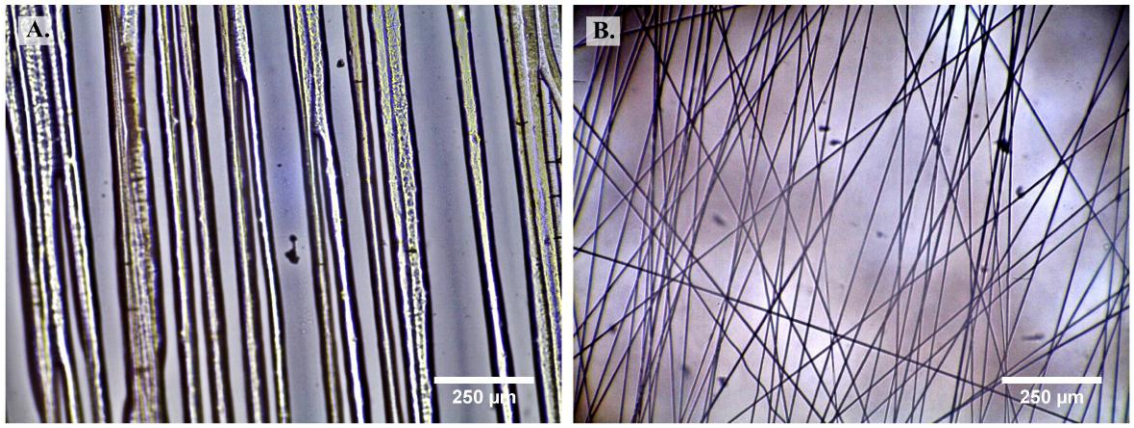

Figure 3.20: Fibres obtained under the parameters chosen for PCL and PEO electrospinning. A. PEO 20%, 400 rpm, 9 mL/h, 8.5 kV, 7 cm. **B.** PCL 10%, 600 rpm, 0.7 mL/h, 12 kV, 20 cm.

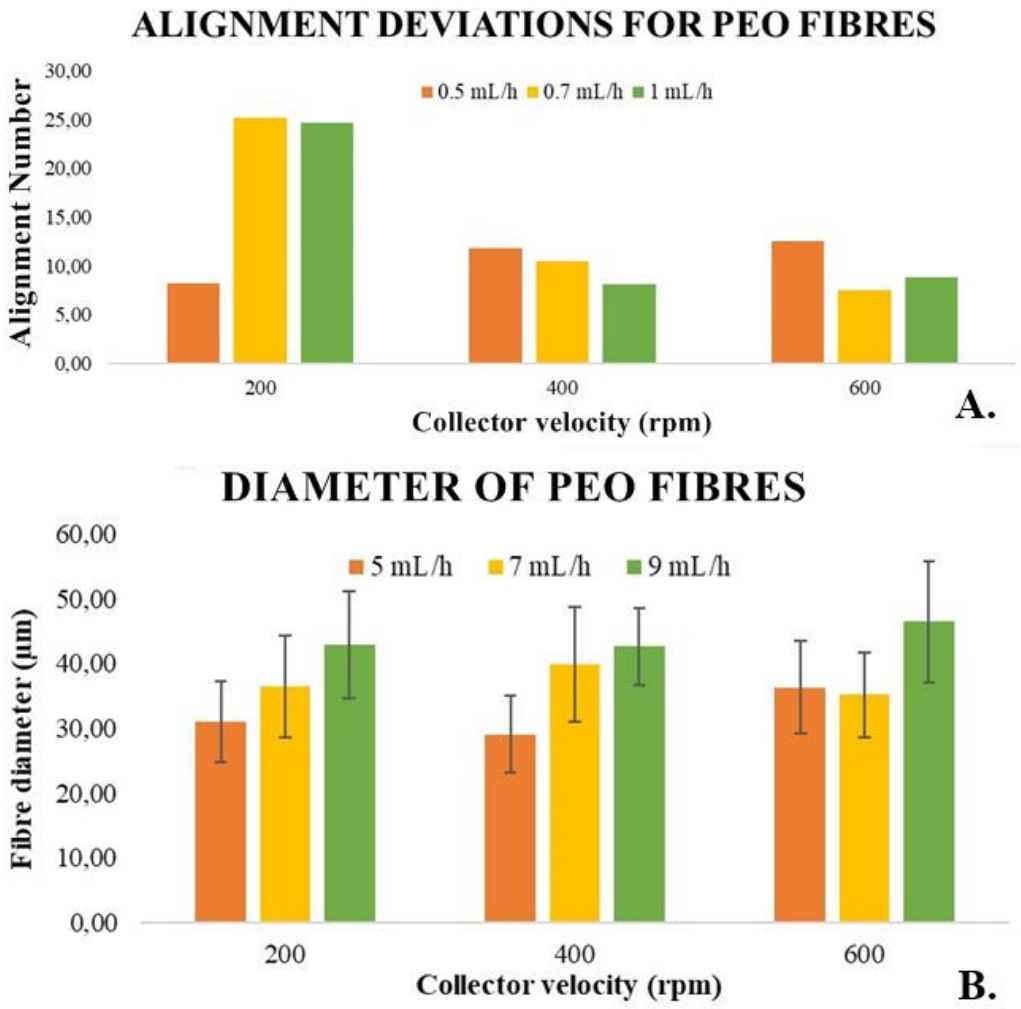

Figure 3.21: Characteristics of PEO electrospun fibres. A. Alignment assessment. **B.** PEO fibre diameter. A velocity of 400 rpm presented the best results in terms of fibre uniformity. Values are an average of four replicates.

3.2.2 The hydrophobicity of PCL: Contact angle measurement

PCL is a highly hydrophilic polymer, often hindering cell adhesion. In order to solve this problem, electrospun PCL matrices were subjected to a treatment with NaOH 0.5 M for a period of 30, 60 or 90 min. As to ensure air removal from the fibres, which could prevent them to come in contact with the solution, they were immersed in 70% ethanol for 15 or 30 min prior to the assay. Table 3.5 displays the contact angle values for the PCL matrices before and after ethanol treatment for 15 or 30 minutes, showcasing a minimal alteration even after 30 minutes of immersion.

All matrices became hydrophilic after the NaOH treatment, with only slight noticeable differences regarding the rate at which the water droplet was absorbed by the material. EtOH 30 conditions and EtOH 15 with an immersion time of 60 and 90 min had a faster rate, being

Table 3.5: Contact Angles for treated and untreated PCL matrices. The displayed values were read 10s past water droplet deposition and are similar for both treated and untreated matrices. Values are an average of six replicates.

Contact Angles		
Untreated	**EtOH 15**	**EtOH 30**
137.0 ± 2.8	136.9 ± 0.6	135.4 ± 3.5

deemed as hyper-hydrophilic, while the remaining one was simply hydrophilic.

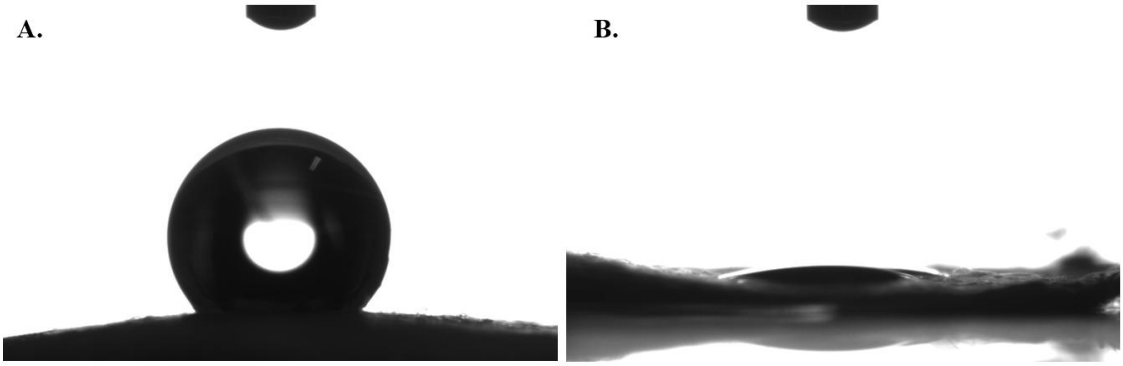

Figure 3.22: Contact angle acquisition images. A. Super-hydrophobic untreated PCL. **B.** Super-hydorphylic EtOH15 60 min matrix.

3.3 Cellular Assays

3.3.1 Resazurin cell viability screening

In order to assess the ideal resazurin concentration for 3T3 and EC, a screening assay was performed. Due to its large use in the lab, Vero cells had already been screened.

For 3T3 cells, a direct proportionality is seen between resazurin concentration and incubation time with absorbance. No significant difference was observed between PBS/DMEM ratios at a resazurin concentration of 0.2 mg/mL. For this reason and in order to be more practical, we have chosen a 40/50 DMEM/PBS ratio and 3h of incubation.

ECs were fairly more susceptible to resazurin toxicity. After three days of culture, a concentration of 0.2 mg/mL was observed to have the best signal/toxicity ratio (data not shown). Cells had the best results for lower ratios of PBS, demonstrating an increased need for nutrients. Considering this, two conditions arose with similar corrected absorbance values, 0% and 30% PBS from which the second was chosen, as a mid-term option that might further help maintain the solution's pH.

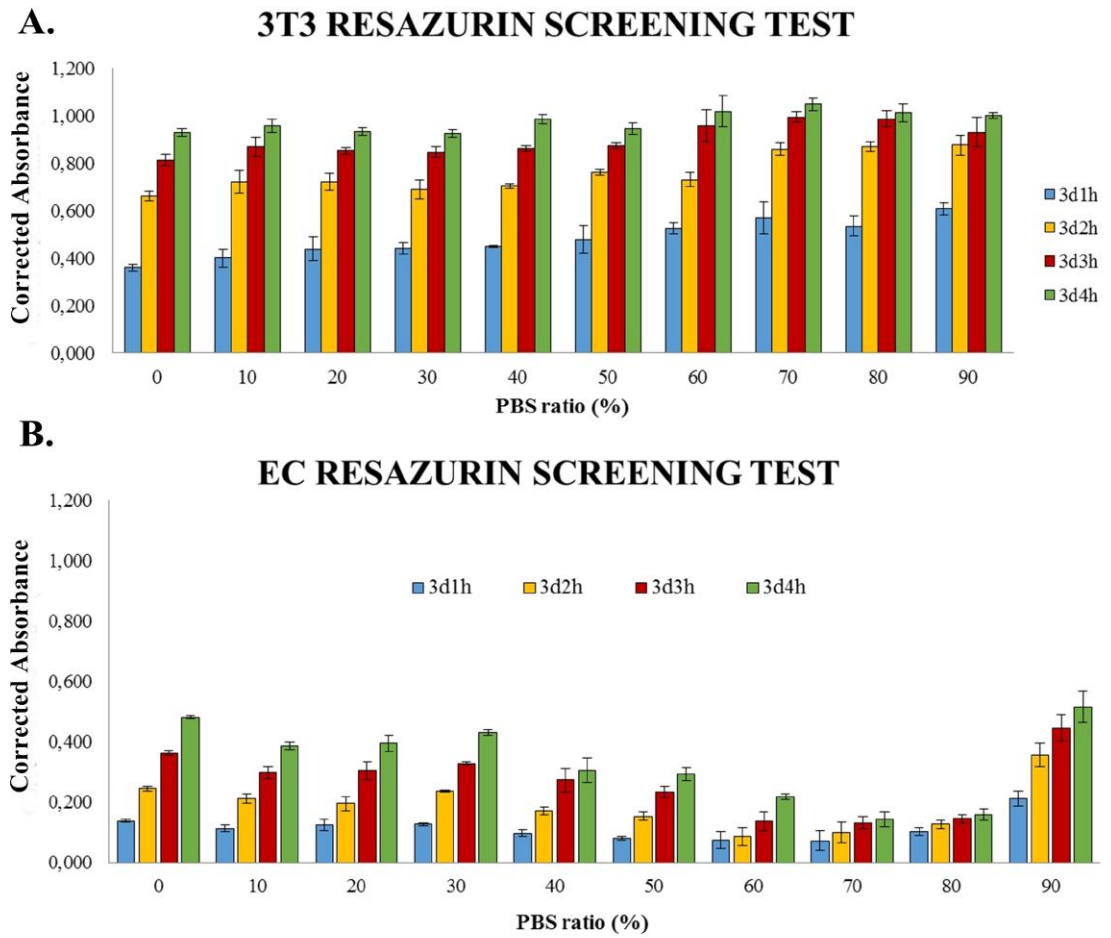

Figure 3.23: **Corrected absorbance values for the 3T3 and EC resazurin screening assay after 3 days of proliferation. A.** 3T3 cell assay. A similar response to resazurin can be observed for all PBS ratios. **B.** EC cell assay. The cells showcase a higher susceptibility to a lower nutrient content. Values are an average of triplicates.

3.3.2 Decellularized leaf scaffolds

Decellularized leaves were grouped by species and cut onto sections as to be used in cell cultures. Due to their fragility, they were not mounted onto a teflon cylinder. In order to calculate the adhesion rate in the leaf itself, they were moved to a different micro-well the day after cell seeding.

Five different conditions were tested using VS, CB or NZ. The sterilization was made in two steps, the first being immersing them in a 70% ethanol solution and the second one a 20 min UV irradiation. Special care was taken so the scaffolds wouldn't dry since that was found to make them loose their shape and stick to the wells, making them difficult to handle afterwards.

3.3.2.1 Condition PCC1

Decellularized 10 mm round sections of VS leaves were seeded with the abaxial surface facing upwards with a density of 80k cells/cm^2 of 3T3, EC or Vero lineages.

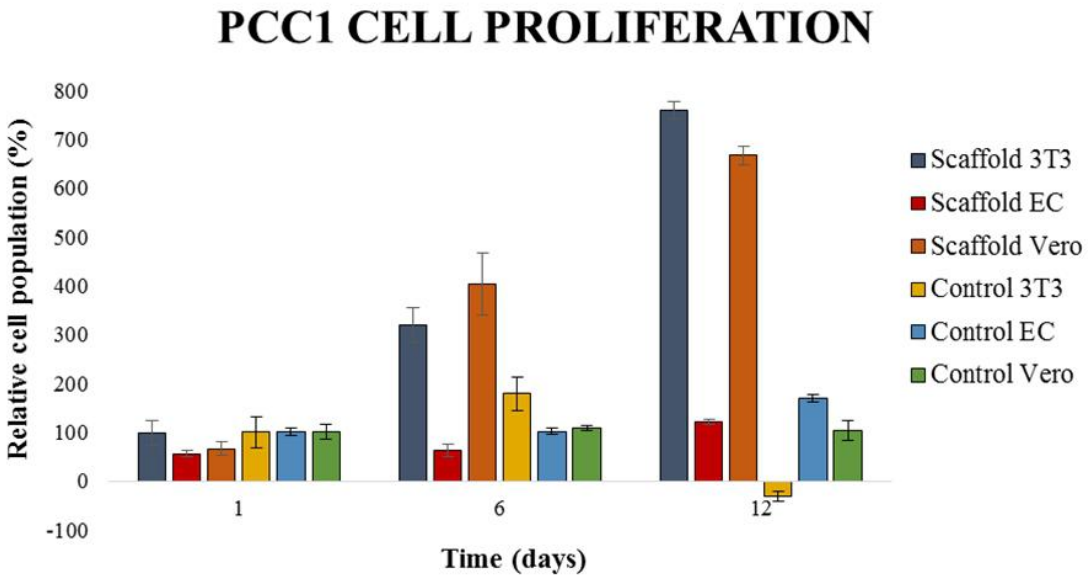

Figure 3.24: PCC1 cell adhesion and proliferation. All values of adhesion percentage were calculated in relation to the control wells at the first day of measuring and represent an average of triplicates.

Being the first test using this type of scaffold, a high cellular density was used in order to increase the probability of cell adhesion and possibly amplify the differences due to the cell lineage's own proliferation rate. Figure 3.24 showcases a notable difference between the 3T3 and EC populations, which is amplified over time. In order to confirm the difference as statistically significant, an ANOVA test was performed between all lineages.

Table 3.6: PCC1 culture and ANOVA results. 3T3 and EC populations are seen to be significantly different and, in the case of 3T3, the high cellular density was shown to be inadequate, as observed on the 12th day. Values are an average of triplicates.

Relative cell population (%)		
3T3	EC	Vero
98 ± 26	55 ± 6	66 ± 14

ANOVA *p-values*			
	3T3	EC	Vero
3T3	-	0.02	0.08
EC	-	-	0.27

One possible explanation is the fact that 3T3 cells, being fibroblasts, have a high cellular turnover, proliferating quickly as long as enough space and nutrients are provided. Since the density used was high, it led to a maximum proliferation rate that lowered once the number of cells got so high that the medium did not provide enough nutrients, explaining the drop in population in the 3T3 and Vero control after 12 days.

Since DAPI is a nuclear stain, it can be used to infer about decellularization. In figure 3.25.A, no nuclei are visible, leading us to the conclusion that the process was successful. Also, differences in cell adhesion mentioned in figure 3.24 can be assessed by DAPI staining. In fact, EC had the lowest number of cells visible which arranged themselves mostly in the vessels (similarly to the other cell lineages), an arrangement pattern that refers to a possible composition or morphology difference between the vessels and the remaining leaf.

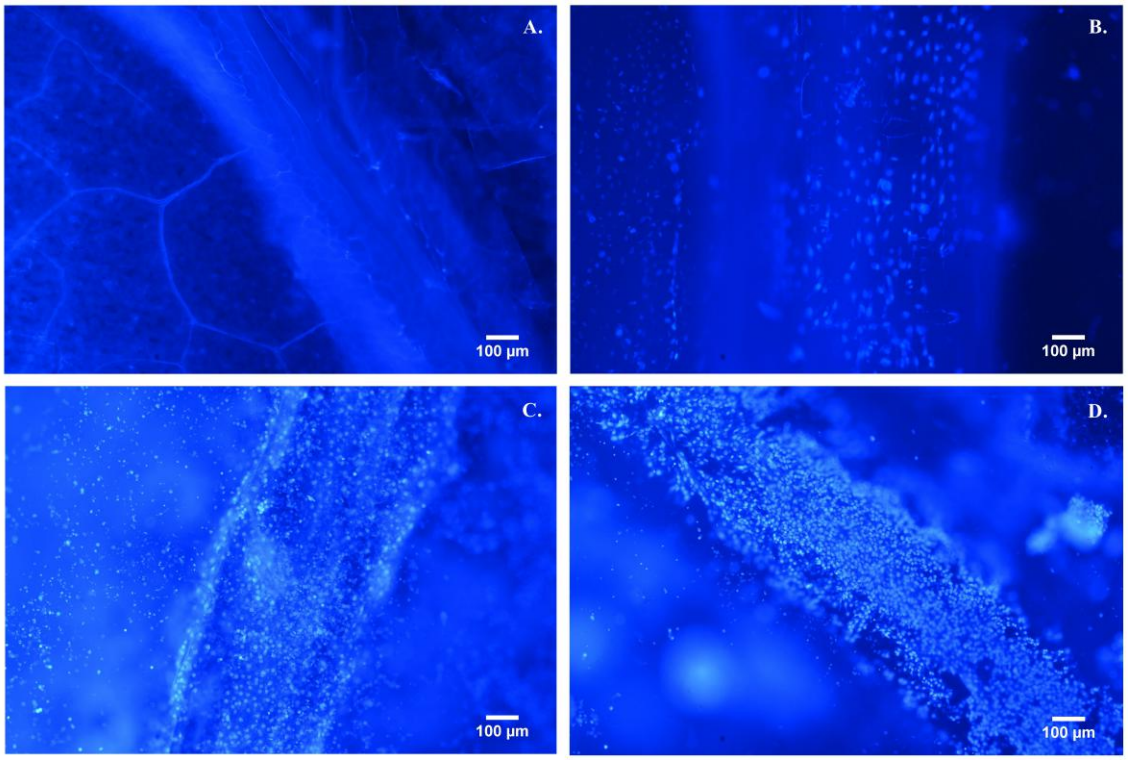

Figure 3.25: DAPI staining imaging for PCC1 after 12 days of incubation. A. Control. No nuclei are observable even in the vascular tissue indicating a successful decellularization procedure. **B.** EC cell culture. Though some nuclei are visible mostly in the leaf's vessels, the seeding process was not ideal. **C.** 3T3 cell culture. A large cellular density can be seen with the cells covering all the surface of the leaf. **D.** Vero cell culture. A large cellular density is observable though not as high as 3T3.

3.3.2.2 Condition PCC2

Decellularized 10 mm round sections of CB leaves were divided in two different conditions. The first were immersed in a sterile 2% bovine gelatin solution for a period of three days and removed from it, before being seeded with the abaxial surface faced upwards with a density of 40k cells/cm^2 of 3T3, EC or Vero lineages. The second (control) group was simply seeded without gelatin.

Gelatin appears to benefit the performance of ECs, achieving an adhesion of almost double the untreated scaffold. However, this effect does not seem to happen along the time

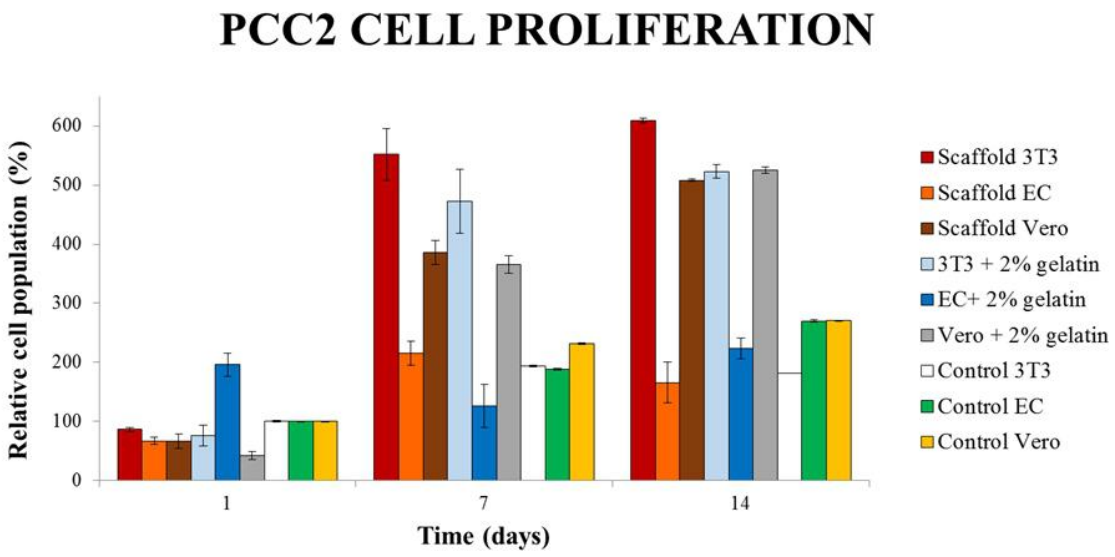

Figure 3.26: PCC2 cell adhesion and proliferation. All cell populations were calculated in relation to the control wells at the first day of measuring. A gelatin treatment appears to improve the adhesion of ECs to the scaffolds. Values are an average of triplicates of two different experiments.

period of the assay since the difference becomes null or slightly negative. Across all other conditions, the presence of gelatin does not seem to cause any considerable effects, either positive or negative. In order to assess for possible differences, the cultured scaffolds were observed by DAPI staining. Since Vero and 3T3 cells appeared to have a similar behaviour, we have decided to not use Vero for future tests and have not observed them.

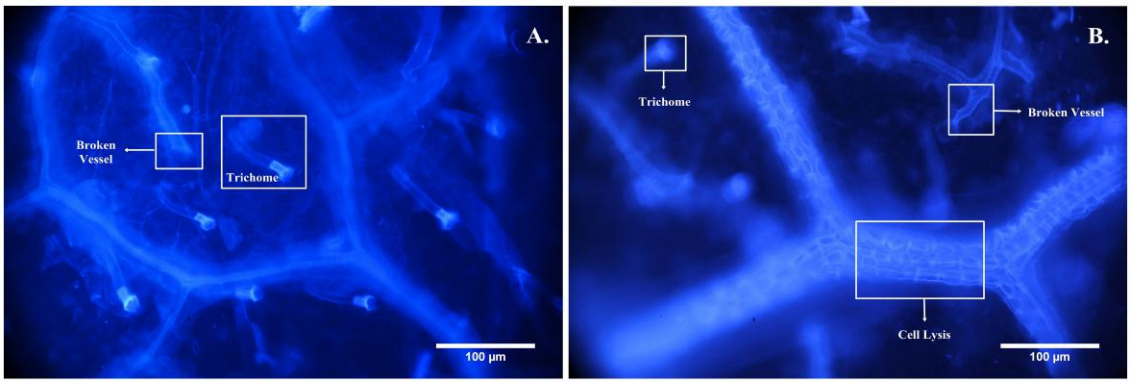

Figure 3.27: Control CB DAPI imaging in condition PCC2. A. The decellularization process did not alter the trichomal structure though a large effect on the structural integrity of the vessels can be observed. **B.** Vessels seem completely decellularized with marks of cell lysis easily visible.

CB leaves are thin, leading to the advantage of being easily observable under the microscope, thus allowing for a better monitoring of possible structural damage. However, as shown in image 3.25, this characteristic also makes the leaves more susceptible to damage from the decellularization process, making them more prone to breakage and holes within

the structure. Also, a large discrepancy is observed between the spacial distribution of 3T3 and ECs likely due to a proliferation issue, where ECs would adhere normally but them perish due to either not finding the ideal conditions to remain anchored to the scaffold or a lack of adequate nutrition coming from the medium used.

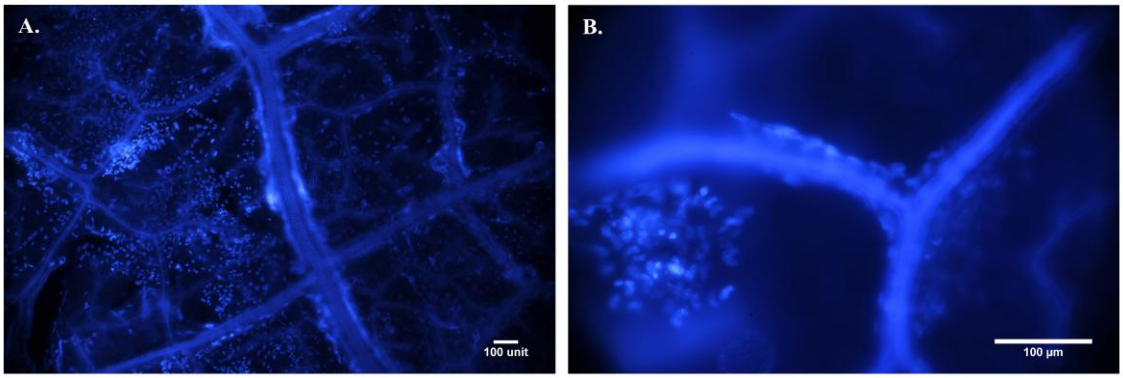

Figure 3.28: DAPI imaging of gelatin coated CB scaffolds in condition PCC2. A. 3T3 coated leaves possess a homogeneous distribution of cells throughout the scaffold. **B.** EC coated leaves showcase a largely inferior cellular density which occurs in spots rather than homogeneously.

3.3.2.3 Condition PCC3

Decellularized 10 mm round sections of post-flowering VS leaves were divided in two different groups. The first group was treated with ECH (see section 2.1.5.1), immersed in a sterile 0.5, 2 or 5% bovine or porcine gelatin solution for a period of three days and seeded with the abaxial surface facing upwards with a density of 40k cells/cm^2 of 3T3 or EC lineages. The second group was immersed in the gelatin solutions and then seeded with no previous ECH treatment.

ECH (C_3H_5ClO) is a chlorinated epoxy compound often used as a cross-linking agent for polymers such as chitin and cellulose. It works by attacking the -OH cellulose functional group, inserting itself between two cellulose monomers at the same time, a reaction that is catalysed by heat. This reaction was employed to attempt the crosslinking between the scaffold and gelatin. [126]

Though the possible cytotoxicity of ECH-crosslinked polymers is inconclusive in the available literature, a lower adhesion percentage and proliferation rate can be observed for ECH treated scaffolds for both tested cellular lineages. This is most likely due to an alteration of the scaffold's structure coming from the heat treatment. However, it is possible that an ECH treatment did not aid the covalent binding of the gelatin to the cellulose. This possibility was not able to be confirmed or denied.

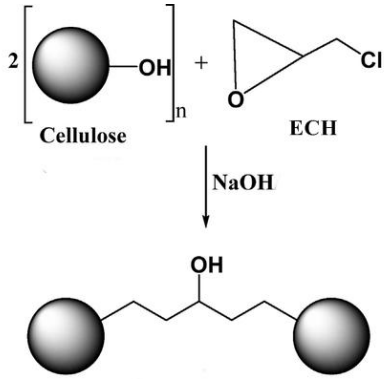

Figure 3.29: Cross-linking reaction between ECH and cellulose. The sphere represents the glucopyranose monomer unit of cellulose. A basic environment improves the yield of the reaction. Adapted from [127].

For both cell lineages, a notable difference between bovine and porcine gelatin can be observed, with a greater amount of cells adhering to the scaffold on the first day but proliferating at a lower rate, a difference directly proportional to gelatin concentration and better seen for 3T3 cells. Porcine gelatin is a highly viscous liquid. For this reason, we postulate that it might be harder for cells to divide since they are subject to the pressure from the surrounding liquid. This difference is felt more strongly on ECs, since their proliferation rate is naturally lower.

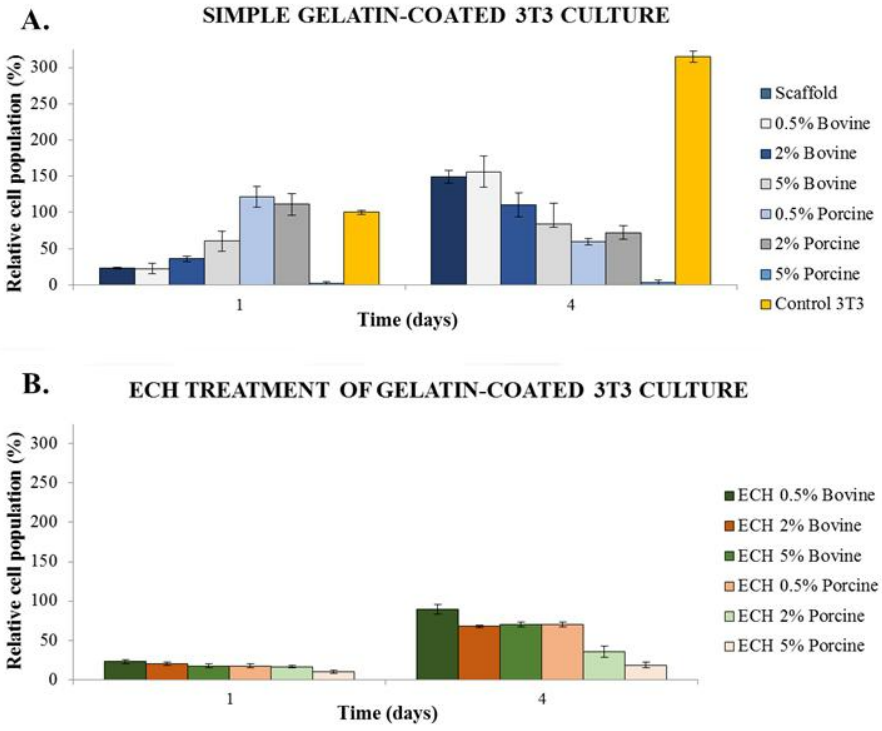

Figure 3.30: PCC3 3T3 cell adhesion and proliferation. A. Gelatin-coated scaffolds. **B.** ECH treated scaffolds coated with gelatin. For all experiments, a 2% bovine gelatin solution holds the best results. Values are an average of triplicates of two different experiments.

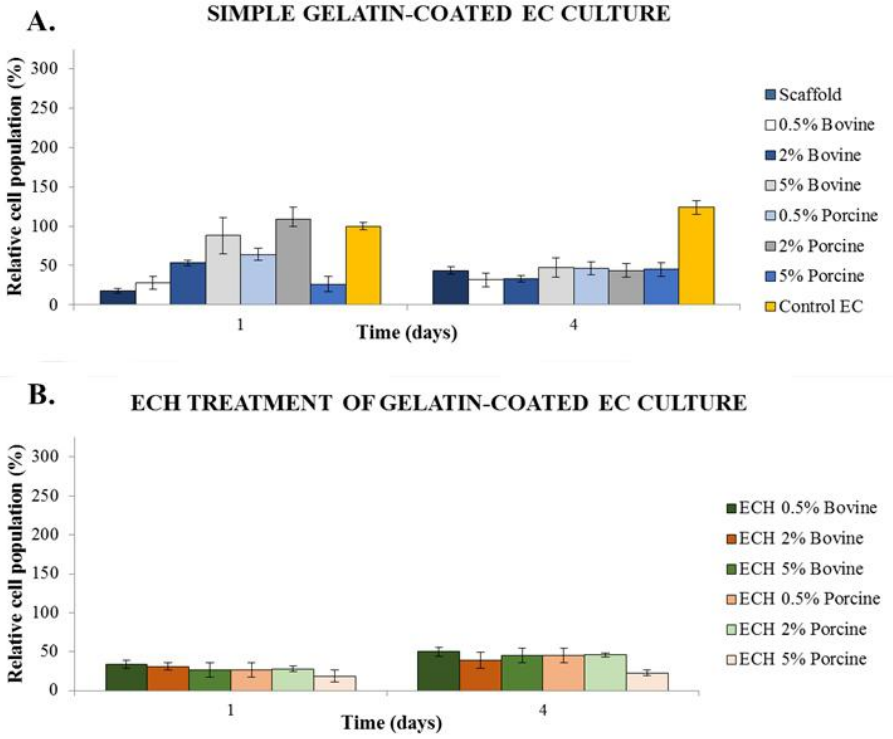

Figure 3.31: PCC3 EC cell adhesion and proliferation. A. Gelatin-coated scaffolds. **B.** ECH treated scaffolds coated with gelatin. Some issues can be seen regarding cell proliferation. However, a tendency can be observed regarding bovine gelatin, which held the best results. Values are an average of triplicates. The experiment was repeated once showcasing a qualitative similarity.

3.3.2.4 Condition PCC4

Considering the information gathered in section 3.3.2.3, a concentration of 2% Bovine solution was chosen for the following test. In order to further analyse the discrepancy between bovine and porcine gelatin, 2% porcine gelatin was also tested.

Decellularized 10 mm round sections of NZ leaves were divided in two groups. The first were immersed in a sterile 2% bovine or porcine gelatin solution for a period of three days and removed from it, before being seeded with the abaxial surface facing upwards with a density of 40k cells/cm^2 of 3T3 or EC lineages. The second (control) group was simply seeded without gelatin.

Similarly to the previous cases, ECs are shown to both adhere and proliferate less than 3T3. However, a lower adhesion occurred when compared to PCC1-3, with only 11.62 ± 1.68 % of ECs adhering to the treated with 2% bovine gelatin. Also, gelatin was not found to have any role, let it be benign or malign, in both adhesion and proliferation, with the best condition being the control for both cell lineages.

DAPI staining images showcase an array or crater-like structures on the abaxial side of NZ leaves inside which cells grow and protrusions. This irregular seeding-site might explain

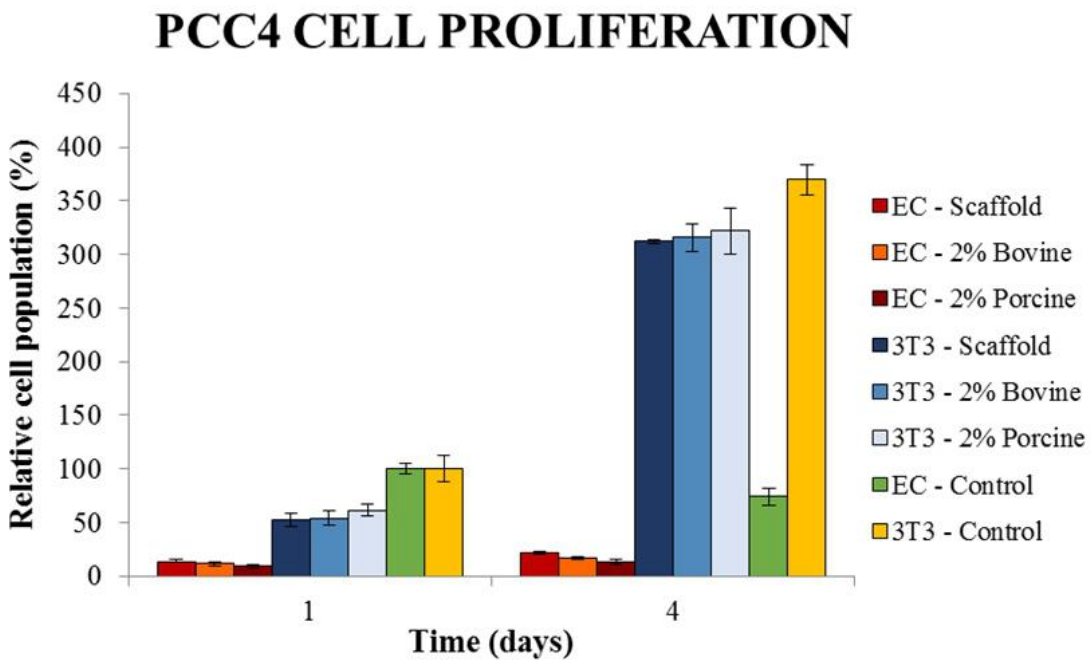

Figure 3.32: PCC4 cell adhesion and proliferation. For NZ, it is not possible to observe differences between gelatin treated and untreated leaves regarding both cell adhesion and proliferation for both used lineages. Values are an average of triplicates.

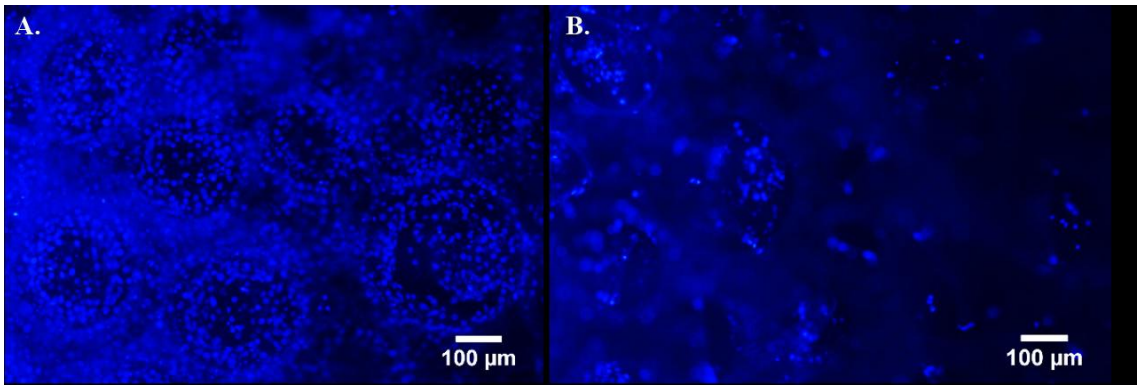

Figure 3.33: DAPI staining of 2% bovine gelatin coated PCC4. A. 3T3 culture. **B.** EC culture. A lower cellular density can be observed.

the reason why proliferation was so poor in ECs for this type of leaf since the physical barrier between "craters"might interfere with the proper proliferation of cells. However, it is more likely that the issues regarding EC proliferation previously assessed, adding to the chemical and morphological alteration of the NZ leaf structure coming from the decellularization process, created an environment not ideal for the proliferation of this particular cell line.

As to shed some light on the matter, non-decellularized and decellularized NZ leaves were stained with DAPI in a similar fashion.

With figure 3.34, we can observe the existence of nuclei on the untreated leaf and the absence in the decellularized leaf, deeming the decellularization process as successful. Also, in

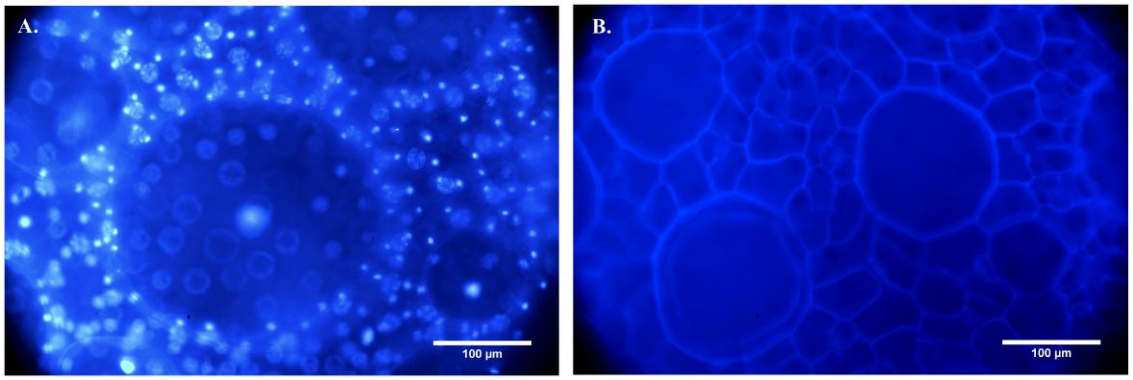

Figure 3.34: DAPI staining decellularized and non-decellularized NZ leaves. A. Non-decellularized leaves. A highly heterogeneous structure is observed. **B.** Decellularized leaves (control assay condition). No cells are observed thus indicating a successful decellularization process.

the untreated leaf, a pattern of cells which is denser in the "crater's"periphery, demonstrates a largely different morphology when compared to VS or CB leaves.

3.3.2.5 Condition PCC5

This condition aimed to assess the feasibility of using decellularized leaves as a vascular substitute. In order to maximize cellular proliferation, we have chosen 3T3 cells.

NZ leaves were tested with and without ECH treatment as well as coated with gelatin. Both the gelatin solutions and cells were inserted through the petiole for the best possible outcome. However, difficulties arose when cells were seeded since the petiole's opening was too narrow and the vessels too opaque, making it hard for the liquid to travel throughout the vascular network. After DAPI staining, we were not able to observe any seeded cells on the leaf though many remained attached to the petri dish itself. This result was common to all conditions tested.

In order to perfect our seeding technique, VS leaves, which have a wider, hollow petiole and vessels were used. During cell perfusion, a much more homogeneous distribution of the seeding liquid was observed. Also, DAPI staining revealed a successful process, with cells localized near (figure 3.36.A) as well as inside the vessels (figure 3.36.B.)

As to assess the amount of cells outside the perfusion site, a resazurin test was conducted after 4 days in both the leaves alone and the petri dish where they were incubated. The obtained results lead to a corrected absorbance for the leaves of 0.32 ± 0.01 and 0.05 ± 0.01 for the petri dishes, meaning that 86 % of the cellular content remained in the leaves. Such a high percentage indicates that the vessels were most likely not damaged by the perfusion protocol.

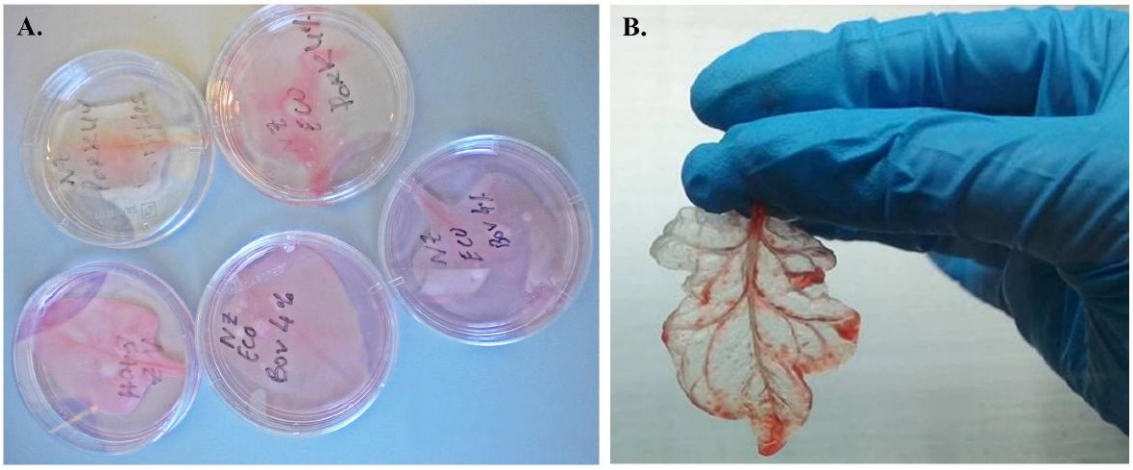

Figure 3.35: Perfusion recellularization samples.a. NZ leaves used for the gelatin test, after incubation with 3T3 cells in a 60mm petri dish. **b.** Viroflay perfusion culture test. Phenol-red dye allows for a better observation of the spacial distribution of the seeding solution.

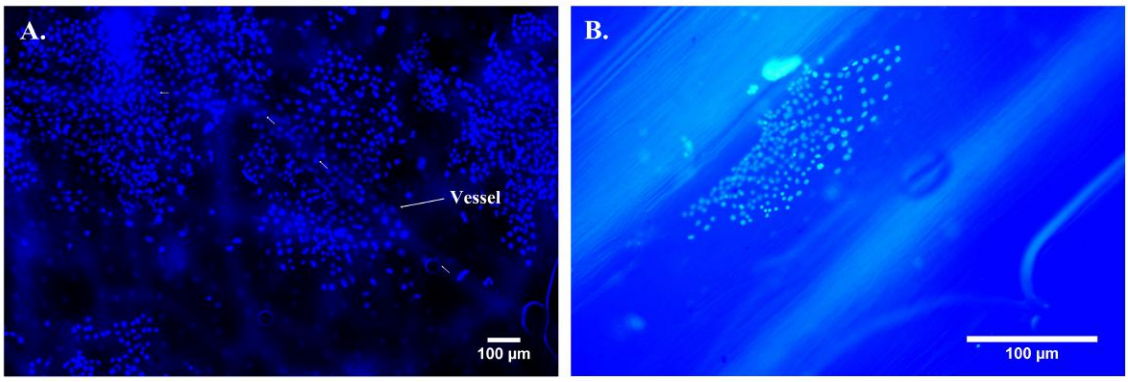

Figure 3.36: DAPI staining of perfusion-based seeded decellularized VS. A. 3T3 cells have largely proliferated in and near the leaf's vessels. **B.** View of 3T3 cells inside the leaf's vessels.

3.3.3 Electrospun scaffolds

Though several different electrospun scaffolds were constructed, not all we able to be used. Due to their thickness, conditions S1-S10 were deemed too hard to manipulate and thus not used for seeding purposes. The behaviour of 3T3, Vero and EC cells was monitored for 12 days in a simple non aligned PCL scaffold. Such as leaf scaffolds, 3T3 and Vero cells had a similar adhesion and proliferation rate (data not shown). Because of this, only 3T3 and EC cells were used afterwards.

3.3.3.1 Condition SCC1

The adhesion and proliferation of 3T3 and EC cells seeded at a density of 40k cells/cm^2 was monitored for both regular PCL, treated PCL (hydrophilic) and the scaffolds S17, S20-21 and S23-24. Though a relative uniformity is observed, some differences can be noted.

For PCL, hydrophilicity appears to have an effect on adhesion but only in EC cells. Since 3T3 cells have a bigger easiness of attachment to scaffolds when compared to ECs, the difference, though existent, dims by the natural standard deviation of biologic systems.

For layered scaffolds, we aimed to analyse whether a higher number of PEO layers would result in a higher proliferation rate. If so, S23, which has three PEO layers of 20 min of spinning, would have the highest value, followed by S23 with three layers of 15 min each, S20 and S21 with two and lastly by S24 with only one. Though this relationship can be somehow observed for 3T3 and ECs in the case of S17 and S23 (with S23 having the best results in EC and S17 in 3T3), the same could not be distinguished for S20, 21 and S24. Also, it is important to indicate that, similar to leaf scaffolds, the proliferation rate of EC cells is much lower than 3T3. However, proliferation actually decreased after 3 days for S17, S21 and S24. In order to understand the reason why, more conditions were tested.

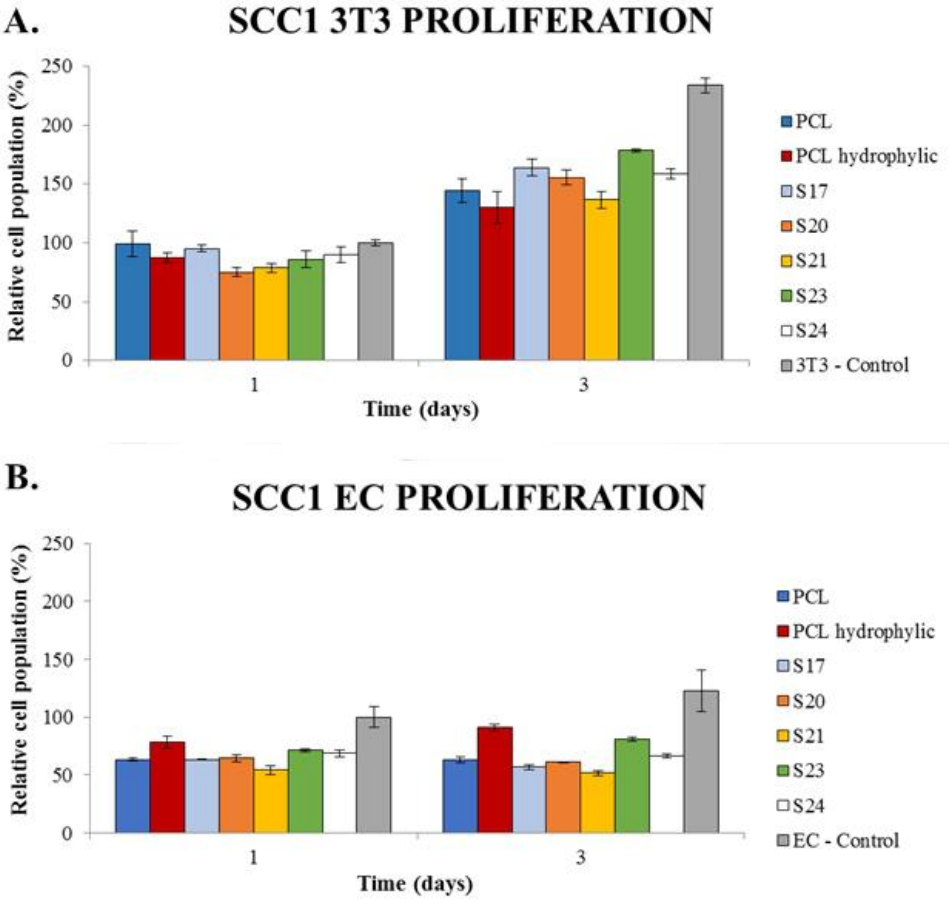

Figure 3.37: SCC1 cell adhesion and proliferation. A. 3T3 proliferation. The values are an average of triplicates of three experiments. **B.** EC proliferation. The experiment was repeated twice showcasing a qualitative similarity. For both lineages, S17 and S23 achieved the best adhesion and proliferation rates.

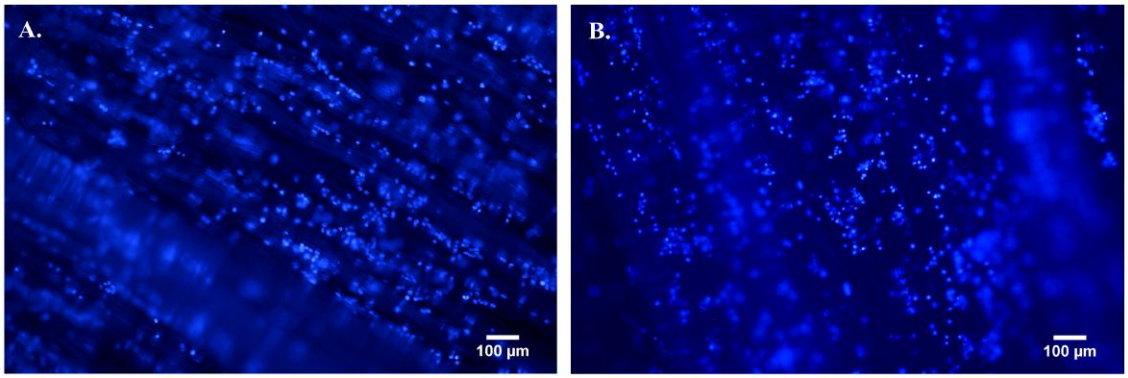

Figure 3.38: DAPI staining of scaffolds S17 and S23 after 3 days of incubation with 3T3 cells. A. Scaffold S17. **B.** Scaffold S23. Two levels of cellular adhesion can be observed both in the inner and outer parts of the channels.

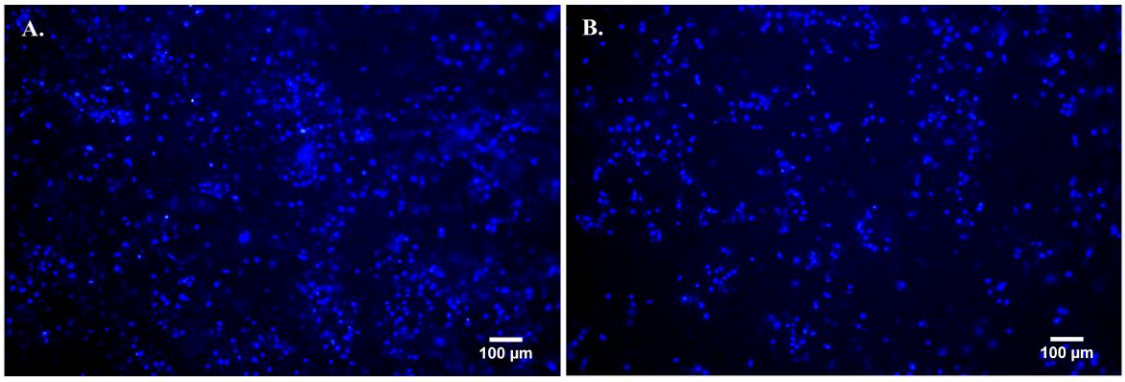

Figure 3.39: DAPI staining hydrophilic and regular PCL after 3 days of incubation with 3T3 cells. A. Hidrophylic PCL scaffold. **B.** Regular PCL scaffold. A lower cellular density is observed.

3.3.3.2 Condition SCC2

The adhesion and proliferation of 3T3 and EC cells seeded at a density of 40k cells/cm^2 was monitored for scaffolds S11-12 and S14-17 for a period of 6 days. These scaffolds differ mainly in the ratio between PEO and PCL, with, considering the theoretical masses of the polymers deposited are an accurate representation of the reality, S11 having 76 % PEO, S12 (which is equivalent to S16), 70 %, S15 54 % and S14 (which is equivalent to S17), 73 %.

Unfortunately, due to the formation of cellular aggregates, we were not able to retrieve any conclusions for the EC culture. In subsequent cultures, aggregates were filtered prior to seeding.

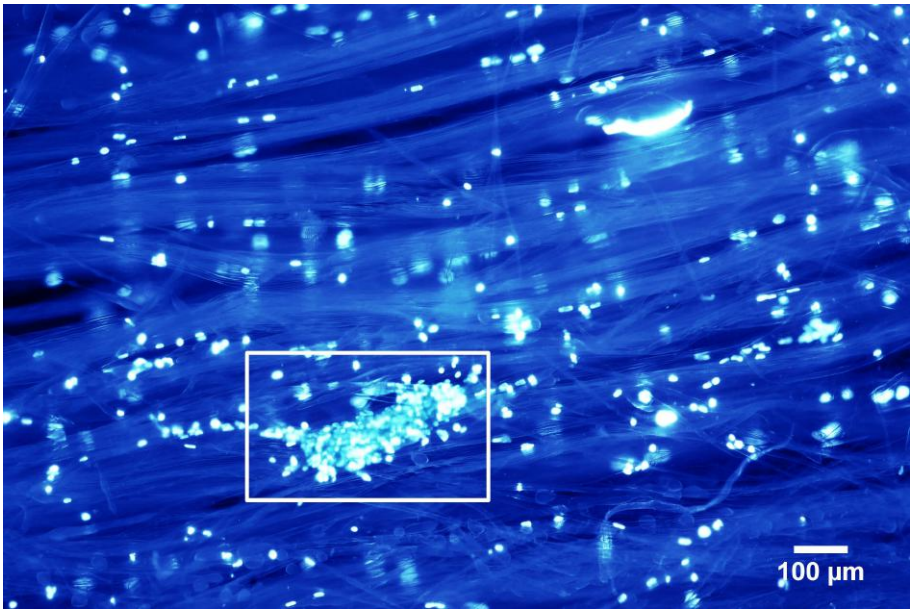

Figure 3.40: DAPI staining of EC aggregate in S14. The presence of aggregates allows for a visual confirmation of the issues with the obtained results. In future experiments, the cellular seeding solution was filtered.

S11, S12 and S14 showcased a much lower adhesion and proliferation when compared to the others. However, by looking at table 2.4, we can see that scaffolds S12 and S16 and S14 and S17 are built using the same specs with the only difference being the fact that they were produced in different days, thus being replicas of each other. This leads us to the assumption that something went wrong in the assay, let it be differences in scaffold production due to humidity issues or, most likely, an heterogeneous seeding procedure. Also, the high standard deviation values for S12, S14 and S15, gives more weight to the seeding issue possibility. Nonetheless, no conclusions can be taken.

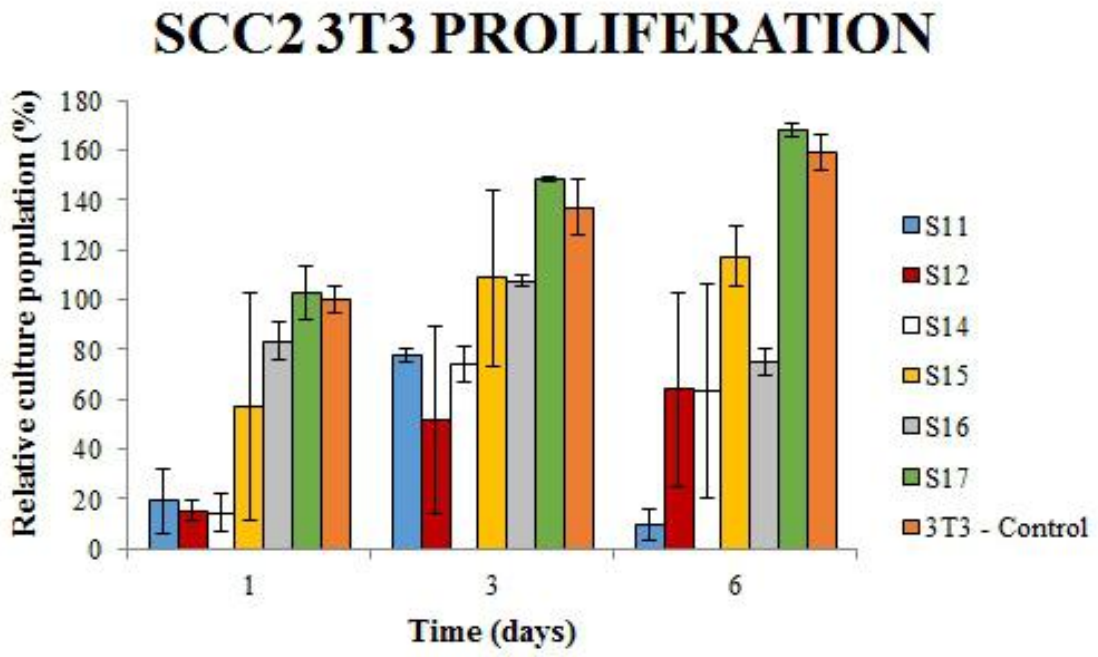

Figure 3.41: SCC2 cell adhesion and proliferation for 3T3. A highly heterogeneous set of results can be observed, mostly due to experimental error. Values are an average of triplicates.

3.3.3.3 Condition SCC3

The adhesion and proliferation of 3T3 and EC cells at a density of 40k cells/cm^2 was monitored for scaffolds S11, S17, S21 and S23, which have relatively similar PEO/PCL ratios and the same number of cellular pathways (three) for a period of 4 days.

For 3T3 cells, the previous tendency can be observed where S23 delivers the best result in adhesion and proliferation followed by S17. As for S11 and S21, a medium success is observed. However, this tendency can not be fully confirmed since the values are not statistically significant. Thus, a repetition of the experiment is necessary.

For ECs, a strange tendency occurred where cells do adhere to the scaffold but do not proliferate properly and actually do seem to have perished during the assay. This tendency was also observed on the control wells which indicates a problem with the cells themselves rather than any toxicity related to the scaffold.

In order to understand the cell's status, the original T25 flask containing the ECs was observed. It is important to note beforehand that these cells had been trypsinated several times which might have harmed them. Figure 3.44 showcases strange black dots forming around the cells which might reflect the presence of apoptotic bodies likely due to an improper culture medium. The ECs used have been harvested directly from the animal and kindly donated by the IGC institute. However, since they are not a commercial line, it becomes harder to pinpoint exactly which medium would be ideal. Trypsin, though rather useful to remove the

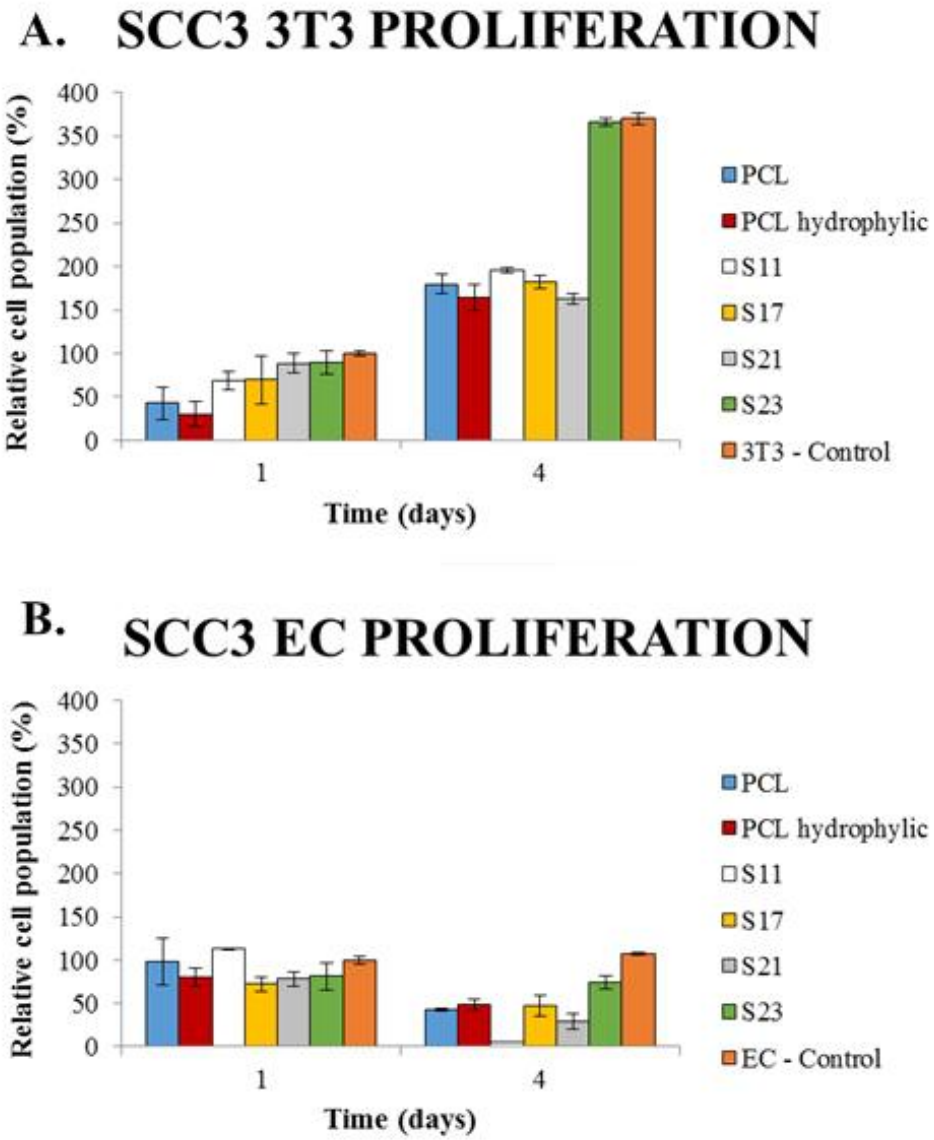

Figure 3.42: SCC3 cell adhesion and proliferation. A. 3T3 cells. As was expected, S23 delivered the best results in terms of proliferation. **B.** EC cells. Issues with cellular proliferation can be observed, likely due to an inadequate culture medium. Values are an average of triplicates. Both experiments were repeated once, showcasing a qualitative similarity.

cells from the flaks, can damage them, making them more vulnerable to other issues. By not using an optimal culture medium, we might have given cells a shorter shelf life than expected, after which their would simply not have a standard pattern of proliferation. This might also explain the reason why the cells proliferate at such a lower rate than 3T3 and have had issues for the previous conditions, including PCC3 (see section 3.3.2.3) and PCC4 (3.3.2.4), which were performed around the same time.

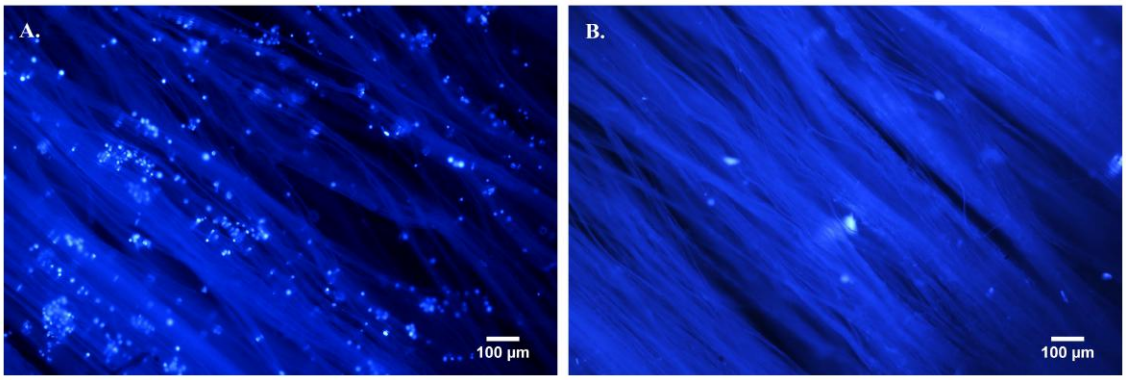

Figure 3.43: **DAPI staining of S11 after 4 days of incubation. A.** 3T3 cell adhesion. A low number of cells is observed, deeming this condition as not ideal for fibroblasts. **B.** EC cell adhesion. Little to no cells can be observed, a result that confirms what was observed in the viability tests.

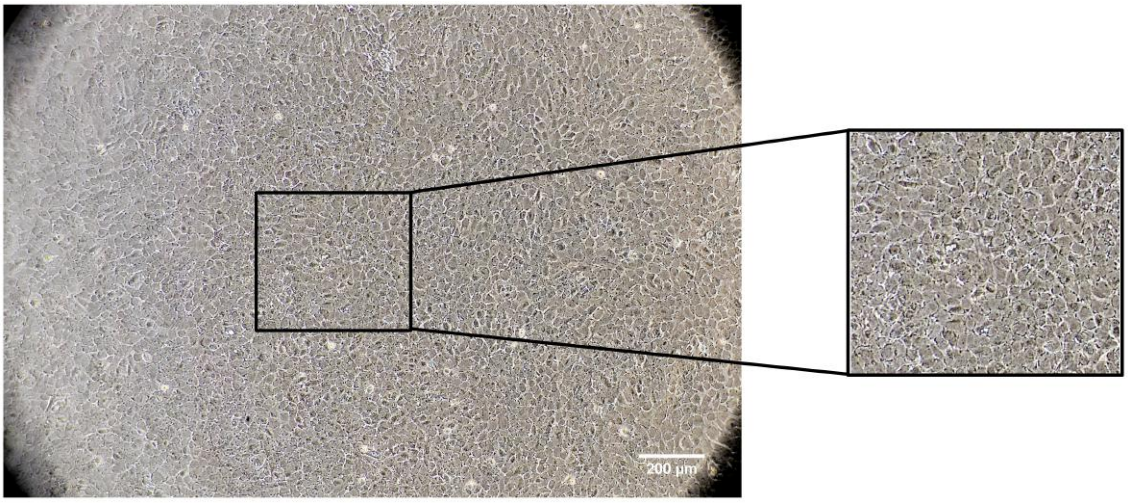

Figure 3.44: **View of T25 flask of confluent EC culture.** Though morphologically normal, the cells present a plethora of black dots which reflect a response to stress (likely a lack of nutrients due to an inappropriate culture medium.

3.3.4 Leaf and Fibre Scaffold SEM imaging

Both scaffold types were observed using SEM imaging in order to understand their structure and confirm their possible effects on cell adhesion.

3.3.4.1 Leaf Scaffolds

SEM imaging further confirms the conservation of structures such as vessels and the stomatal complex in both NZ and VS leaves. As for cell adhesion, no particular areas are preferred , with an all in all global cellular proliferation. Due to their high cellular density it is not possible to differentiate individual cells in 3T3 coated scaffolds.

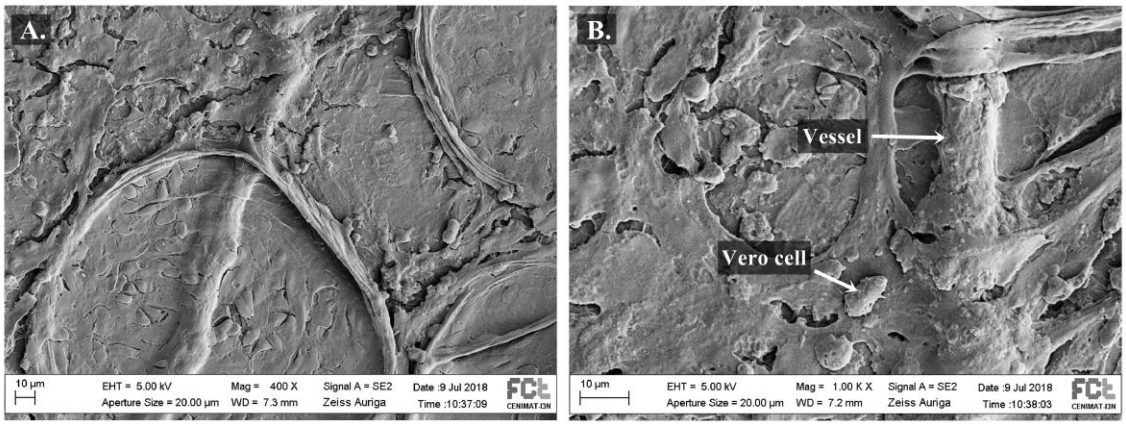

Figure 3.45: Abaxial view of decellularized NZ leaf seeded with Vero cells. A. 400x ampliation. **B.** 1000x ampliation. The structure of the vessels is seen to be intact, with a relatively high cellular density adhered to them.

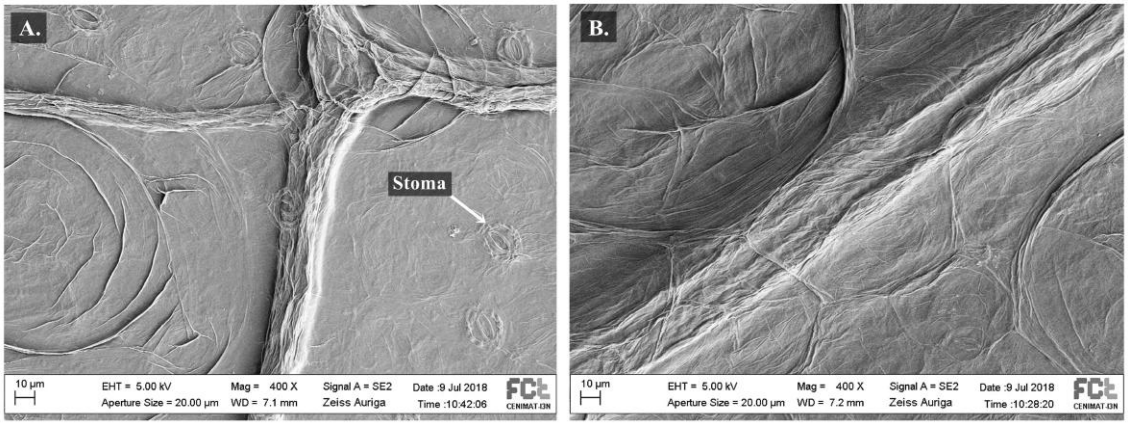

Figure 3.46: Abaxial view of decellularized NZ leaf with and without seeding with 3T3 cells. A. Control condition. Stomata structure can be easily seen though their cells have been removed through the decellularization process. **B.** 3T3 seeded scaffolds. Not many cells can be observed.

The quantity, spatial distribution and pattern of lignin varies in different plant species and varieties, influencing the plant's agro-industrial utility. Protoxylem, the most abundant in young vascular plants, can be young or mature, a difference best seen in the thickenings of their cell wall. With SEM, we can observe a mature protoxylem, as noted on image 3.47. This structure was also able to be seen in lesser detail in some DAPI stained images.

SEM microscopy shed some light over the stability of the leave's structures. Figure 3.48 alerts for a sample drying that was too abrupt. Trichomes possess cells that help them maintain their erect position. Since the process of decellularization removes those cells, trichomes become more susceptible to the effects of sample preparation, leading to their collapse when dried too quickly.

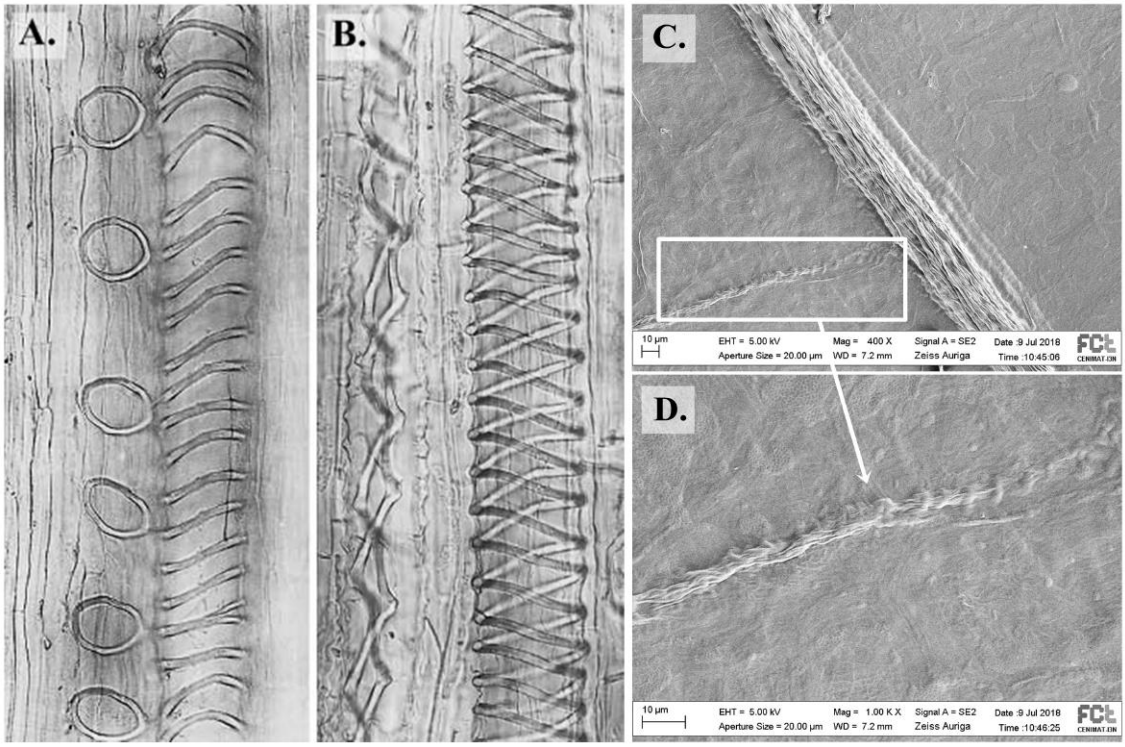

Figure 3.47: Structure of primary xylem vessels. A. Tilted annular and helical wall thickenings in *Ricinus communis*, typical of young protoxylem.**B.** Double helical thickenings in stretched mature protoxylem in *Ricinus communis*. Images A. and B. were adapted from Evert *et al.* [31]. **C.** Vero seeded VS leaf. A good conservation of vessel anatomy can be observed. **D.** Zoomed view of mature xylem in decellularized VS leaf.

3.3.4.2 Electrospun fibre scaffolds

For electrospun scaffolds, the aim of SEM imaging was to understand their structure, mostly regarding the presence of PEO. Both seeded and unseeded scaffolds were observed to assess both PEO presence and the channels themselves.

Regular and treated (hydrophilic) PCL fibres were observed to assess possible structural alterations. No significant differences were noted, demonstrating NaOH treatment to be non-damaging (see figure 3.49).

It was possible to shed a brighter light over the reason why some worked better than others, mainly, the difference between S17 and S23. S11 has previously been seen as having a lower range adhesion and proliferation when compared to, for example, non-aligned PCL. Figure 3.50.A showcases large empty spaces between PCL and PEO fibres, with broken PEO fibres, demonstrating a high structural fragility. As for S17 and S23, S23 possesses much more regular fibres, with spaces between them which allow cells to both adhere and migrate across the PCL fibres towards the first open channel. In comparison, though cellular adhesion and proliferation is observed in S17, SEM imaging evinces a more heterogeneous surface, with a thinner PCL layer that does not adequately cover the PEO channels.

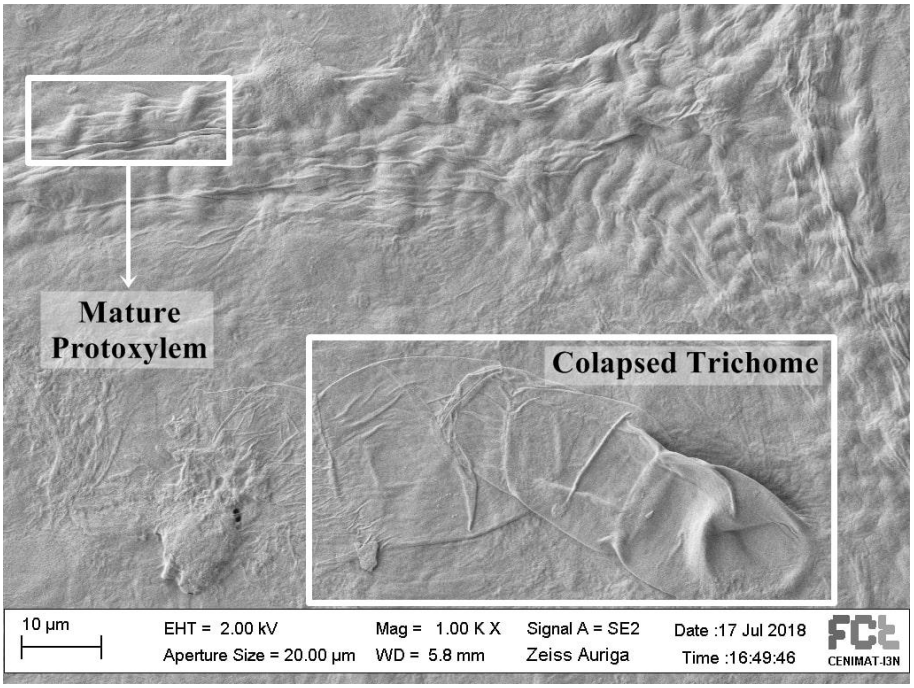

Figure 3.48: SEM imaging of decellularized VS leaf seeded with 3T3 cells. Again, it is possible to observe the structure of a mature protoxylem. Also, a collapsed trichome indicates a rapid drying of the leaf prior to SEM preparation.

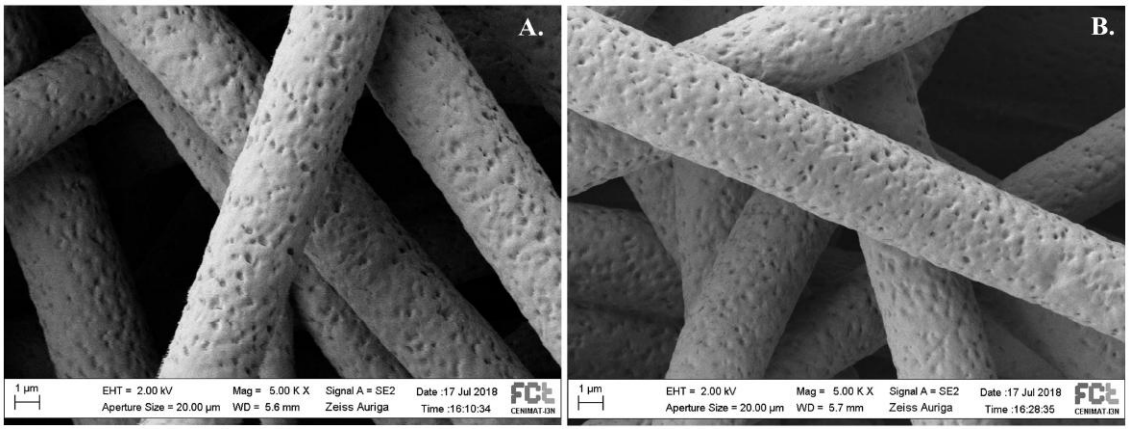

Figure 3.49: SEM imaging of unseeded PCL fibres. A. Untreated fibres. **B.** Hydrophilic PCL fibres. No significant differences can be observed.

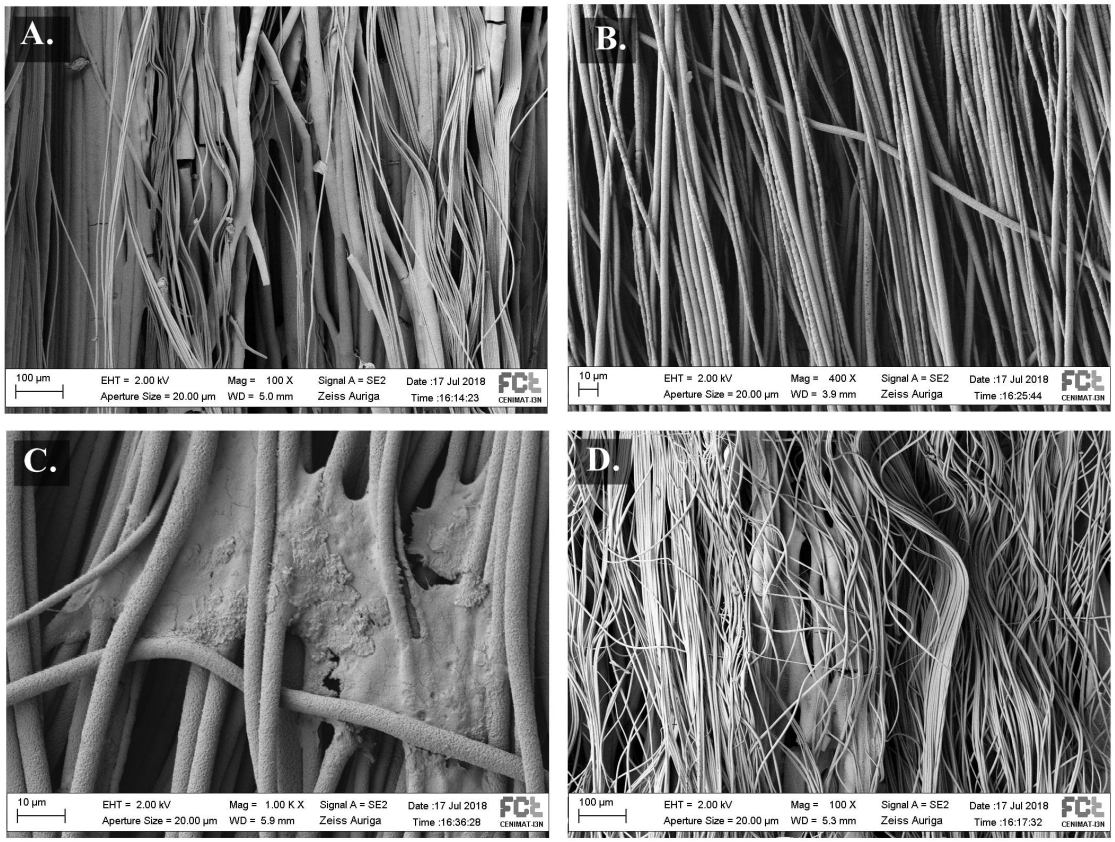

Figure 3.50: SEM imaging of S11, S17 and S23 scaffolds. A. Unseeded S11 **B.** Unseeded S23. **C.** S23 seeded with 3T3 cells. **D.** Unseeded S17. The thicker PCL layers in S23 increase its homogeneity, allowing for a better adhesion environment for cells. Contrarily, S11, a scaffold with a much lower PCL/PEO ratio, showcases larger pathways for cells to migrate towards, preventing them to be conveniently trapped within the PEO channels.

Chapter 4

Conclusions and Future Perspectives

4.1 Conclusions

It was possible to both fully decellularize and re-seed plant leaves with 3T3, EC and Vero cells, resulting in a functional vascular network. Also, it was possible to build PCL scaffolds interleaved with PEO open channels and assess the proliferation of 3T3 and EC cells.

CB, VS, RC, NZ and WGS leaves were successfully grown, transported and conserved for up to three weeks in a 15 % PEG solution stored at 4°C. No significant difference was observed in pigment quantities after 11 days of CB storage when compared to freshly harvested leaves. WGS was deemed as not ideal to decellularization due to their curled inwards leaf structure.

CB leaves, though highly vascularized, were anatomical impractical for decellularization, due to their fine leaf tip that has a tendency to break while immersion decellularization was performed. RC leaves had the opposite problem, with a highly resistant structure that could not be decellularized by any of the perfusion or immersion techniques tested. Chloroform was more effective than acetone for wax solubilization, with the cycle programs of three 15s for VS, two 15s for CB and three 60s cycles for NZ having the best results. Acetone was, however, helpful in aiding pigment removal though it led to structural damage in young VS leaves. As for immersion, SDS was found to be necessary for decellularization, though a 10% solution was too structurally damaging for VS leaves. A basic solution of pH 8.5 was observed to be helpful though not fully effective, deeming it as a good first step approach to decellularization. Bleach had no utility other than being visually deceiving. Perfusion decellularization was attempted, but insufficient on its own, nonetheless being useful as a last step to remove the remaining cellular debris from the vessels.

We found a 3% SDS + 3% Triton-X-100 solution to be best suited for young and post-flowering WGS and VS leaves, 5% SDS + 1% Triton X-100 for NZ and 5% SDS + 3% Triton X-100 for CB leaves. The success of the process was confirmed by DNA quantification, with a 99.6 ± 0.4 % loss of nucleic acids reported for CB, 99 ± 1% for VS and 89 ± 11 % for NZ leaves.

Mechanical testing allowed us to understand how the structure compared to human vessels, with a similar bi-curve behaviour being observed. NZ was the most similar to human vessels with a Young's Modulus of 0.62 ± 0.07 MPa. Nonetheless, CB held the best ultimate tensile strength at 0.34 ± 0.01 MPa. ECH treated leaves did not handle the test, breaking immediately in CB and VS due to severe structural damage.

As for electrospun scaffolds, for PCL a 10% solution electrospun at 600 rpm, with a 0.7 mL/h flow (as to achieve a medium diameter), 12 kV tension and 20 cm collector distance (to ensure homogeneous fibres) was chosen. As For PEO, a 20% solution electrospun at 400 rpm (to achieve the most uniform fibre alignment and diameter), with a 9 mL/h flow (to ensure larger channels), 8.5 kV tension and 7 cm collector distance. PCL was electrospun horizontally while PEO was electrospun vertically to aid the deposition of the highly viscous liquid. A low humidity was observed to help the separation of PEO fibres and, therefore, the homogeneity of fibre diameter.

Cellular assays were performed for both scaffold types. 3T3 and Vero cells were observed to have a similar adhesion and proliferation behaviour. EC were difficult to work with, with slow proliferation rates and adhesion difficulties likely due to an inadequate culture medium.

For leaf scaffolds, decellulazation was confirmed through DAPI staining in all tested conditions. Gelatin, particularly 2% Bovine skin type B gelatin was found to be helpful in the adhesion of EC cells. ECH treatment was deemed as harmful due to its suspected cytotoxicity and bad mechanical properties. NZ leaves were difficult to seed due to their irregular abaxial anatomy and opaque vessels. A successful perfusion seeding of VS with 3T3 cells was achieved with 88 % of cells remaining inside the perfusion site.

Un-aligned PCL scaffolds were made hydrophilic through their immersion for 60 min in NaOH 0.5 M after being treated for 15 min in 70% ethanol and tested against regular PCL. A slight improvement in cellular adhesion was observed. The constructed open channels of PEO were helpful in improving cellular adhesion, with a three PEO layered scaffold interleaved with thick PCL layers having the best results when seeded with 3T3 cells.

Lastly, SEM imaging showcased a good preservation of vessel structure in leaf scaffolds. It was also possible to observe the fragility of a high PEO amount and thin PCL layers, with large empty spaces that are likely not useful for the objective at hand. The best electrospun condition, S23, was seen to have the most homogeneous fibres with adequate pathways towards the PEO channels.

4.2 Troubleshooting and Future Perspectives

The present work showcases the potential of leaf scaffolds, as an easily available, biocompatible and cost effective approach to the issue of vascularization in tissue engineering. Though not currently ideal due to their mechanical properties, a further optimization of the decellularization process as to diminish the amount of time necessary as well as its cross-linking with different polymers might increase their endurance.

In order to optimize the decellularization process, it is important to test a pre-treatment with trypsin perfusion and final step with 1-5% Triton X-100. An optimization of the perfusion apparatus is also necessary. Also, it would be important to test other plant varieties that might have more interesting characteristics for the task at hand.

As for electrospun scaffolds, the role of the open channels should be better assessed by testing a greater number of PEO layers, all interleaved with thick PCL. After that, the next step would be the creation of the vessels themselves by rolling the scaffold, mechanical testing and lastly, animal implantation.

Perhaps the most important issue that hindered some of the conclusions was the inadequacy of the medium used. It is thus important to change it or use a different line of endothelial cells. Also, tests using smooth muscle cells would further ground the conclusions.

Being a project in its first steps of development, many possibilities are ahead of us. In particular, a closed-system perfusion bio-reactor for decellularization with solution pumps and a drainage system would be useful since it would concentrate out efforts in the actual vessels, which we have seen to be the most difficult to reach. This system would also be of use for cell seeding, with a constant supply of cell medium pumped at low pressures. Likewise, mix cultures of both endothelial and smooth muscle cells, supplemented with angiogenic factors would best mimic the behaviour of vessels *in vivo*. An injection of 2% bovine skin type B gelatin prior to cell seeding would also be helpful for achieving the best adhesion results. Furthermore, we postulate that these fully vascularized leaf scaffolds would best show their abilities when attached to damaged tissue, as to stimulate tissue regeneration on, for example, myocardium damage. As for the electrospun versions, we believe them to have particularly interesting characteristics to substitute damaged vessels, a technique that would be able to work together with the leaf scaffolds since most cardiac damage is coexistent with vessel blockage and impairment.

Bibliography

[1] B. Subia, J. Kundu, and S. C. "Biomaterial Scaffold Fabrication Techniques for Potential Tissue Engineering Applications." In: *Tissue Engineering*. InTech, 2010. ISBN: 19373368. DOI: 10.5772/8581.

[2] F. Colombo, G. Sampogna, G. Cocozza, S. Y. Guraya, and A. Forgione. "Regenerative medicine: Clinical applications and future perspectives." In: *Journal of microscopy and ultrastructure* 5.1 (2017), pp. 1–8. ISSN: 2213-8803. DOI: 10.1016/j.jmau.2016.05.002. URL: http://www.ncbi.nlm.nih.gov/pubmed/30023231http://www.pubmedcentral.nih.gov/articlerender.fcgi?artid=PMC6014261.

[3] J. C.-Y. Chung and D. Shum-Tim. "Neovascularization in tissue engineering." In: *Cells* 1.4 (2012), pp. 1246–60. ISSN: 2073-4409. DOI: 10.3390/cells1041246. URL: http://www.ncbi.nlm.nih.gov/pubmed/24710553http://www.pubmedcentral.nih.gov/articlerender.fcgi?artid=PMC3901123.

[4] C. E. R. and E. L. Clark. "Microscopic studies on the regeneration of medullated nerves in the living mammal." In: *The American journal of anatomy* 81.2 (1947), pp. 233–268. ISSN: 00029106. DOI: 10.1002/aja.1000810204.

[5] J. Rouwkema, N. C. Rivron, and C. A. van Blitterswijk. "Vascularization in tissue engineering." In: *Trends in Biotechnology* 26.8 (2008), pp. 434–441. ISSN: 01677799. DOI: 10.1016/j.tibtech.2008.04.009. arXiv: NIHMS150003.

[6] E. C. Novosel, C. Kleinhans, and P. J. Kluger. "Vascularization is the key challenge in tissue engineering." In: *Advanced Drug Delivery Reviews* 63.4 (2011), pp. 300–311. ISSN: 0169409X. DOI: 10.1016/j.addr.2011.03.004.

[7] A. Atala, F. Kurtis Kasper, and A. G. Mikos. "Engineering complex tissues." In: *Science Translational Medicine* 4.160 (2012), 160rv12–160rv12. ISSN: 19466234. DOI: 10.1126/scitranslmed.3004890. arXiv: NIHMS150003.

[8] N. C. Rivron, J. Liu, J. Rouwkema, J. De Boer, and C. A. Van Blitterswijk. "Engineering vascularised tissues in vitro." In: *European Cells and Materials* 15 (2008), pp. 27–40. ISSN: 14732262. DOI: 10.22203/eCM.v015a03.

[9] P. L. Tremblay, V. Hudon, F. Berthod, L. Germain, and F. A. Auger. "Inosculation of tissue-engineered capillaries with the host's vasculature in a reconstructed skin transplanted on mice." In: *American Journal of Transplantation* 5.5 (2005), pp. 1002–1010. ISSN: 16006135. DOI: 10.1111/j.1600-6143.2005.00790.x.

[10] M. W. Laschke, B. Vollmar, and M. D. Menger. "Inosculation: Connecting the Life-Sustaining Pipelines." In: *Tissue Engineering Part B: Reviews* 15.4 (2009), pp. 455–465. ISSN: 1937-3368. DOI: 10.1089/ten.teb.2009.0252.

[11] K. K. Hirschi, T. C. Skalak, S. M. Peirce, and C. D. Little. "Vascular assembly in natural and engineered tissues." In: *Annals of the New York Academy of Sciences* 961 (2002), pp. 223–242. ISSN: 00778923. DOI: 10.1111/j.1749-6632.2002.tb03090.x.

[12] R. K. Jain, P. Au, J. Tam, D. G. Duda, and D. Fukumura. "Engineering vascularized tissue." In: *Nature Biotechnology* 23.7 (2005), pp. 821–823. ISSN: 10870156. DOI: 10.1038/nbt0705-821.

[13] L. Dew, S. Macneil, and C. K. Chong. "Vascularization strategies for tissue engineers." In: *Regenerative Medicine* 10.2 (2015), pp. 211–224. ISSN: 1746076X. DOI: 10.2217/rme.14.83.

[14] D. Druecke, S. Langer, E. Lamme, J. Pieper, M. Ugarkovic, H. U. Steinau, and H. H. Homann. "Neovascularization of poly(ether ester) block-copolymer scaffolds in vivo: Long-term investigations using intravital fluorescent microscopy." In: *Journal of Biomedical Materials Research - Part A* 68.1 (2004), pp. 10–18. ISSN: 00219304. DOI: 10.1002/jbm.a.20016.

[15] V. Karageorgiou and D. Kaplan. "Porosity of 3D biomaterial scaffolds and osteogenesis." In: *Biomaterials* 26.27 (2005), pp. 5474–5491. ISSN: 01429612. DOI: 10.1016/j.biomaterials.2005.02.002.

[16] S. J. Hollister. "Porous scaffold design for tissue engineering." In: *Nature Materials* 4.7 (2005), pp. 518–524. ISSN: 14761122. DOI: 10.1038/nmat1421. arXiv: {_}barataMaterialsandTechniquesofpolychromewoodensculpture.

[17] T. Lu, Y. Li, and T. Chen. "Techniques for fabrication and construction of three-dimensional scaffolds for tissue engineering." In: *International Journal of Nanomedicine* 8.1 (2013), pp. 337–350. ISSN: 11769114. DOI: 10.2147/IJN.S38635.

[18] C. Frantz, K. M. Stewart, and V. M. Weaver. "The extracellular matrix at a glance." In: *Journal of Cell Science* 123.24 (2010), pp. 4195–4200. ISSN: 0021-9533. DOI: 10.1242/jcs.023820.

[19] G. Karp. *Cell and molecular biology : concepts and experiments*. John Wiley, 2010. ISBN: 0470483377.

[20] M. Yanagishita. "Function of proteoglycans in the extracellular matrix." In: *Pathology International* 43.6 (1993), pp. 283–293. ISSN: 14401827. DOI: 10.1111/j.1440-1827.1993.tb02569.x.

[21] B. R. Olsen. *Cell Biology of Extracellular Matrix*. 2nd. 1988, pp. 139–177. ISBN: 978-1-4612-8226-6. DOI: 10.1007/978-1-4613-0881-2.

[22] M. A. Schwartz. "Integrins and extracellular matrix in mechanotransduction." In: *Cold Spring Harbor perspectives in biology* 2.12 (2010), a005066. ISSN: 1943-0264. DOI: 10.1101/cshperspect.a005066.

[23] A. Akalu and P. C. Brooks. "Matrix, Extracellular and Interstitial." In: *Encyclopedia of Molecular Cell Biology and Molecular Medicine*. Vol. 8. Weinheim, Germany: Wiley-VCH Verlag GmbH & Co. KGaA, 2005, pp. 45–79. ISBN: 3527305505. DOI: 10.1002/3527600906.mcb.200400091.

[24] J. K. Kular, S. Basu, and R. I. Sharma. "The extracellular matrix: Structure, composition, age-related differences, tools for analysis and applications for tissue engineering." In: *Journal of Tissue Engineering* 5.17 (2014), p. 204173141455711. ISSN: 2041-7314. DOI: 10.1177/2041731414557112.

[25] K. J. Hamill, K. Kligys, S. B. Hopkinson, and J. C. R. Jones. "Laminin deposition in the extracellular matrix: a complex picture emerges." In: *Journal of Cell Science* 122.24 (2009), pp. 4409–4417. ISSN: 0021-9533. DOI: 10.1242/jcs.041095.

[26] T. Rozario and D. W. DeSimone. "The extracellular matrix in development and morphogenesis: A dynamic view." In: *Developmental Biology* 341.1 (2010), pp. 126–140. ISSN: 1095564X. DOI: 10.1016/j.ydbio.2009.10.026.

[27] J. H. Kristensen and M. A. Karsdal. "Elastin." In: *Biochemistry of Collagens, Laminins and Elastin: Structure, Function and Biomarkers*. Academic Press, 2016. Chap. 30, pp. 197–201. ISBN: 9780128098998. DOI: 10.1016/B978-0-12-809847-9.00030-1.

[28] R. Pankov. "Fibronectin at a glance." In: *Journal of Cell Science* 115.20 (2002), pp. 3861–3863. ISSN: 00219533. DOI: 10.1242/jcs.00059.

[29] C. Reuzeau and R. F. Pont-Lezica. "Comparing plant and animal extracellular matrix-cytoskeleton connections - are they alike?" In: *Protoplasma* 186.3-4 (1995), pp. 113–121. ISSN: 0033183X. DOI: 10.1007/BF01281321.

[30] L. Guerra-Guimarães, C. Pinheiro, I. Chaves, D. Barros, and C. Ricardo. "Protein Dynamics in the Plant Extracellular Space." In: *Proteomes* 4.3 (2016), p. 22. ISSN: 2227-7382. DOI: 10.3390/proteomes4030022. URL: http://www.ncbi.nlm.nih.gov/pubmed/28248232http://www.pubmedcentral.nih.gov/

articlerender.fcgi?artid=PMC5217353http://www.mdpi.com/2227-7382/4/3/22.

[31] R. F. Evert, S. E. Eichhorn, K. Esau, K. Esau, and John Wiley & Sons. *Esau's Plant anatomy : meristems, cells, and tissues of the plant body : their structure, function, and development*. Wiley-Interscience, 2006, p. 601. ISBN: 9780470047385.

[32] M. Chabannes, K. Ruel, A. Yoshinaga, B. Chabbert, A. Jauneau, J.-P. Joseleau, and A.-M. Boudet. "In situ analysis of lignins in transgenic tobacco reveals a differential impact of individual transformations on the spatial patterns of lignin deposition at the cellular and subcellular levels." In: *The Plant Journal* 28.3 (2001), pp. 271–282. ISSN: 09607412. DOI: 10.1046/j.1365-313X.2001.01159.x.

[33] R. Bailey. *Plant Leaves and Leaf Anatomy*. 2018. URL: https://www.thoughtco.com/plant-leaves-and-leaf-anatomy-373618 (visited on 09/26/2018).

[34] P. J. White. *Crop Plant Anatomy*. Vol. 49. 02. Cambridge University Press, 2013, p. 320. ISBN: 978 1 78064 019 8. DOI: 10.1017/S0014479712001469.

[35] D. Carlson. *Leaf Structure||Carlson Stock Art*. URL: https://www.carlsonstockart.com/photo/leaf-structure-anatomy-illustration/ (visited on 09/26/2018).

[36] E. C. Reynhardt and M. Riederer. "Structures and molecular dynamics of plant waxes - II. Cuticular waxes from leaves of Fagus sylvatica L. and Hordeum vulgare L." In: *European Biophysics Journal* 23.1 (1994), pp. 59–70. ISSN: 01757571. DOI: 10.1007/BF00192206.

[37] V. Fernández, P. Guzmán-Delgado, J. Graça, S. Santos, and L. Gil. "Cuticle Structure in Relation to Chemical Composition: Re-assessing the Prevailing Model." In: *Frontiers in Plant Science* 7 (2016), p. 427. ISSN: 1664-462X. DOI: 10.3389/fpls.2016.00427.

[38] M. W. Szyndler, K. F. Haynes, M. F. Potter, R. M. Corn, and C. Loudon. "Entrapment of bed bugs by leaf trichomes inspires microfabrication of biomimetic surfaces." In: *Journal of the Royal Society Interface* 10.83 (2013), p. 20130174. ISSN: 17425662. DOI: 10.1098/rsif.2013.0174.

[39] M. Knoblauch, J. Knoblauch, D. L. Mullendore, J. A. Savage, B. A. Babst, S. D. Beecher, A. C. Dodgen, K. H. Jensen, and N. M. Holbrook. "Testing the Münch hypothesis of long distance phloem transport in plants." In: *eLife* 5.JUN2016 (2016). ISSN: 2050084X. DOI: 10.7554/eLife.15341.

[40] U. Hacke. *Functional and ecological Xylem anatomy*. Tech. rep. 2. 2015, pp. 1–281. DOI: 10.1007/978-3-319-15783-2.

[41] A. J. Van Bel. "Evolution, polymorphology and multifunctionality of the phloem system." In: *Perspectives in Plant Ecology, Evolution and Systematics* 2.2 (1999), pp. 163–184. ISSN: 14338319. DOI: 10.1078/1433-8319-00069.

[42] B. Staff. "Medical gallery of Blausen Medical 2014." In: *WikiJournal of Medicine* 1.2 (2014), p. 10. DOI: 10.15347/wjm/2014.010. URL: https://en.wikiversity.org/wiki/WikiJournal{_}of{_}Medicine/Medical{_}gallery{_}of{_}Blausen{_}Medical{_}2014.

[43] M Tennant and J. K. McGeachie. "Blood vessel structure and function: a brief update on recent advances." In: *The Australian and New Zealand journal of surgery* 60.10 (1990), pp. 747–53. ISSN: 0004-8682.

[44] F. Moroni and T. Mirabella. "Decellularized matrices for cardiovascular tissue engineering." In: *Am J Stem Cells* 3.1 (2014), pp. 1–20.

[45] P. M. Crapo, T. W. Gilbert, and S. F. Badylak. "An overview of tissue and whole organ decellularization processes." In: *Biomaterials* 32.12 (2011), pp. 3233–3243. ISSN: 01429612. DOI: 10.1016/j.biomaterials.2011.01.057. arXiv: NIHMS150003.

[46] T. W. Gilbert, S. Wognum, E. M. Joyce, D. O. Freytes, M. S. Sacks, and S. F. Badylak. "Collagen fiber alignment and biaxial mechanical behavior of porcine urinary bladder derived extracellular matrix." In: *Biomaterials* 29.36 (2008), pp. 4775–4782. ISSN: 01429612. DOI: 10.1016/j.biomaterials.2008.08.022.

[47] I. Prasertsung, S. Kanokpanont, T. Bunaprasert, V. Thanakit, and S. Damrongsakkul. "Development of acellular dermis from porcine skin using periodic pressurized technique." In: *Journal of Biomedical Materials Research - Part B Applied Biomaterials* 85.1 (2008), pp. 210–219. ISSN: 15524973. DOI: 10.1002/jbm.b.30938.

[48] J. E. Reing, B. N. Brown, K. A. Daly, J. M. Freund, T. W. Gilbert, S. X. Hsiong, A. Huber, K. E. Kullas, S. Tottey, M. T. Wolf, and S. F. Badylak. "The effects of processing methods upon mechanical and biologic properties of porcine dermal extracellular matrix scaffolds." In: *Biomaterials* 31.33 (2010), pp. 8626–8633. ISSN: 01429612. DOI: 10.1016/j.biomaterials.2010.07.083.

[49] A. Gilpin and Y. Yang. "Decellularization Strategies for Regenerative Medicine: From Processing Techniques to Applications." In: *BioMed Research International* 2017 (2017), p. 9831534. ISSN: 23146141. DOI: 10.1155/2017/9831534.

[50] S. R. Meyer, B. Chiu, T. A. Churchill, L. Zhu, J. R. Lakey, and D. B. Ross. "Comparison of aortic valve allograft decellularization techniques in the rat." In: *Journal of Biomedical Materials Research - Part A* 79.2 (2006), pp. 254–262. ISSN: 00219304. DOI: 10.1002/jbm.a.30777. arXiv: NIHMS150003.

[51] B. Mendoza-Novelo, E. E. Avila, J. V. Cauich-Rodríguez, E. Jorge-Herrero, F. J. Rojo, G. V. Guinea, and J. L. Mata-Mata. "Decellularization of pericardial tissue and its impact on tensile viscoelasticity and glycosaminoglycan content." In: *Acta Biomaterialia* 7.3 (2011), pp. 1241–1248. ISSN: 17427061. DOI: 10.1016/j.actbio.2010.11.017.

[52] T. H. Petersen, E. A. Calle, L. Zhao, E. J. Lee, L. Gui, M. S. B. Raredon, K. Gavrilov, T. Yi, Z. W. Zhuang, C. Breuer, E. Herzog, and L. E. Niklason. "Tissue-engineered lungs for in vivo implantation." In: *Science* 329.5991 (2010), pp. 538–541. ISSN: 00368075. DOI: 10.1126/science.1189345.

[53] T. W. Hudson, S. Zawko, C. Deister, S. Lundy, C. Y. Hu, K. Lee, and C. E. Schmidt. "Optimized Acellular Nerve Graft Is Immunologically Tolerated and Supports Regeneration." In: *Tissue Engineering* 10.11-12 (2004), pp. 1641–1651. ISSN: 1076-3279. DOI: 10.1089/ten.2004.10.1641.

[54] T. W. Gilbert, T. L. Sellaro, and S. F. Badylak. "Decellularization of tissues and organs." In: *Biomaterials* 27.19 (2006), pp. 3675–3683. ISSN: 01429612. DOI: 10.1016/j.biomaterials.2006.02.014.

[55] J. D. O'Neill, R. Anfang, A. Anandappa, J. Costa, J. Javidfar, H. M. Wobma, G. Singh, D. O. Freytes, M. D. Bacchetta, J. R. Sonett, and G. Vunjak-Novakovic. "Decellularization of human and porcine lung tissues for pulmonary tissue engineering." In: *Annals of Thoracic Surgery* 96.3 (2013), pp. 1046–1055. ISSN: 00034975. DOI: 10.1016/j.athoracsur.2013.04.022. arXiv: NIHMS150003.

[56] T. H. Petersen, E. A. Calle, M. B. Colehour, and L. E. Niklason. "Matrix composition and mechanics of decellularized lung scaffolds." In: *Cells Tissues Organs* 195.3 (2012), pp. 222–231. ISSN: 14226421. DOI: 10.1159/000324896.

[57] C. C. Xu, R. W. Chan, and N. Tirunagari. "A Biodegradable, Acellular Xenogeneic Scaffold for Regeneration of the Vocal Fold Lamina Propria." In: *Tissue Engineering* 13.3 (2007), pp. 551–566. ISSN: 1076-3279. DOI: 10.1089/ten.2006.0169.

[58] R. Capoulade, K. L. Chan, C. Yeang, P. Mathieu, Y. Bossé, J. G. Dumesnil, J. W. Tam, K. K. Teo, A. Mahmut, X. Yang, J. L. Witztum, B. J. Arsenault, J. P. Després, P. Pibarot, and S. Tsimikas. "Oxidized phospholipids, lipoprotein(a), and progression of calcific aortic valve stenosis." In: *Journal of the American College of Cardiology* 66.11 (2015), pp. 1236–1246. ISSN: 15583597. DOI: 10.1016/j.jacc.2015.07.020.

[59] R. J. Levy, N. Vyavahare, M. Ogle, P. Ashworth, R. Bianco, and F. J. Schoen. "Inhibition of cusp and aortic wall calcification in ethanol- and aluminum-treated bioprosthetic heart valves in sheep: background, mechanisms, and synergism." In: *The Journal of heart valve disease* 12.2 (2003), 209–216; discussion 216. ISSN: 09668519.

[60] B. Yang, Y. Zhang, L. Zhou, Z. Sun, J. Zheng, Y. Chen, and Y. Dai. "Development of a Porcine Bladder Acellular Matrix with Well-Preserved Extracellular Bioactive Factors for Tissue Engineering." In: *Tissue Engineering Part C: Methods* 16.5 (2010), pp. 1201–1211. ISSN: 1937-3384. DOI: 10.1089/ten.tec.2009.0311.

[61] U. Böer, A. Lohrenz, M. Klingenberg, A. Pich, A. Haverich, and M. Wilhelmi. "The effect of detergent-based decellularization procedures on cellular proteins and immunogenicity in equine carotid artery grafts." In: *Biomaterials* 32.36 (2011), pp. 9730–9737. ISSN: 01429612. DOI: 10.1016/j.biomaterials.2011.09.015.

[62] D. Voet, J. G. Voet, and C. W. Pratt. *Fundamentals of Biochemistry: Life at the Molecular Level*. Wiley, 2012, p. 1200. ISBN: 0470547847. DOI: 0-471-74268-6. arXiv: arXiv:1011.1669v3.

[63] R. W. Grauss, M. G. Hazekamp, F. Oppenhuizen, C. J. Van Munsteren, A. C. Gittenberger-De Groot, and M. C. DeRuiter. "Histological evaluation of decellularised porcine aortic valves: Matrix changes due to different decellularisation methods." In: *European Journal of Cardio-thoracic Surgery* 27.4 (2005), pp. 566–571. ISSN: 10107940. DOI: 10.1016/j.ejcts.2004.12.052.

[64] M. Yang, C. Z. Chen, X. N. Wang, Y. B. Zhu, and Y. J. Gu. "Favorable effects of the detergent and enzyme extraction method for preparing decellularized bovine pericardium scaffold for tissue engineered heart valves." In: *Journal of Biomedical Materials Research - Part B Applied Biomaterials* 91.1 (2009), pp. 354–361. ISSN: 15524973. DOI: 10.1002/jbm.b.31409.

[65] J. Cortiella, J. Niles, A. Cantu, A. Brettler, A. Pham, G. Vargas, S. Winston, J. Wang, S. Walls, and J. E. Nichols. "Influence of Acellular Natural Lung Matrix on Murine Embryonic Stem Cell Differentiation and Tissue Formation." In: *Tissue Engineering Part A* 16.8 (2010), pp. 2565–2580. ISSN: 1937-3341. DOI: 10.1089/ten.tea.2009.0730.

[66] L. E. Flynn. "The use of decellularized adipose tissue to provide an inductive microenvironment for the adipogenic differentiation of human adipose-derived stem cells." In: *Biomaterials* 31.17 (2010), pp. 4715–4724. ISSN: 01429612. DOI: 10.1016/j.biomaterials.2010.02.046.

[67] P. N. Nonaka, N. Campillo, J. J. Uriarte, E. Garreta, E. Melo, L. V. De Oliveira, D. Navajas, and R. Farré. "Effects of freezing/thawing on the mechanical properties of decellularized lungs." In: *Journal of Biomedical Materials Research - Part A* 102.2 (2014), pp. 413–419. ISSN: 15493296. DOI: 10.1002/jbm.a.34708.

[68] N. T. Remlinger, C. A. Czajka, M. E. Juhas, D. A. Vorp, D. B. Stolz, S. F. Badylak, S. Gilbert, and T. W. Gilbert. "Hydrated xenogeneic decellularized tracheal matrix as a scaffold for tracheal reconstruction." In: *Biomaterials* 31.13 (2010), pp. 3520–3526. ISSN: 01429612. DOI: 10.1016/j.biomaterials.2010.01.067.

[69] N.-C. Cheng, B. T. Estes, H. A. Awad, and F. Guilak. "Chondrogenic Differentiation of Adipose-Derived Adult Stem Cells by a Porous Scaffold Derived from Native Articular Cartilage Extracellular Matrix." In: *Tissue Engineering Part A* 15.2 (2009), pp. 231–241. ISSN: 1937-3341. DOI: 10.1089/ten.tea.2008.0253.

[70] S. Cebotari, I. Tudorache, T. Jaekel, A. Hilfiker, S. Dorfman, W. Ternes, A. Haverich, and A. Lichtenberg. "Detergent decellularization of heart valves for tissue engineering: Toxicological effects of residual detergents on human endothelial cells." In: *Artificial Organs* 34.3 (2010), pp. 206–210. ISSN: 0160564X. DOI: 10.1111/j.1525-1594.2009.00796.x.

[71] T. J. Keane, I. T. Swinehart, and S. F. Badylak. "Methods of tissue decellularization used for preparation of biologic scaffolds and in vivo relevance." In: *Methods* 84 (2015), pp. 25–34. ISSN: 10959130. DOI: 10.1016/j.ymeth.2015.03.005.

[72] J. M. Wainwright, R. Hashizume, K. L. Fujimoto, N. T. Remlinger, C. Pesyna, W. R. Wagner, K. Tobita, T. W. Gilbert, and S. F. Badylak. "Right ventricular outflow tract repair with a cardiac biologic scaffold." In: *Cells Tissues Organs* 195.1-2 (2011), pp. 159–170. ISSN: 14226405. DOI: 10.1159/000331400.

[73] C. V. Montoya and P. S. McFetridge. "Preparation of ex vivo-based biomaterials using convective flow decellularization." In: *Tissue engineering. Part C, Methods* 15.2 (2009), pp. 191–200. ISSN: 1937-3384. DOI: 10.1089/ten.tec.2008.0372.

[74] D. E. Wagner, N. R. Bonenfant, C. S. Parsons, D. Sokocevic, E. M. Brooks, Z. D. Borg, M. J. Lathrop, J. D. Wallis, A. B. Daly, Y. W. Lam, B. Deng, M. J. DeSarno, T. Ashikaga, R. Loi, and D. J. Weiss. "Comparative decellularization and recellularization of normal versus emphysematous human lungs." In: *Biomaterials* 35.10 (2014), pp. 3281–3297. ISSN: 01429612. DOI: 10.1016/j.biomaterials.2013.12.103. arXiv: NIHMS150003.

[75] E. Uchimura, Y. Sawa, S. Taketani, Y. Yamanaka, M. Hara, H. Matsuda, and J. Miyake. "Novel method of preparing acellular cardiovascular grafts by decellularization with poly(ethylene glycol)." In: *Journal of Biomedical Materials Research - Part A* 67.3 (2003), pp. 834–837. ISSN: 00219304. DOI: 10.1002/jbm.a.10097.

[76] S. L. Dahl, J. Koh, V. Prabhakar, and L. E. Niklason. "Decellularized native and engineered arterial scaffolds for transplantation." In: *Cell Transplantation* 12.6 (2003), pp. 659–666. ISSN: 09636897. DOI: 10.3727/000000003108747136.

[77] C. Quint, Y. Kondo, R. J. Manson, J. H. Lawson, A. Dardik, and L. E. Niklason. "Decellularized tissue-engineered blood vessel as an arterial conduit." In: *Proceedings of the National Academy of Sciences* 108.22 (2011), pp. 9214–9219. ISSN: 0027-8424. DOI: 10.1073/pnas.1019506108. arXiv: arXiv:1604.05974v2.

[78] J. Liao, E. M. Joyce, and M. S. Sacks. "Effects of decellularization on the mechanical and structural properties of the porcine aortic valve leaflet." In: *Biomaterials* 29.8 (2008), pp. 1065–1074. ISSN: 01429612. DOI: 10.1016/j.biomaterials.2007.11.007.

[79] P. E. Dijkman, A. Driessen-Mol, L. Frese, S. P. Hoerstrup, and F. P. Baaijens. "Decellularized homologous tissue-engineered heart valves as off-the-shelf alternatives to xeno- and homografts." In: *Biomaterials* 33.18 (2012), pp. 4545–4554. ISSN: 01429612. DOI: 10.1016/j.biomaterials.2012.03.015.

[80] P. J. Schaner, N. D. Martin, T. N. Tulenko, I. M. Shapiro, N. A. Tarola, R. F. Leichter, R. A. Carabasi, and P. J. DiMuzio. "Decellularized vein as a potential scaffold for vascular tissue engineering." In: *Journal of Vascular Surgery* 40.1 (2004), pp. 146–153. ISSN: 07415214. DOI: 10.1016/j.jvs.2004.03.033.

[81] H. C. Ott, T. S. Matthiesen, S. K. Goh, L. D. Black, S. M. Kren, T. I. Netoff, and D. A. Taylor. "Perfusion-decellularized matrix: Using nature's platform to engineer a bioartificial heart." In: *Nature Medicine* 14.2 (2008), pp. 213–221. ISSN: 10788956. DOI: 10.1038/nm1684.

[82] J. R. Gershlak, S. Hernandez, G. Fontana, L. R. Perreault, K. J. Hansen, S. A. Larson, B. Y. Binder, D. M. Dolivo, T. Yang, T. Dominko, M. W. Rolle, P. J. Weathers, F. Medina-Bolivar, C. L. Cramer, W. L. Murphy, and G. R. Gaudette. "Crossing kingdoms: Using decellularized plants as perfusable tissue engineering scaffolds." In: *Biomaterials* 125 (2017), pp. 13–22. ISSN: 18785905. DOI: 10.1016/j.biomaterials.2017.02.011.

[83] D. J. Modulevsky, C. Lefebvre, K. Haase, Z. Al-Rekabi, and A. E. Pelling. "Apple derived cellulose scaffolds for 3D mammalian cell culture." In: *PLoS ONE* 9.5 (2014). Ed. by I. Kerkis, e97835. ISSN: 19326203. DOI: 10.1371/journal.pone.0097835.

[84] D. J. Modulevsky, C. M. Cuerrier, and A. E. Pelling. "Biocompatibility of Subcutaneously Implanted Plant-Derived Cellulose Biomaterials." In: *PLoS ONE* 11.6 (2016). Ed. by F. Zhao, e0157894. ISSN: 19326203. DOI: 10.1371/journal.pone.0157894.

[85] J. Doshi and D. H. Reneker. "Electrospinning process and applications of electrospun fibers." In: *Journal of Electrostatics* 35.2-3 (1995), pp. 151–160. ISSN: 03043886. DOI: 10.1016/0304-3886(95)00041-8.

[86] D. Li and Y. Xia. "Electrospinning of nanofibers: Reinventing the wheel?" In: *Advanced Materials* 16.14 (2004), pp. 1151–1170. ISSN: 09359648. DOI: 10.1002/adma.200400719.

[87] Z. M. Huang, Y. Z. Zhang, M. Kotaki, and S. Ramakrishna. "A review on polymer nanofibers by electrospinning and their applications in nanocomposites." In: *Composites Science and Technology* 63.15 (2003), pp. 2223–2253. ISSN: 02663538. DOI: 10.1016/S0266-3538(03)00178-7. arXiv: {_}barataMaterialsandTechniquesofpolychrom

[88] M. Labet and W. Thielemans. "Synthesis of polycaprolactone: A review." In: *Chemical Society Reviews* 38.12 (2009), pp. 3484–3504. ISSN: 03060012. DOI: 10.1039/b820162p.

[89] L. S. Nair and C. T. Laurencin. "Biodegradable polymers as biomaterials." In: *Progress in Polymer Science (Oxford)* 32.8-9 (2007), pp. 762–798. ISSN: 00796700. DOI: 10.1016/j.progpolymsci.2007.05.017. arXiv: NIHMS150003.

[90] M. A. Woodruff and D. W. Hutmacher. "The return of a forgotten polymer - Polycaprolactone in the 21st century." In: *Progress in Polymer Science (Oxford)* 35.10 (2010), pp. 1217–1256. ISSN: 00796700. DOI: 10.1016/j.progpolymsci.2010.04.002.

[91] O. Coulembier, P. Degée, J. L. Hedrick, and P. Dubois. "From controlled ring-opening polymerization to biodegradable aliphatic polyester: Especially poly(β-malic acid) derivatives." In: *Progress in Polymer Science (Oxford)* 31.8 (2006), pp. 723–747. ISSN: 00796700. DOI: 10.1016/j.progpolymsci.2006.08.004.

[92] M. Vert. "Degradable and bioresorbable polymers in surgery and in pharmacology: Beliefs and facts." In: *Journal of Materials Science: Materials in Medicine* 20.2 (2009), pp. 437–446. ISSN: 09574530. DOI: 10.1007/s10856-008-3581-4.

[93] C. X. Lam, S. H. Teoh, and D. W. Hutmacher. "Comparison of the degradation of polycaprolactone and polycaprolactone-(β-tricalcium phosphate) scaffolds in alkaline medium." In: *Polymer International* 56.6 (2007), pp. 718–728. ISSN: 09598103. DOI: 10.1002/pi.2195.

[94] S. I. Jeong, B. S. Kim, S. W. Kang, J. H. Kwon, Y. M. Lee, S. H. Kim, and Y. H. Kim. "In vivo biocompatibilty and degradation behavior of elastic poly(L-lactide-co-ϵ-caprolactone) scaffolds." In: *Biomaterials* 25.28 (2004), pp. 5939–5946. ISSN: 01429612. DOI: 10.1016/j.biomaterials.2004.01.057.

[95] C. M. Vaz, S. van Tuijl, C. V. C. Bouten, and F. P. T. Baaijens. "Design of scaffolds for blood vessel tissue engineering using a multi-layering electrospinning technique." In: *Acta Biomaterialia* 1.5 (2005), pp. 575–582. ISSN: 17427061. DOI: 10.1016/j.actbio.2005.06.006.

[96] B. Nottelet, E. Pektok, D. Mandracchia, J. C. Tille, B. Walpoth, R. Gurny, and M. Möller. "Factorial design optimization and in vivo feasibility of poly(ϵ-caprolactone)-micro- and nanofiber-based small diameter vascular grafts." In: *Journal of Biomedical Materials Research - Part A* 89.4 (2009), pp. 865–875. ISSN: 15493296. DOI: 10.1002/jbm.a.32023.

[97] B. W. Tillman, S. K. Yazdani, S. J. Lee, R. L. Geary, A. Atala, and J. J. Yoo. "The in vivo stability of electrospun polycaprolactone-collagen scaffolds in vascular reconstruction." In: *Biomaterials* 30.4 (2009), pp. 583–588. ISSN: 01429612. DOI: 10.1016/j.biomaterials.2008.10.006.

[98] S. de Valence, J. C. Tille, D. Mugnai, W. Mrowczynski, R. Gurny, M. Möller, and B. H. Walpoth. "Long term performance of polycaprolactone vascular grafts in a rat abdominal aorta replacement model." In: *Biomaterials* 33.1 (2012), pp. 38–47. ISSN: 01429612. DOI: 10.1016/j.biomaterials.2011.09.024.

[99] E. Pektok, B. Nottelet, J. C. Tille, R. Gurny, A. Kalangos, M. Moeller, and B. H. Walpoth. "Degradation and healing characteristics of small-diameter poly(ϵ-caprolactone) vascular grafts in the rat systemic arterial circulation." In: *Circulation* 118.24 (2008), pp. 2563–2570. ISSN: 00097322. DOI: 10.1161/CIRCULATIONAHA.108.795732.

[100] H. Ahn, Y. M. Ju, H. Takahashi, D. F. Williams, J. J. Yoo, S. J. Lee, T. Okano, and A. Atala. "Engineered small diameter vascular grafts by combining cell sheet engineering and electrospinning technology." In: *Acta Biomaterialia* 16 (2015), pp. 14–22. ISSN: 1742-7061. DOI: 10.1016/J.ACTBIO.2015.01.030.

[101] Y.-C. Jiang, L. Jiang, A. Huang, X.-F. Wang, Q. Li, and L.-S. Turng. "Electrospun polycaprolactone/gelatin composites with enhanced cell–matrix interactions as blood vessel endothelial layer scaffolds." In: *Materials Science and Engineering: C* 71 (2017), pp. 901–908. ISSN: 0928-4931. DOI: 10.1016/J.MSEC.2016.10.083.

[102] G. Marchioli, A. D. Luca, E. de Koning, M. Engelse, C. A. Van Blitterswijk, M. Karperien, A. A. Van Apeldoorn, and L. Moroni. "Hybrid Polycaprolactone/Alginate Scaffolds Functionalized with VEGF to Promote de Novo Vessel Formation for the Transplantation of Islets of Langerhans." In: *Advanced Healthcare Materials* 5.13 (2016), pp. 1606–1616. ISSN: 21922640. DOI: 10.1002/adhm.201600058.

[103] K.-H. Sun, Z. Liu, C.-J. Liu, T. Yu, M. Zhou, C. Liu, F. Ran, L.-J. Pan, and H. Zhang. "In vivo study of alginate hydrogel conglutinating cells to polycaprolactone vascular scaffolds fabricated by electrospinning." In: *Journal of Biomedical Materials Research Part B: Applied Biomaterials* 105.8 (2017), pp. 2443–2454. DOI: 10.1002/jbm.b.33731.

[104] E. E. Fenn, D. E. Moilanen, N. E. Levinger, and M. D. Fayer. "Water dynamics and interactions in water-polyether binary mixtures." In: *Journal of the American Chemical Society* 131.15 (2009), pp. 5530–5539. ISSN: 00027863. DOI: 10.1021/ja809261d.

[105] M. Spitzer, E. Sabadini, and W. Loh. "Poly(ethylene glycol) or poly(ethylene oxide)? Magnitude of end-group contribution to the partitioning of ethylene oxide oligomers and polymers between water and organic phases." In: *Journal of the Brazilian Chemical Society* 13.1 (2002), pp. 7–9. ISSN: 01035053. DOI: 10.1590/S0103-50532002000100002.

[106] J. Israelachvili. *The different faces of poly(ethylene glycol)*. Tech. rep. 16. 1997, pp. 8378–8379. DOI: 10.1073/pnas.94.16.8378.

[107] C. W. McGary. "Degradation of poly(ethylene oxide)." In: *Journal of Polymer Science* 46.147 (1960), pp. 51–57. ISSN: 00223832. DOI: 10.1002/pol.1960.1204614705.

[108] D. I. Arnon. "Microelements in culture solution experiments with higher plants." In: *American Journal of Botany* 25.5 (1938), pp. 322–325. DOI: 10.1002/j.1537-2197.1938.tb09223.x.

[109] D. I. Arnon and D. R Hoagland. "Soil science." In: *Soil Science* 50 (1940), pp. 463–485.

[110] F Yamazaki, H Yokomise, S. H. Keshavjee, S Miyoshi, P. F. Cardoso, A. S. Slutsky, and G. A. Patterson. "The superiority of an extracellular fluid solution over Euro-Collins' solution for pulmonary preservation." In: *Transplantation* 49.4 (1990), pp. 690–4. ISSN: 0041-1337.

[111] J. C. Ramalho, N. C. Marques, J. N. Semedo, M. C. Matos, and V. L. Quartin. "Photosynthetic Performance and Pigment Composition of Leaves from two Tropical Species is Determined by Light Quality." In: *Plant Biology* 4.1 (2002), pp. 112–120. ISSN: 1435-8603. DOI: 10.1055/s-2002-20443.

[112] H. K. Lichtenthaler. "Chlorophylls and carotenoids: Pigments of photosynthetic biomembranes." In: *Methods in Enzymology*. Vol. 148. Academic Press, 1987. Chap. 34, pp. 350–382. ISBN: 9780121820480. DOI: 10.1016/0076-6879(87)48036-1.

[113] A. C.C.d. S. Pádua. "Projecto de um bio-reactor para cultura celular em membranas tubulares." Doctoral dissertation. Universidade Nova de Lisboa, 2014. URL: https://run.unl.pt/handle/10362/14286.

[114] D. Tolivia and J. Tolivia. "Fasga: A new polychromatic method for simultaneous and differential staining of plant tissues." In: *Journal of Microscopy* 148.1 (1987), pp. 113–117. ISSN: 00222720. DOI: 10.1111/j.1365-2818.1987.tb02859.x.

[115] X. Zeng and E. Ruckenstein. "Control of Pore Sizes in Macroporous Chitosan and Chitin Membranes." In: *Ind. Eng. Chem. Res* 35.11 (1996), pp. 4169–4175. DOI: 10.1021/IE960270J.

[116] M. Keb-Llanes, G. González, B. Chi-Manzanero, and D. Infante. "A rapid and simple method for small-scale DNA extraction inAgavaceae and other tropical plants." In: *Plant Molecular Biology Reporter* 20.3 (2002), pp. 299–299. ISSN: 0735-9640. DOI: 10.1007/BF02782465. URL: http://link.springer.com/10.1007/BF02782465.

[117] *Vita-Blue Cell Viability Reagent*. URL: http://file.biotool.com/downloads/Vita-Blue-Cell-Viability-Reagent.pdf (visited on 08/18/2018).

[118] *PrestoBlue® Cell Viability Reagent Documentation*. URL: https://tools.thermofisher.com/content/sfs/manuals/PrestoBlueFAQ.pdf (visited on 08/18/2018).

[119] J. Kapuscinski. "DAPI: a DNA-Specific Fluorescent Probe." In: *Biotechnic & Histochemistry* 70.5 (1995), pp. 220–233. ISSN: 1052-0295. DOI: 10.3109/10520299509108199.

[120] T Kono, O Suzuki, and Y Tsunoda. "Cryopreservation of rat blastocysts by vitrification." In: *Cryobiology* 25.2 (1988), pp. 170–3. ISSN: 0011-2240.

[121] S Ohboshi, N Fujihara, T Yoshida, and H Tomogane. "Usefulness of polyethylene glycol for cryopreservation by vitrification of in vitro-derived bovine blastocysts." In: *Animal reproduction science* 48.1 (1997), pp. 27–36. ISSN: 0378-4320.

[122] G. Pasut, A. Panisello, E. Folch-Puy, A. Lopez, C. Castro-Benítez, M. Calvo, T. Carbonell, A. García-Gil, R. Adam, and J. Roselló-Catafau. "Polyethylene glycols: An effective strategy for limiting liver ischemia reperfusion injury." In: *World Journal of Gastroenterology* 22.28 (2016), p. 6501. ISSN: 1007-9327. DOI: 10.3748/wjg.v22.i28.6501.

[123] T. Hauet, J. M. Goujon, H. Baumert, I. Petit, M. Carretier, M. Eugene, and A. Vandewalle. "Polyethylene glycol reduces the inflammatory injury due to cold ischemia/reperfusion in autotransplanted pig kidneys1Drs. Hauet and Goujon contributed equally to this work." In: *Kidney International* 62.2 (2002), pp. 654–667. ISSN: 00852538. DOI: 10.1046/j.1523-1755.2002.00473.x. URL: http://www.ncbi.nlm.nih.gov/pubmed/12110031http://linkinghub.elsevier.com/retrieve/pii/S0085253815485977.

[124] I. NanoDrop Technologies. *260/280 and 260/230 Ratios*. Tech. rep. 2007. URL: http://www.bio.davidson.edu/projects/gcat/protocols/NanoDrop{_}tip.pdf.

[125] A. P. Ebrahimi. "Mechanical properties of normal and diseased cerebrovascular system." In: *Journal of vascular and interventional neurology* 2.2 (2009), pp. 155–62. ISSN: 1941-5893.

[126] J. B. Mckelvey, R. J. Berni, and R. R. Benerito. *Alkaline catalyzed cellulose-epichlorohydrin reactions wherein cellulose is pretreated with aqueous salt solutions*. 1963. URL: https://patents.google.com/patent/US3382029.

[127] I. A. Udoetok, R. M. Dimmick, L. D. Wilson, and J. V. Headley. "Adsorption properties of cross-linked cellulose-epichlorohydrin polymers in aqueous solution." In: *Carbohydrate Polymers* 136 (2016), pp. 329–340. ISSN: 01448617. DOI: 10.1016/j.carbpol.2015.09.032. URL: https://linkinghub.elsevier.com/retrieve/pii/S0144861715008887.